Master's thesis

NTNU
Norwegian University of Science and Technology
Faculty of Information Technology and Electrical Engineering
Department of Electric Power Engineering

Arjan van Dijk Festøy

Voltage Regulation in Low Voltage Distribution Grids

A Study of Different Technologies and Implementation of a VSC Based Series Regulator

Master's thesis in Electric Power Engineering
Supervisor: Kjetil Uhlen
June 2020

NTNU
Norwegian University of Science and Technology

Arjan van Dijk Festøy

Voltage Regulation in Low Voltage Distribution Grids

A Study of Different Technologies and Implementation of a VSC Based Series Regulator

Master's thesis in Electric Power Engineering
Supervisor: Kjetil Uhlen
June 2020

Norwegian University of Science and Technology
Faculty of Information Technology and Electrical Engineering
Department of Electric Power Engineering

NTNU
Norwegian University of
Science and Technology

Summary

These days, more power demanding equipment such as charging of electric vehicles (EV), induction cooktops and power electronics based devices are installed in low voltage distribution grids in every part of the country. This introduces potential problems regarding voltage quality due to the state of the overhead lines and cables supplying consumers, especially in rural areas where the trend of old infrastructure with low short circuit capacity is high.

In this thesis, a real IT-based low voltage distribution grid is modelled in the Simulink environment where two series-connected voltage regulators, the Magtech Voltage Booster (MVB) and the Dynamic Voltage Restorer (DVR), are installed and simulated during the start of an induction motor. By analysing the response and impact of the voltage regulators, the goal is to establish a set of guidelines for choosing the correct voltage regulation method followed by the grid's topology based on the $\frac{R}{X}$ factor and short circuit capacity.

Through the simulations done, it is clear that both the modelled voltage regulators manage to control the voltage at the secondary side to 1 pu, supporting the induction machine in a way that the startup sequence finishes without problems. However, the MVB is consuming significant amounts of reactive power which leads to voltage drops upstream in the grid. This is further empowered if the network has a $\frac{R}{X}$ factor lower than 1. The DVR on the other hand is producing the necessary amounts of active and reactive power needed to inject the correct voltage, without consuming from the grid due to the VSC and energy storage. This is an important point as the DVRs impact in the grid compared to the MVB is minimal and enables the DVR to theoretically fully protect loads for the safety of supply during short circuit contingencies and other great voltage sag events.

Installing the DVR in grids with a resistive $\frac{R}{X}$ factor, however, is not ideal since the DVR cannot supply unlimited amounts of active power, and is significantly more expensive than other installations such as the MVB - and the ultimate goal for these devices is to be a cheaper and more convenient alternative to a total reinvestment in the grid.

Sammendrag

Lading av elbiler, induksjonskokeplater og laster med kraftelektronikk blir mer og mer vanlig i det norske lavspentnettet og trekker høy effekt over kortere tid. Dette introduserer nye utfordringer knyttet til spenningsproblemer grunnet tilstanden som mye av dagens distribusjonskabler og luftledninger befinner seg i. Gammel kraftinfrastruktur i lavspentnettet med høy kortslutningsytelse er svært vanlig i grisegrendte strøk, og alternative løsninger til reinvestering i nettet har i økende grad vært forsket på med målsetning om å utnytte den eksisterende nettinfrastrukturen bedre.

I denne masteroppgaven har et IT-basert lavspentnett blitt modellert i programvaren Simulink basert på data fra nettselskapet Elvia. To seriekoblede spenningsregulatorer, en Magtech Voltage Booster (MVB) og en Dynamic Voltage Restorer (DVR), er modellert og implementert i lavspentnettet. Starten av en standard trefase 4kVA induksjonsmotor er gjort ved en last lokalisert på sekundærsiden av de implementerte spenningsregulatorene, hvor responsen og regulatorenes effekt på spenningsprofilen i nettet under- og etter maskinstarten er analysert. Målet med oppgaven er å gi noen generelle anbefalinger for hvilke spenningsreguleringsteknologier som kan være aktuelle for ulike nettopologier basert på den spesifikke $\frac{R}{X}$ faktoren og kortslutningsytelsen.

Simuleringene som har blitt gjennomført viser at begge de modellerte spenningsregulatorene klarer å gjenopprette spenningen ved motorterminalene på sekundærsiden til 1 pu under motorstarten. Regulatorenes påvirkning i nettet ellers er derimot svært forskjellig, hvor MVB trekker store mengder reaktiv effekt. Dette fører til større spenningsfall lenger oppe i nettet, en trend som blir mer tydelig når $\frac{R}{X}$ faktoren synker. Dette er ikke tilfelle med en DVR da den produserer den nødvendige reaktive effekten selv gjennom den interne kraftelektronikkløsningen. I tillegg kan den kompensere for manglende aktiv effekt gjennom energilageret, som er et viktig punkt, da denne regulatoren potensielt kan beskytte laster gjennom kortslutningshendelser eller større spenningsfall mye mer effektivt enn eksempelvis en MVB.

Installasjon av en DVR i lavspentnett med ensartede spenningsproblemer grunnet lav kortslutningsytelse hvor $\frac{R}{X}$ faktoren i all hovedsak er resistiv anbefales i utgangspunktet ikke, siden spenningsstøtte via aktiv kompensering krever tilgjengelig kapasitet på energilageret. En spenningsbooster lignende MVBen kan da være et bedre alternativ, hovedsakelig grunnet den store investeringskostnaden til kraftelektronikkbaserte spenningsregulatorer med energilager. Dette

er viktig siden målsetningen med disse installasjonene er å være et billigere og mer gunstig alternativ til store reinvesteringer i nettet.

Preface

This thesis marks the very end of my five years of studies at the Norwegian University of Science and Technology in Trondheim, concluding in an M.Sc., in Electrical Power Engineering.

The last years have been hard and challenging, but extremely motivating and informative where I have gained invaluable insight and passion for the Electrical Engineering discipline. I would like to thank family and friends for important support throughout the years, as well as all the persons involved with NTNUI Volleyball, which has been my second family during my stay in Trondheim.

In regards of this thesis, I would like to thank Andreas Rosendahl Simonsen and the DSO company Elvia and my supervisor Kjetil Uhlen for supplying a very interesting and relevant topic as well as valuable insights and ideas. I would also like to explicitly thank Bendik Nybakk Torsæter from SINTEF with supplying measurement data from the laboratory testing of the Magtech Voltage Booster during the autumn of 2019 as well as important feedback.

Trondheim, June 2020
Arjan van Dijk Festøy

Table of Contents

List of Tables

List of Figures

Abbreviations

BESS	=	Battery Energy Storage System
DER	=	Distributed Energy Sources
DG	=	Distributed Generation
DSO	=	Distribution System Operator
DVR	=	Dynamic Voltage Restorer
EHS	=	Environment, Health, Security
EV	=	Electric Vehicles
FACTS	=	Flexible Alternating Current Transmission System
FoL	=	Forskrift om Leveringskvalitet
IEC	=	International Electrotechnical Commission
LVR	=	Line Voltage Regulator
MCI	=	Magnetic Controllable Inductor
MMF	=	Magneto-Motive Force
MVB	=	Magtech Voltage Booster
NVE	=	Norges Vassdrags- og Energidirektorat
OLTC	=	On-Load Tap changer
PCS	=	Power Converter System
PV	=	Photovoltaic Cells
PWM	=	Pulse Width Modulation
SCC	=	Short Circuit Capacity
SPS	=	Specialized Power Systems
SSSC	=	Static Synchronous Series Compensator
ST	=	Series Transformer
STATCOM	=	Static Compensator
SVC	=	Static VAR Compensator
SVR	=	Series Voltage Regulator
TCR	=	Thyristor Controlled Reactor
TSC	=	Thyristor Controlled Capacitor
TSO	=	Transmission System Operator
UPFC	=	Unified Power Flow Controller
VSC	=	Voltage Source Converter

Chapter 1

Introduction

The Norwegian power system is divided into three different categories. The transmission grid (132-400 kV) operated by the Norwegian transmission system operator (TSO) Statnett, the regional grid (66-132 kV) and the distribution grid (0.23-22kV) both operated by distribution system operators (DSO). The different grid levels have different characteristics but all share some similar traits. Huge parts of the Norwegian power grid is old and require reinvestments to uphold new regulations in voltage quality and safety in the meeting of modern load profiles dominated by electric vehicles, electrical motors and other power demanding applications.

In the distribution grid, it is estimated that one-third of all lines are older than 40 years [6]. The general load profile of a modern home greatly differs from back then until today, with more equipment requiring higher load peaks and introducing other distortions. Examples being the direct start of induction motors, heat pumps, induction cooktops, charging of EVs and power electronics based devices. In a weak distribution grid with long distances and low short circuit capacity, the large load variations can lead to undesirable voltage phenomena such as voltage dips, asymmetry between phases and harmonic disturbances. The DSOs is underlaid the Norwegian regulation of voltage quality (FoL) which introduces requirements and regulations. Besides, the low short circuit capacity (SCC) introduces challenges in implementing proper protection schemes in the network, which is increasingly more difficult as more distributed generation units are dispatched in the grid.

Methods and techniques to improve voltage quality in weak grids as explained above is of great importance for DSOs, as finding cheaper alternatives to large reinvestments in the grid makes it easier to further invest in new technologies which give economical and environmental benefits for the consumers as well as the DSO.

1.1 Scope of Work

In the specialization project conducted the autumn of 2019, test results regarding an actual MVB were acquired from SINTEF, and analysed intending to confirm the validity of the previously established MVB model from [15].

This thesis is a continuation of the named project and evolves with the implementation of a power electronics based series voltage regulator, the Dynamic Voltage Restorer (DVR), enabled for reactive and active power control. The device will be modelled in the simulation software Simulink, and its behaviour in a modelled low voltage distribution grid will be investigated and compared to the existing MVB model which previously has been established. The startup of a 4 kVA induction motor downstream of the modelled devices is used to simulate a taxing dynamic voltage distortion to properly challenge the voltage regulators.

The goal of this project is to investigate on a scientific basis how the two modelled series voltage regulators (the DVR and the MVB) can cope with the dynamics of the induction machine during startup. The regulators' impact in the voltage profile of the modelled distribution grid as a whole will be investigated, with the goal of establishing some general guidelines for which type of regulation devices is the most effective depending on grid topology, $\frac{R}{X}$ factor and short circuit capacity.

1.2 Project Outline

The thesis is split into three parts that focus on different aspects of the theme of voltage regulation in the low voltage distribution grid. In the first part (chapters 1-2), some general characteristics and challenges of the distribution grid are explained. Major parts of the content (chapters 1, 2 and 4) are transported from the specialization project [11] with modifications.

In the second part (chapters 3-6), a modelling approach of the induction motor, the MVB and the DVR will be conducted. Also, the modelling of an actual test grid from the DSO Elvia will be done.

In the third part (chapters 7-9), the simulation results relating the Simulink models of the DVR and the MVB in the appointed grid will be presented. The results are further discussed with a basis in the presented and known theory, before resulting in a conclusion which will give some general guidelines about which regulation technology is the most effective for different network topologies.

Chapter 2

The Distribution Grid - Characteristics and Challenges

The Norwegian distribution grid is the final step of the transmission chain from producer to consumer in the power grid. The main objective of the distribution grid is to distribute electrical power at voltage levels ranging from 22kV (highest voltage) to household voltages of 230-400V. The distribution grid is divided into two parts as seen below and operated by local DSO's. The total length of the Norwegian distribution grid (0.230 - 22kV) is estimated to be around 300.000 km of lines and cables [7].

- **High voltage distribution grid:** Voltages between 1kV and 22kV [7].
- **Low voltage distribution grid:** Voltages between 230V and 1kV. The last step before the consumer.

The Norwegian distribution grid has some fundamental characteristics which imply challenges that have to be faced in order to maintain the security of supply and environment, health and security (EHS). In essence, the most important characteristic (that poses a problem) is that the distribution grid is not built for the load profiles of today, and certainly not for the future [10]. With a significant part of cables being old with high resistance and ageing insulation, the modern trends of more power-demanding applications such as charging electric vehicles, heat pumps, power electronics and induction ovens (to mention a few) introduce new problems to voltage quality with emphasis on flickers, harmonics, asymmetric phases and under/overvoltages [8]. In addition, older grids tend to have a low short circuit capacity (SCC) - which heavily implies that the distribution network in question responds poorly to load changes due to high system impedance, and introduces problems referring to setup of protection schemes. This will be further explained below.

The introduction of more distributed generation (DG) also poses a significant challenge for the current distribution grid [33], but is important for both environmental and economic standpoints. Increased implementation of DG units can pose problems for protection schemes, but also overvoltages as a result of the bidirectional flow of power [30]. The implementation of DG will briefly be explained and discussed in accordance with voltage regulation techniques presented in the thesis.

2.1 Simplified Model

In figure 2.1, a simplified model of a distribution network with one voltage source, one impedance and one load is presented. The load is here representing a common household, the impedance is representing the line and the voltage source is the step-down distribution transformer. It can be seen that by increasing the load in the model, the increased current will lead to higher voltage losses across the lines which will result in U_2 being reduced.

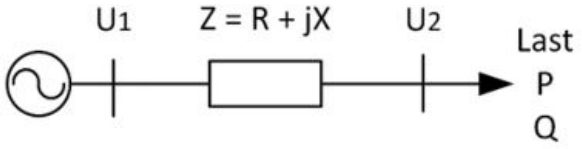

Figure 2.1: Simplified circuit model of distribution network [17].

To derive the expression for the voltage drop of the model above in figure 2.1, Kirchoff's Voltage Law is used to derive the voltage balance of the model.

$$U_1 = U_2 + I \cdot (R + jX) \tag{2.1}$$

$$S = U_1 \cdot I^* = P + jQ \rightarrow I = \frac{P - jQ}{U_1} \tag{2.2}$$

Inserting equation 2.2 into 2.1 and we get 2.3

$$U_1 = U_2 + \frac{(P - jQ)(R + jX)}{U_1} = U_2 + \frac{(P \cdot R + Q \cdot X) + j(X \cdot P - Q \cdot R)}{U_1} \tag{2.3}$$

By setting $\Delta U = U_2 - U_1$ and acknowledging the fact that the angle between the voltage source and the load is very low [35], equation 2.3 compiles to 2.4

$$\Delta U = \frac{P \cdot R + Q \cdot X}{U_1} \tag{2.4}$$

By utilizing standard p.u. notation, $U_1 = 1$ pu since the voltage at the source is assumed ideal. Equation 2.4 then results in equation 2.5.

$$\Delta U = P \cdot R + Q \cdot X \tag{2.5}$$

The voltage drop across the line can in other words be estimated using equation 2.5, and is important for the continuity of this thesis. It should be noted that both active- and reactive powers have a connection with the voltage drop connected to the resistance and reactance of the system impedance, respectively. To minimize the voltage drop, the impedance of the distribution lines should ideally be kept as low as possible [17]. Figure 2.4 visualizes the concept of voltage drop in the lines.

2.2 Network Structure: Radial and Meshed

There are mainly two ways to structurize the electrical grid. Radial, and meshed. Radial grids typically operate through a single supply line, giving a simple layout and ofter easier operation. However, this structure is outdated and offers low selectivity with alternative supply paths during faults. I.e., if a fault occurs right after the fuse/relay in the substation, the whole supply path will be cut off for all the loads connected on that specific feeder [3]. This topology is commonly used in the distribution grid. As can be seen, with no further DG production - the voltage and SCC will be at the very lowest at the farthest end of the line. Figure 2.2 illustrates a simple sketch of a radial layout.

A meshed grid or open-loop structure is a more modern form of grid - with more than one supply alternative for different households, giving greater dependability of power supply for the connected loads. However, the operation is more complicated and designing proper protection schemes with satisfying selectivity is challenging [3]. The HV distribution grid, regional grid and the transmission system should all be as meshed as possible to secure safety of supply [3].

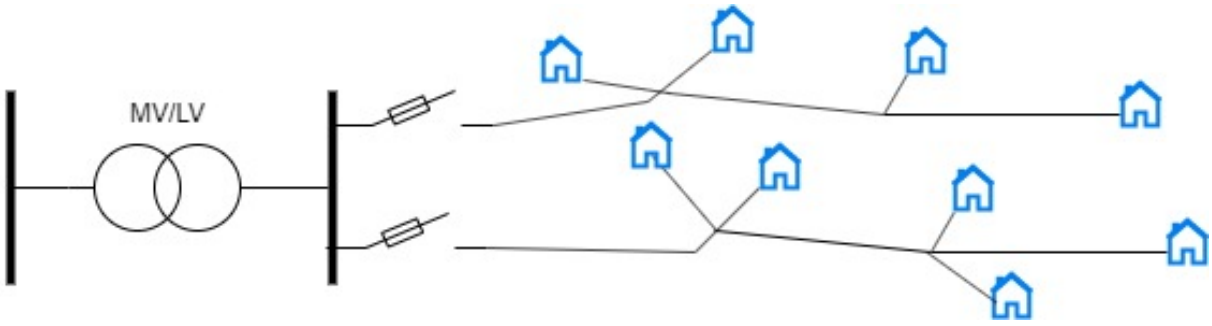

Figure 2.2: Radial structure, typical for older parts of the distribution grid.

2.3 R/X Ratio

As shown above, in the simplified model in figure 2.1 and equation 2.5, the voltage drop over the distribution lines is dependent on both the system resistance and reactance, and the active and reactive powers. In turn, different voltage regulation applications utilize different technologies. Some technologies are better suited for grids with a more reactive impedance/load profile and vice versa. The $\frac{R}{X}$ ratio is calculated by dividing the system resistance with the system reactance and is simply a measurement for the relationship between the resistance and reactance in the network impedance. In general, overhead lines have a lower $\frac{R}{X}$ ratio than cables [20] (but not always), and is reduced with increased cross-section since the inductance of conductors in a three-phase system is heavily dependent on the geometrical mean radius.

With $\frac{R}{X} > 1$ the distribution lines are more resistive, and changes in active power injections influence the voltage response more than a change in reactive power. The opposite is also true, with $\frac{R}{X} < 1$ the changes in reactive power injections will influence the voltage more. In the low voltage distribution grid, the typical $\frac{R}{X}$ ratio of a low voltage distribution grid is in the range of $2 > \frac{R}{X} > 0.5$ [17]. A table with $\frac{R}{X}$ factors for different cables and overhead lines represented in the high and low voltage distribution grids can be seen in figure 9.1 in the Appendix. In a distribution network, the other households/loads which are connected in parallel is neglected for simplicity. The $\frac{R}{X}$ ratio can be a good indication for choosing the correct voltage regulation method [17].

At higher voltage levels, like in the transmission grid, the $\frac{R}{X}$ factor corresponds to the $\frac{X}{R}$ factor, where they are the inverse of each other. The reactance component in transmission lines is usually several times larger than the resistance component due to the increased geometrical mean radius, as well as the length of the lines. Besides, the cross-sectional area of transmission cables is larger, effectively reducing the resistance [12]. Consequently, voltage regulation through reactive power compensation is much more common at higher voltage levels compared to the low voltage distribution grid.

2.4 Short Circuit Capacity

In the low voltage distribution network, the term short circuit capacity (SCC) is of vital importance. NVE defines the SCC as S_k in equation 2.6 [21].

$$S_k = \sqrt{3} U_n I_n = \sqrt{3} \frac{U_n^2}{Z_k} \tag{2.6}$$

Where U_n is the nominal system voltage, and I_k is the short circuit current during a three-phase

symmetrical fault. Using Ohms law and substituting I_k, it can be noted that the systems short circuit impedance Z_k is critical for the size of the SCC. Since the system voltage in the Norwegian grid *mainly* is 230V, the SCC is often denoted as the short circuit current $I_{2k,min}$, the minimum fault current between two phases. In an IT configured network, the two-phased fault current is the minimum fault current than can occur, giving the term additional information regarding the setup of relays and fuses.

The SCC is a general measurement for the stiffness of the network, with a low value making the network less ”stiff” and vice versa. The term ”stiff” refers to the network's ability to counteract and stabilize its voltage after load changes [16]. The SCC is a function of the impedance of the network to the voltage source. The networks impedance increases with the distance to the step-down transformer, implying that nodes/households built at some distance to the transformer are most often exposed to voltage problems. A stiff network has a very static voltage response, with negligible changes. A weak network with low SCC is often associated with voltage problems consisting of e.g. subsequent voltage dips during notable load changes in the system, or asymmetric behaviour between the phases [16]. Using the SCC as a comparison parameter of stiffness between grids of the IT and TN type cannot be done, which will be further explained in the next section.

Another important aspect with the SCC, is the proper installation of protective devices such as overcurrent relays/fuses, ensuring safe disconnection during a fault scenario. If the short circuit current is in the same range as the general load current, problems will arise. E.g., the reference network in the Norwegian distribution grid has a SCC of around 1.1kA while the main fuse of a standard household is usually 63A per phase [16]. The topic of proper protection selectivity during faults will not be investigated in great detail in this project but is very important for both safety and proper operation of the distribution grid. This is especially true with the increased implementation of DG [30].

2.4.1 Reference Values and Fault Current Sizes

In Norway, the majority of the low voltage distribution grid is constructed through an IT configuration. An IT configuration means that all three-phases are grounded through the neutral point, and there is no external neutral conductor [37]. All new constructions of the low voltage distribution grid are today in general built in a TN configuration, with 400V system voltage between phases compared to 230V between phases in an IT configuration. The TN configuration has an additional neutral phase that is used for grounding in the system [16].

The short circuit current in a TN configuration during a fault will naturally be larger than the

short circuit current for the same fault in an IT configuration (i.e., phase-phase, phase-ground). This follows by equation 2.6 above as the voltage is larger. However, the voltage drop during operation of the grid *will still be the same* for both cases - since the connection of a 230V load is between the neutral and phase (TN) or two phases (IT). The system impedance from the fault location will then be equal for both cases, but the short circuit current between two phases will be larger for the TN case due to the increased voltage in the phases [16]. There are some differences between loads connected in a one or three-phase configuration, but the main point is that using the SCC as a comparing parameter between networks of different configurations can be problematic without further groundwork.

A more natural approach for a comparable parameter between both network configurations could be the system impedance, where the main rule of thumb follows: two networks with IT and TN configuration respectively have the same stiffness if the system impedance is equal. For three-phase loads, the IT impedance has to be one-third of the TN impedance for the same stiffness [16]. I.e, if an IT configurated network has voltage problems due to the increased connection of three-phase loads such as electric cars or heat pumps, upgrading from an IT configuration to a TN configuration *with the same conductors* will improve the voltage situation. Upgrading *will not* improve voltage problems caused by one-phase loads [16].

There are no specific reference values that indicate maximum or minimum short circuit currents for different networks, but there are some guidelines and regulations that have to be followed and be kept in mind

- In the "*Regulations on safety when working in and operating electrical installations*" it is stated that an electrical system should be installed such that the probability of harm is minimal for human life and materialistic values [22].
- A normal main fuse installed in Norway has a capacity of 63A. A rule of thumb is that the minimal I_{k2} is 5 times this size, i.e., 315A [17].
- IEC has reference values for system impedance in the distribution grid that ensure that electrical components do not influence the general voltage quality or cause inherent phenomena as voltage flickering. Calculating $I_{k2,min}$ with this value, the current of 1172A is obtained. This value is quite large [16].
- Based on [16] and NVE, it is recommended that the minimal I_{k2} should not be lower than 371A in an IT configuration. With a lower value, the usage of normal equipment can lead to violations of FoL.

Based on [16], it is recommended that the minimal I_{k2} should not be lower than 371A in an IT configuration. With a lower value, the usage of normal equipment can lead to violations of FoL.

With $I_{k2,min} = 371\text{A}$ as lowest current, the corresponding system impedance can be calculated to 0.23Ω using equation 2.7 from [16].

$$I_{k2min} = \frac{c \cdot U_n}{|Z_+ + Z_-|} \tag{2.7}$$

Where $U_n = 230\text{V}$, and $Z_+ = Z_- = R_f + jX_f$ is the impedance in the network with the fault location at a distance from the transformer. The two-phase to ground fault current is the lowest fault current in an IT network.

The value of $Z_{min} = 0.23\Omega$ should be noted. Installing voltage regulation instalments such as series voltage regulators (SVRs) will increase this value, and further reduce the short circuit current.

2.5 Distributed Generation

According to Wikipedia, Distributed Generation (DG) can be defined as electrical generation and storage performed by a variety of small, grid-connected or distribution-system-connected devices called distributed energy resources (DER). DER systems typically use renewable energy sources such as small hydro, solar power, wind power and are characterized by the fact that they are decentralized, inherits a high degree of modularity and rated at 10 MW or less [42].

In the context of this thesis, DG units will mainly consist of small scale photovoltaic (PV) cells connected downstream in radials in the low voltage distribution network. As of 2020, the Norwegian government subsidize the instalment of PV panels for both households and companies, to increase the renewable power generation. PV cells as an energy source are rapidly increasing worldwide, and is purely renewable [9].

The introduction of more renewables through DG is from an environmental perspective is unquestionable positive, however, the effects of installing DG in weak distribution grids can be large, with extra emphasis on voltage quality and protection schemes. Some general advantages with increased DG in distribution systems can be related to improved efficiency of the system, reduced maintenance cost for DSO due to less power through lines, increased renewable production, increased ability to regulate voltage through inverter and storage solutions [30].

2.6 Regulations for Voltage Quality

The operation of the Norwegian power grid is controlled through strict laws and regulations, where one of the more notable regulations is the Regulation for Quality of Delivery (FoL). One

of the objectives of the FoL is to ensure the satisfactory quality of voltage in the system. Every instance that operates or owns electrical equipment connected to the Norwegian power grid is underlaid this regulation. Chapter 3 in this regulation sets requirements and boundaries for several parameters of interest [21]. These boundaries should be noted and are critical for the successful implementation of grid reinvestments.

System Frequency

The TSO is responsible for the frequency of the system. The frequency should normally be in the interval $50\ \text{Hz} \pm 2\%$.

Slow Variations in System Voltage

The DSO is responsible for that the slow variations of the RMS value of the system voltage are inside the boundaries of $U_n \pm 10\%$. This value is measured over a period of 1 minute in the low voltage distribution grid.

Short Over and Undervoltages and Voltage Sags:

There is a maximum number of allowed short over and undervoltages (transients) at any node in the distribution grid. The values from table 2.1 are to be followed. It should be noted that voltage transients that occur as a result of switching breakers, short circuits or necessary switching operations to ensure the proper operation of the system is not covered by this regulation.

Kortvarige overspenninger, kortvarige underspenninger og spenningssprang	***Maksimalt antall tillatt pr. flytende 24-timersperiode***	
	$0{,}23\ \text{kV} \leq U_N \leq 35\ \text{kV}$	$35\ \text{kV} < U_N$
$\Delta U_{\text{stasjonær}} \geq 3\ \%$	24	12
$\Delta U_{\text{maks}} \geq 5\ \%$	24	12

Table 2.1: Maximum allowed short over and undervoltage variations within 24 hours [21].

Voltage Asymmetry:

The DSO is responsible that the voltage asymmetry between the phases is within $\pm 2\%$ measured over 10 minutes.

2.7 Technologies for Voltage Regulation

The fact that voltage problems can occur as a result of poor/old network design has been properly established. To reduce voltage problems there are several alternatives that should be considered. The most obvious solution that usually is the technical most ideal, is to reinvest and rebuild the distribution network in question by investing in cables/overhead lines with larger cross-section or moving the distribution transformer closer to the loads, effectively reducing the system impedance. Looking at reinvesting from a cost-benefit perspective, this is often not the ideal solution for the DSO - and other solutions should be investigated before taking this action. In the following subsections, a number of available technologies will briefly be presented.

2.7.1 On-load Tap Changer

The most common and simple method of controlling the voltage in a distribution network is to vary the transformer ratio in the distribution transformer. Manual tap changing on transformers is an option available on most models, but models in low voltage distribution networks cannot be tap-changed during load. Manual tap changers in the low voltage distribution grids are often installed at the high voltage (HV) side of the transformer (11-22 kV), and can be trinned in several steps (typically $\pm 2x2.5\%$).

Another option is to install an On-Load Tap Changer (OLTC) in the transformer to be able to change the voltage set point during operation based on voltage measurements in the system to prevent over- and undervoltages. Transformers connected to industrial applications or nodes with a high level of power fluctuation usually have such applications installed. See figure 2.4 for an illustration. In the transformers between HV/MV voltages, OLTC is standard - and required such that voltage variations at higher voltage levels do not spread towards the distribution level [35].

As of yet and current knowledge, Helgeland Kraft is the only company which owns a distribution transformer with OLTC technology installed in Norway through the DGnett project yielding very good results [33]. The transformer used in the DGnett project is produced by Norsk Transformator, with Maschinenfabrik Reinhausen delivering the OLTC and control system. Additionally, Hafslund Nett will be conducting an installation of a distribution transformer with OLTC in an ongoing research & development project. Several transformer producers have available products, but the Siemens FitFormer REG is a well tested complete solution.

The switching procedure in the Siemens FITformer can be seen in figure 2.3. The switching consists of activating a bypass by closing a contactor. To make sure that the switch is faultless,

the current flows through the bypass. This implies that any occurrences of unwanted voltage drops/peaks during switching are minimal. After the switching is finished, the bypass is re-opened and deactivated after reaching desirable regulation [36].

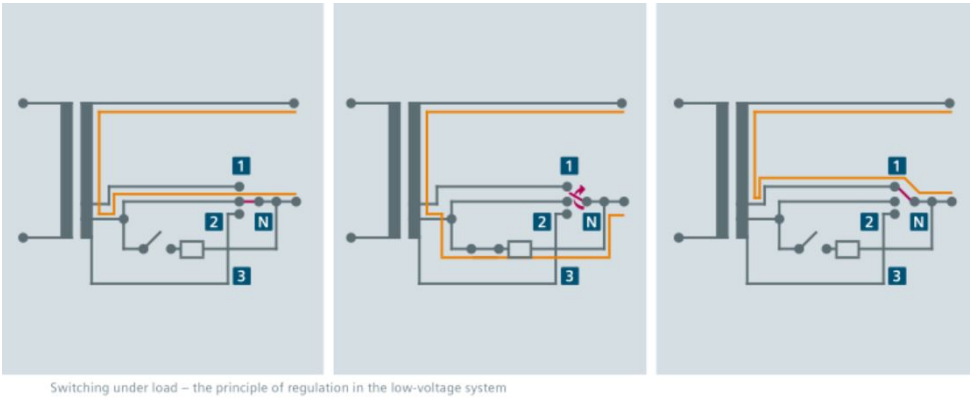

Figure 2.3: Siemens FITformer REG, principle of switching during load [36].

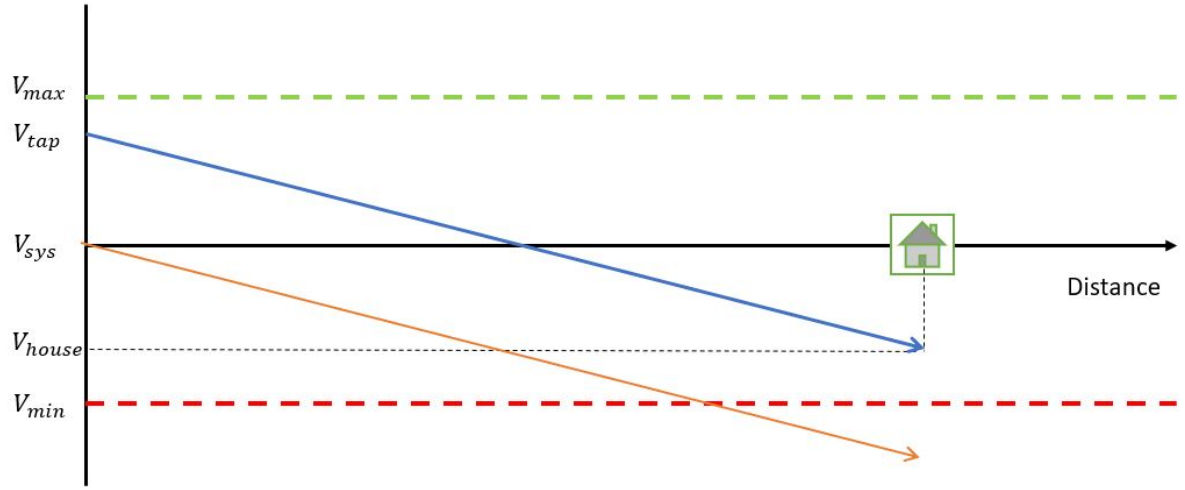

Figure 2.4: Voltage development with trinned voltage at distribution transformer.

2.7.2 Series Voltage Regulation

In general, Series Voltage Regulators (SVRs) functions by implementing a voltage regulation device in series with the load, effectively boosting or reducing the voltage seen as fit. There are mainly two types of series voltage regulators available that work in two fundamentally different ways. Namely the series compensator and the line voltage regulator (LVR). Whereas the series compensator functions by connecting capacitor banks in series with the line to offset the inductive reactance of a line, the LVR decouples the initial line voltage and boosts it through a series-connected transformer solution as can be seen in figure 2.5 below. In short, the LVR can be modelled as a controllable voltage source connected in series with the line, injecting the

missing voltage between the reference and the signal.

In this thesis two SVRs are modelled, where both the MVB and the DVR are variants of the LVR type. Both the MVB and DVR functions in different ways, as the MVB utilizes a magnetic controllable inductor (MCI) to change the inductance of an internal autotransformer, whereas the DVR consists of a Voltage Source Converter (VSC) coupled with an energy storage which can supply active and reactive power without increasing the reactive consumption of the line. A more thorough explanation of the DVR and the modelled MVB will be done in chapters 3 and 4 respectively. Below, a brief explanation of the LVR and series compensation technology will be done.

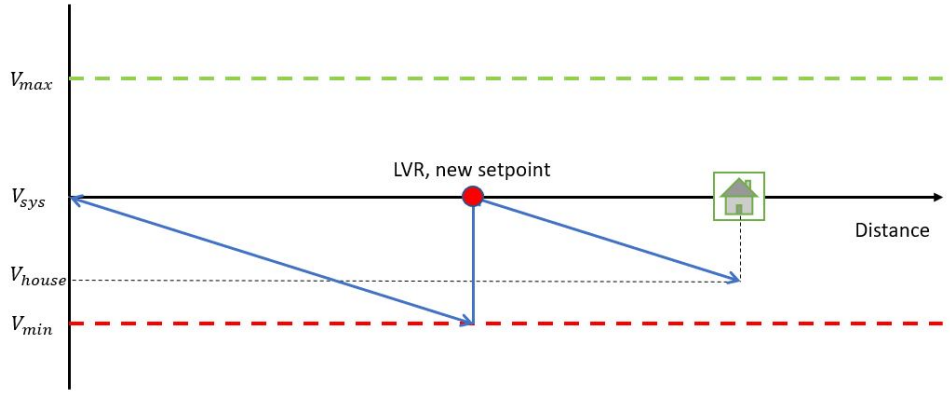

Figure 2.5: Example of voltage development with a LVR.

Line Voltage Regulators

Line Voltage Regulators (LVR) (as illustrated in figure 2.5) decouples the system voltage, and resets it to a new set point according to the instalment [13], or injects the voltage missing between the reference and the measured value at the secondary. There are different LVR technologies, but they all consist of a transformer solution connected in series with the load which can be modelled as a controllable voltage source. The differences between technologies comes down to the method of changing the injected voltage. Figure 2.6 illustrates a basic single line diagram of a LVR.

Different technologies to control the injected voltage of the LVR is used by different companies. I.e., Magtech is using the MCI to seamlessly change the inductance of an integrated autotransformer [24], while other manufacturers utilize power electronics, transformer cascades or separate tap changers to change the output voltage. Some basic single line diagrams of these technologies are illustrated in figure 2.7 [13].

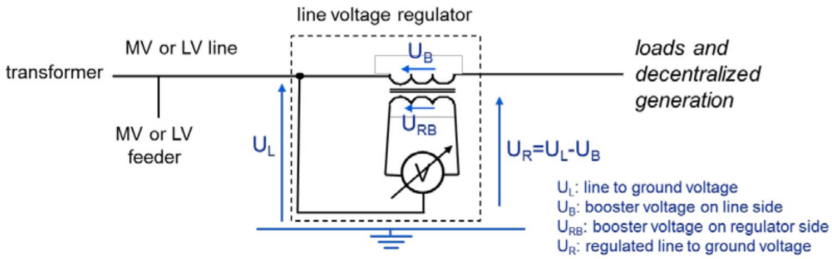

Figure 2.6: Single line diagram of a standard LVR regulator [13].

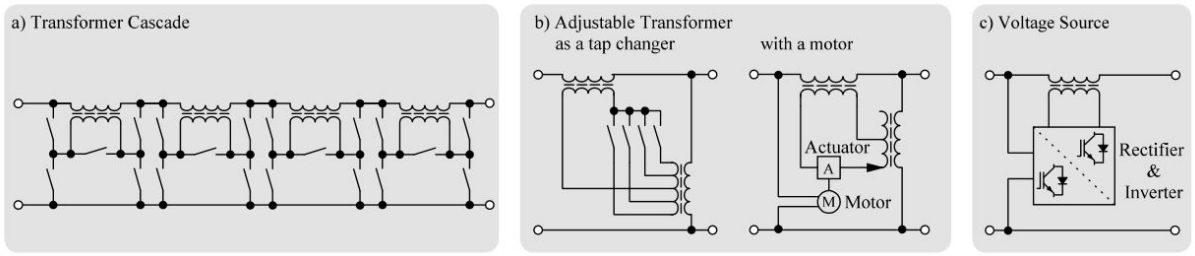

Figure 2.7: Different LVR technologies [13].

Adjusting inductance through tap changing is one of the more common solutions, with ABB and a-eberle marketing solutions which utilizes this technology in some way [1]. Smart switching through thyristor controlling or other measures can be used to seamlessly change the voltage. However, the downside of using switching technology is moving parts and increased wear & tear in the installations [13]. It should be noted that installations like LVRs can be used as an alternative to reinvesting in grids in sparsely populated areas in the countryside. Having robust installations with low maintenance costs are a huge advantage for the operator.

Series Compensation

Series impedance compensation is done by connecting capacitors in series with the line, and is a common technique to offset the inductive reactance of the line in question to minimize power losses. According to [23], the inductive reactance of a transmission line is compensated to between 25 - 70% whereas full 100% compensation makes the line flows extremely sensitive to changes in angle, and the risk of harmonic resonance occurring at the line increases. The use of impedance compensation through series connecting of capacitors are mainly used in the transmission system [5]. The working principle is briefly explained below.

Assume an ideal power line with a series inductance X_L. The series capacitor X_c is connected at the midpoint of the line according to 2.8. Then the active power transfer across the line and series reactance is given by equations 2.8 - 2.9.

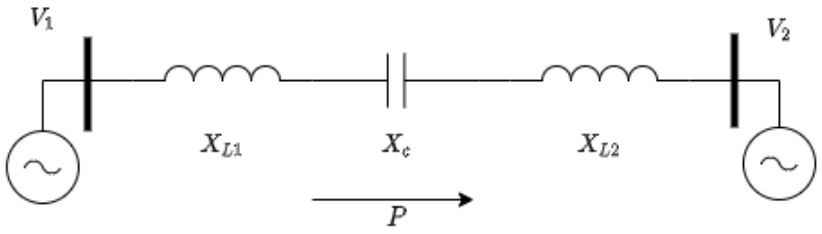

Figure 2.8: Simple transmission line model.

$$P = \frac{V_1 V_2}{X} \sin \delta \tag{2.8}$$

$$X = X_L - X_c = X_{L1} + X_{L2} - X_c \tag{2.9}$$

Substituting 2.9 into 2.8 results into 2.10.

$$P = \frac{V_1 V_2}{X_L - X_c} \sin \delta \tag{2.10}$$

Where

- P is the active power transferred per phase
- V_1 and V_2 is the sending and receiving end voltages respectively
- X_L is the series inductive reactance of the line per phase
- X_c is the series capacitive reactance of the capacitor bank per phase
- δ is the phase angle between V_1 and V_2

It should then be observed that by varying X_c the total reactance of the line can be increased or decreased, enabling for greater values of power transfer. X_c can be varied by changing the number of capacitor banks connected through smart switching according to needs.

Series compensation is a great tool to enhance system stability, but also introduces problems regarding sub-synchronous resonance, instalment of distance relays and potential high voltages across any breakers. These are moments that will not be regarded any further in this thesis.

2.7.3 Shunt Compensation

The usage of shunt compensation methods through shunt-connected reactors and capacitor banks are widespread, and an absolute necessity at higher voltage levels to maintain the high

power factor and compensate for reactive consumption or production of power in transmission cables [23]. This is often done through Flexible AC Transimssion System (FACTS) technology. The idea of connecting a capacitor or inductor in parallel with a transmission line is to compensate for an either inductive or capacitive power factor in the system, maximizing the transmission of active power. By shunt connecting a capacitor, the capacitor bank will supply reactive power and thus increasing the voltage. Vice versa, the shunt reactor will consume reactive power, thus lowering the voltage. Reactors are often installed in high voltage distribution systems with high variations in generation and load due to DG. Installing separate capacitor banks and reactors for shunt compensation in the distribution grid is often associated with static switching and small scale of controllability [30], however, newer installations are depending more on implementation of power electronics - and gives greater controllability and performance.

In the following, the ideal derivation of the working method of shunt compensation is to be explained.

Consider a no-loss line with set impedance $Z = jX$ and the voltage at both ends is the same $V_s = V_r = V$ as in figure 2.9.

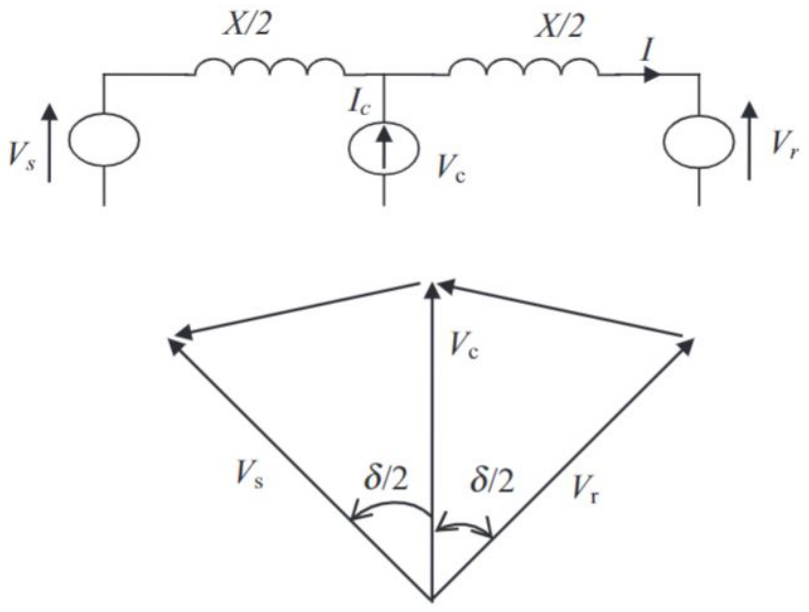

Figure 2.9: Lossless line with equal voltage [41].

Due to the reactance of the line, there will be a phase lag between the voltages δ. Thus V_r, V_s and I can be derived as in equations 2.11 - 2.13.

$$V_s = V\cos\frac{\delta}{2} + jV\sin\frac{\delta}{2} \tag{2.11}$$

$$V_r = V\cos\frac{\delta}{2} - jV\sin\frac{\delta}{2} \tag{2.12}$$

$$I = \frac{V_s - V_r}{jX} = \frac{2V\sin\frac{\delta}{2}}{X} \tag{2.13}$$

Since the line has $R = 0$ there are no real losses in the line, meaning the active power P is equal at any point of the line. The reactive power at the sending end has to be the opposite of the reactive power at the receiving end due to the phase shift. This gives the following equations 2.14 - 2.15.

$$P_s = P_r = P = \Re(V)\cdot I = V\cos(\frac{\delta}{2})\cdot\frac{2V\sin(\frac{\delta}{2})}{X} = 2\frac{V^2}{X}\sin(\frac{\delta}{2}) \tag{2.14}$$

$$Q_s = -Q_r = Q = \Im(V)\cdot I = V\sin(\frac{\delta}{2})\cdot\frac{2V\sin(\frac{\delta}{2})}{X} = 4\frac{V^2}{X}(1-\cos(\frac{\delta}{2})) \tag{2.15}$$

Equation 2.14 is the transmitted active power in the line, while equation 2.15 is the injected reactive power from the midpoint shunt compensator. It can be noted that the maximum active power possible to transmit equals $2\frac{V^2}{X}$ and happens when $\delta = 90°$. The shunt compensator then has to inject $4\frac{V^2}{X}$ of reactive power. The shunt compensator will then inject or consume reactive power based on the power factor of the system.

The general working method of shunt compensation is briefly explained above by [41], but it is important to note the fact that the shunt compensator injects or consumes reactive power. The effectiveness of voltage regulation by reactive power compensation is quite dependent on the topology of the network, i.e., the $\frac{R}{X}$ factor, and not necessary the best solution for the standard low voltage distribution network.

2.7.4 FACTS

According to Machowski [23], the main control actions in a power system have traditionally been utilized by the means of mechanical devices like tap changing transformers and switching capacitors/inductors. FACTS devices are power electronic based devices that enable fast, robust and accurate control of voltage variation through i.e., consumption and injection of active and reactive powers. Nearly all FACTS devices have a power converter consisting of semiconductors such as thyristors, whereas one of the more common converter types are the VSC.

Different types of FACTS devices exist, and they can be connected both in series and shunt based on the need. Examples of shunt-connected FACTS devices are braking resistors and reactive power compensators. Examples of series-connected FACTS devices are series compensators, power controllers and phase angle regulators [23]. Below, a few well-known devices will be briefly explained. The modelled DVR in this project is a variant of a series connected FACTS device and is similar to the Static Synchronous Series Compensator (SSSC) and the Static Synchronous Compensator (STATCOM).

Static VAR Compensator

The Static VAR Compensator (SVC) is a shunt compensation device that can be found in several different configurations, but are in general made up of thyristor controlled reactors (TCR), thyristor switched capacitors (TSC) and Fixed Capacitors (FC) [23]. Examples of a few configurations can be seen in figure 2.10. Through the operation of the SVC with power electronics, a flexible and continuous reactive power compensation scheme can be established that operates in both the inductive and capacitive regions. The operation is seamless, and is highly effective in terms of improving voltage quality in transmission grids at higher voltage levels, but also to improve voltages at industrial loads [23].

In the Norwegian distribution grid, the SVC is not used at lower voltage levels. A leading reason is probably connected to cost, and distribution grids with mostly $\frac{R}{X} > 1$ where reactive compensation is not as effective as other methods. The SVC is however much more common at higher voltage levels. In other countries, the SVC is more commonly seen in lower voltage distribution grids [39].

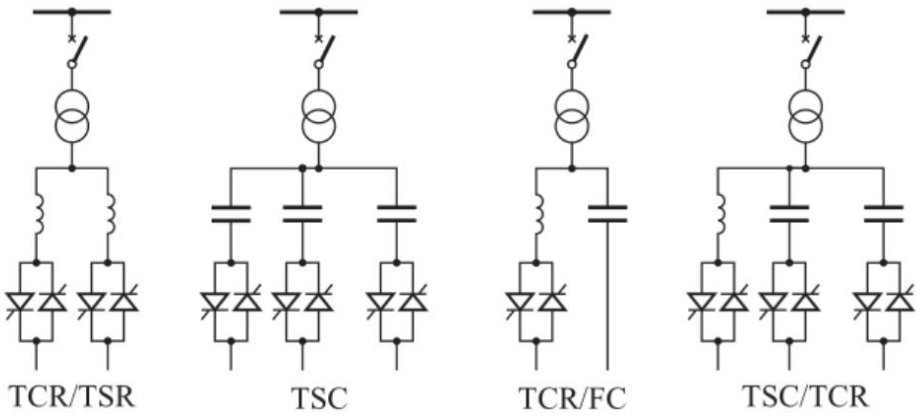

Figure 2.10: Different types of SVCs [23].

Static Compensator

The STATCOM is another FACTS device that is similar to the SVC in many ways, but instead of being thyristor controlled, the STATCOM utilizes the VSC. The STATCOM incorporates a very high content of power electronics, but the other components mainly consist of a transformer and a capacitor [23]. See figure 2.11a for a simple model. The VSC is equipped with a pulse-width modulation (PWM) controller which controls the AC voltage delivered by the VSC, by changing the control parameters m and ψ as given by equation 2.16. The transformer has a reactance X, and the resulting voltage V_{AC} from the VSC influences a change of alternating current across the transformer I_{AC} as given in equation 2.17 [23].

$$V_{AC} = mkV_{DC}(cos\psi + jcos\psi) \tag{2.16}$$

$$I_{AC} = \frac{(V_i - V_{AC})}{jX} \tag{2.17}$$

Since the impedance in I_{AC} is purely reactive, the flow of current is controlled by the size of the voltage produced by the VSC. I.e., if $V_{AC} > V_i$, the STATCOM will deliver reactive power to the busbar and vice versa. The AVR is regulating the sizes of m and ψ according to the bus voltage.

In general, the STATCOM cannot deliver active power to the system, but by installing an energy storage system in parallel with the capacitor, this enables the STATCOM to consume and inject active power in addition to reactive compensation. This solution is also known as a Battery Energy Storage System (BESS) [23]. Figure 2.11b illustrates a simple model of the STATCOM/BESS with energy storage.

The modelled DVR in this thesis is similar to other FACTS devices like the STATCOM by its general design. The latter, however, is connected in shunt with the subjected distribution line/load, and where the DVR is injecting a voltage in series with the load, the STATCOM is injecting a controllable shunt current. The difference of series and shunt connection makes a difference during greater voltage sags and outages (i.e., short circuits upstream in the grid). According to [19] the DVR is more robust during greater voltage sags than the STATCOM, giving cleaner voltage sags with less harmonics and noise. Both the DVR and the STATCOM can support with active power if there is an energy storage element available.

PCS and AVR are acronyms for Power Converter System and Automatic Voltage Regulator, respectively.

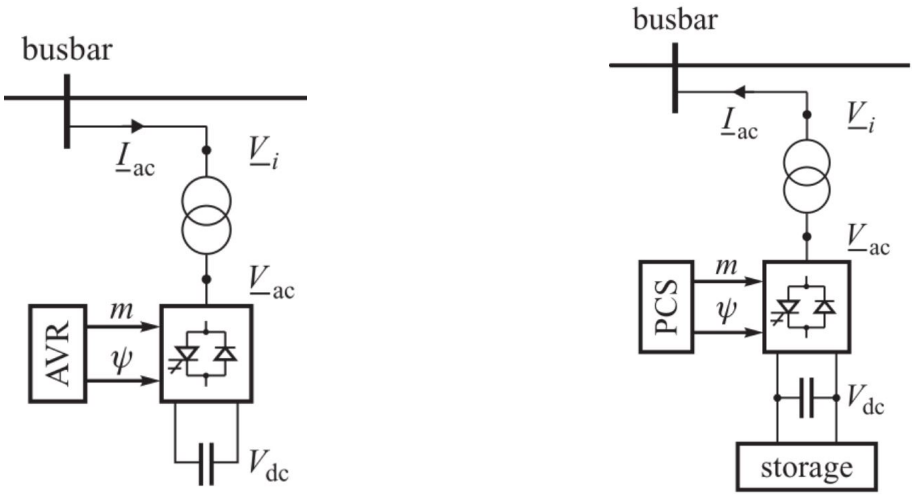

(a) General model of a STATCOM.

(b) STATCOM with connected storage system for active power regulation (BESS).

Figure 2.11: Simple models of a STATCOM and a BESS [23].

Static Synchronous Series Compensator (SSSC)

The SSSC, in essence, is very similar to the STATCOM, and is often referred to as the series STATCOM [23]. The AC voltage is generated by a VSC interconnected with a regular DC link. The control of the SSSC is done by PWM by the parameters ψ and m in a similar manner as above. The converter operates as a voltage source and is directly feeding the transmission link through the transformer [23]. A general one-line diagram is shown in figure 2.12. ST is short for series-transformer.

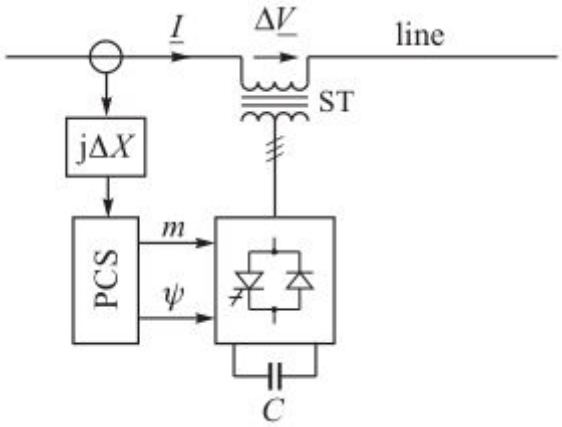

Figure 2.12: One-line diagram of the SSSC. [23]

Unified Power Flow Controller (UPFC)

The equivalent circuit as well as a one-line diagram of the UPFC can be found in figure 2.13. The UPFC is divided into two parts, one series and one shunt-connected. The shunt part is

similar to a STATCOM, while the series part functions as a SSSC which is briefly described above. The power converters are of the VSC type and are back-to-back connected through a regular DC link. Through different control methods the UPFC enables three important functions (the following is directly from [23]):

- Control of real power flows by adjusting the quadrature component of the booster voltage in the series part.
- Control of reactive power flows by adjusting the direct component of the booster voltage in the series part.
- Control of the voltage V_i in the connection node by controlling the reactive current supplied by the network to the shunt part.

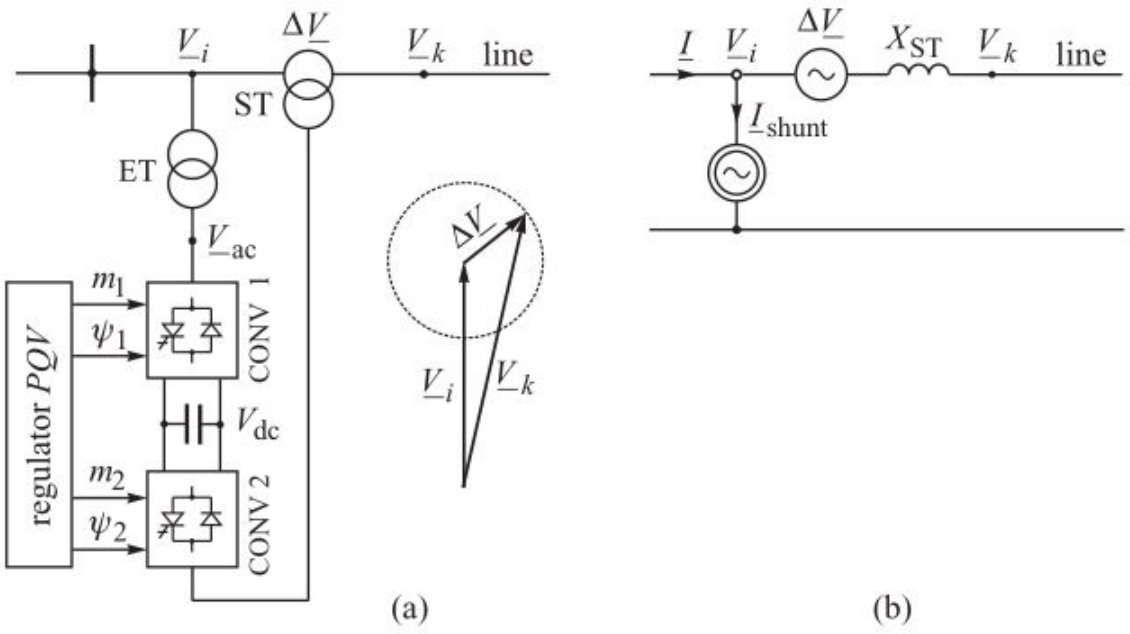

Figure 2.13: The UPFC; a) functional diagram and b) equivalent circuit from [23].

2.7.5 Distributed Generation

From sections 2.3 and 2.1, it is already established that distribution grids usually have $\frac{R}{X}$ between 2 and 0.5, giving that changes in active power injection in the system *mainly* will affect the system voltage the most according to equation 2.5. The motivations for a private instance to invest in PV cells are often economical, therefore the PV cells are set to produce active power at unity power factor, in turn heavily influencing the voltage in the distribution network [30]. In Norway, the power generated is coincidentally at the highest during the time of the year where

the loads are lowest (during the summer), and the production is at its lowest when the loads are the largest (during the winter). The corresponding voltage change ΔU can be expressed with equation 2.18 (which is identical to 2.5) [25]. Q_g and P_g is the reactive and active power generated, whereas P_l and Q_l is the active and reactive loads.

$$\Delta U = R \cdot (P_l - P_g) + X \cdot (\pm Q_l - Q_g) \tag{2.18}$$

Neglecting reactive power production/generation, the voltage drop over the line will be negative when $P_g > P_l$, simply implying that the DG application is increasing the system voltage since the generation is greater than the load. Depending on the network impedance, the PV cells have to reduce its production capacity which is not desirable from an economic or environmental perspective during hours of high production and low load [25]. This is especially true in weak grids with a high system impedance. For grids with a $\frac{R}{X}$ ratio close to 1, inverters in the DG installation can contribute to nullifying the voltage increase due to active power injection by consuming reactive power [20].

The scenarios stated above are of the worst case, and in normal situations in the average grid, the installed DG often contributes to maintaining acceptable voltage levels, ensuring that when sudden load changes arise - the FoL regulations are upheld. I.e, if a voltage dip should arise as a result of a sudden load change downstream in the system, the DG may prevent the voltage from violating the -10% barrier of the system voltage as figure 2.14 illustrates.

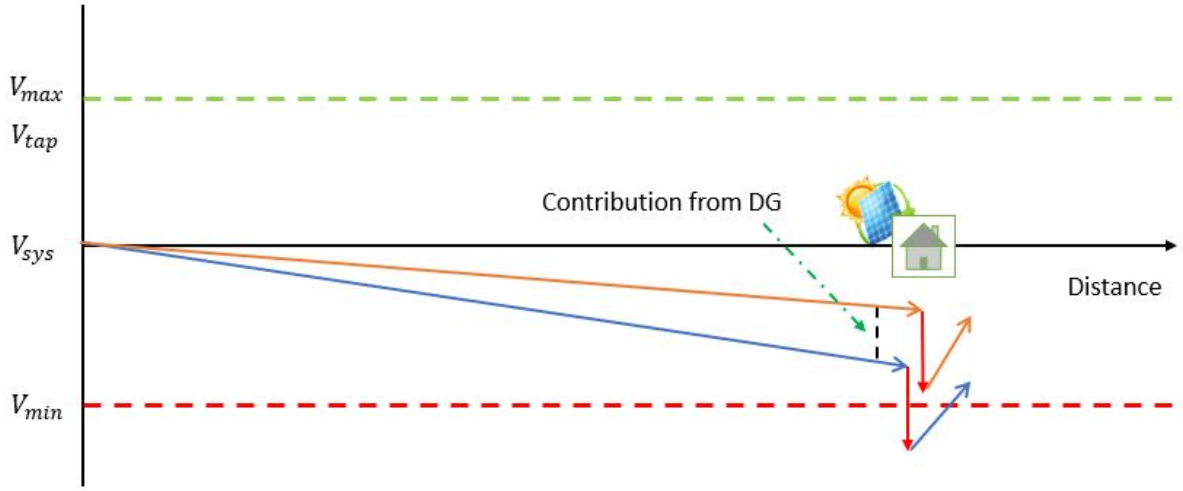

Figure 2.14: Simplified illustration of how DG can contribute to the system voltage.

However, as mentioned earlier - DG units based on PV cells are highly fluctuating, and should therefore not be used as a primary solution for voltage regulation. DG units are installed privately, making it challenging to adjust the power factor of the inverters in the system [17].

Utilizing Energy Storage such as lithium batteries to inject active and reactive power and storing excess energy from DG units is technically a viable option, but practically not realistic as of today due to ownership regulations of batteries [17]. It should also be noted that in the low voltage distribution grid, the $\frac{R}{X}$ ratio is usually larger than 1. Inverter based solutions such as DG and energy storage can always consume reactive power, but can only inject active power to increase the voltage as long as the production or storage capacity allows it [17]. In networks with $\frac{R}{X}$ around 1 to 0.5, installing simple shunt reactors for voltage control is a very viable option that is used several places in grids internationally [30] with a high degree of implemented DG.

2.7.6 Consequences for SCC

Series Voltage Regulators

The instalment of series voltage regulators, especially of the LVR type will affect the SCC of the network. This is especially true if the network is based on an IT scheme [16]. Some LVRs can contribute to the SCC if the network is of the TN type. I.e., the TN models of the MVB has this functionality as stated in [24]. In general, since almost all new instalments of TN networks in Norway is of newer date, it should be appropriate to assume that SVRs will mainly be installed in IT grids.

As mentioned in section 2.4, the lowest possible $I_{k2,min}$ an IT network should have is around 371A, which gives a system impedance of 0.23Ω. Installing different LVRs gives an additional impedance in series, potentially decreasing this current. Some applications like the MVB has a bypass function that activates during a fault on the secondary side. This function can be seen in figure 4.1.

It's a bit challenging to acquire the correct series impedance of different SVRs since the series impedance will vary according to the degree of voltage boosting and load. In [17], the additional impedance of the MVB was estimated to be between $0.16 - 0.31\Omega$ depending on the total $\frac{R}{X}$ ratio of the network and the booster. Installing the MVB in a grid with 0.23Ω system impedance, the $I_{k2,min}$ will be reduced from 371A to 295-213A. .

Distributed Generation

The instalment of DG units such as PV cells without energy storage solutions is challenging for DSOs, since the traditional power flow in radial distribution systems is compromised, with situations where some households produce power to the grid. Neglecting the problems with

overvoltages as explained above, the real contribution to the voltage is the increased set point.

The voltage consequences have been properly explained earlier, however, from the perspective of existing protection schemes, DG units with and without energy storage solutions can drastically affect the $I_{k2,min}$ [30]. In section 2.4, it was stated that the $I_{k2,min}$ varied as a function of the system voltage and the system impedance of the grid. The combination of distribution networks with DG creates situations where the $I_{k2,min}$ will differ greatly as a function of the production of the DG. The higher the local production and capacity of DG is, the bigger the change. This can contribute to problematic situations with the tuning of overcurrent relays, effectively leading to false trips or no trips at all during faults [30].

I.e, in a situation at the end of a long line with three households in close proximity where all have installed DG as in figure 2.15. With one fault at one of the households, the $I_{k2,min}$ flowing in the line and in the fault will vary according to the production of DG [30]. If the fault happens during full production in a weak grid, the possibility of the DG units feeding the fault, and increasing the set voltage at the node at the end of the line - can lead to the relay at the substation not tripping as it should. More extensive protection schemes should be applied in such systems [30].

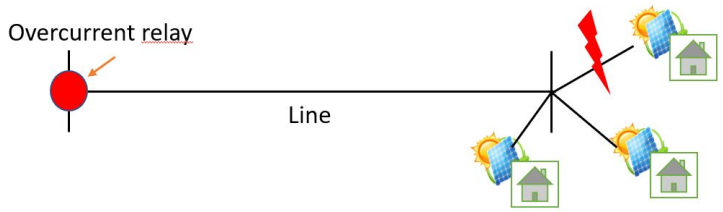

Figure 2.15: Example of a fault at one household in an area with DG production.

Chapter 3

Dynamic Voltage Restorer

The principle of the DVR is similarly to the MVB a transformer installation connected in series with the appointed load. The DVR is, however, utilizing the VSC coupled with an energy storage device to be able to inject active power in addition to reactive power. The installation is used in different scenarios at different voltage levels in the world but is currently not significantly utilized in the Norwegian low voltage distribution system. The DVR shares several similarities to the FACTS devices SSST, the STATCOM and the UPFC. An illustrative one-line diagram for a proposed DVR installation is found in figure 3.1 below.

According to [31] the DVR consists of 7 fundamental elements which is listed in table 3.1 below. A brief explanation of the elements listed will be done later in this chapter.

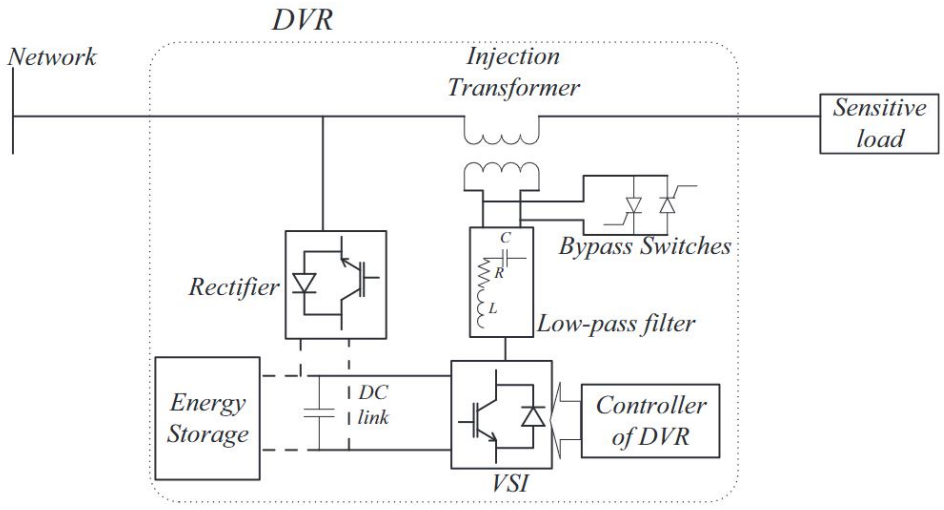

Figure 3.1: Illustrative one line diagram of DVR [38].

Element	Main Function
Energy Storage	Source of real power
DC-link Capacitor	Stabilizing voltage
Power Converter	Converting between AC/DC
Filter	Filtering harmonics
Injection Transformer	Minimize converter rating
Bypass Equipment	Bypass large currents during faults or contingencies
Disconnection Equipment	Disconnecting DVR from grid

Table 3.1: Fundamental elements of the DVR and their main function.

3.1 Technology and Working Principle

In this section, the working principle and fundamental technology of the general DVR model is explained. Like other FACTS devices the DVR is equipped with a power converter (i.e., the VSC) on the secondary side of the power transformer. The DVR utilizes voltage measurements downstream of the device to control the stream of reactive power, as well as active power if there is an energy source on the DC side of the power converter. DC energy sources that are applicable for utilization could be batteries, super capacitors and flywheels to name a few [2]. The converter is controlled through a PI controller utilizing PWM. Since the DVR is regulating by utilizing power electronics, the regulation is both fast and accurate. However, these abilities comes at a cost since devices based on these technologies are often more expensive than cheaper solutions, such as the MVB.

3.1.1 Circuit Model and Phasor Diagram

As a SVR of the LVR type, the DVR can be modelled as a variable or controllable voltage source connected in series with the load, and functions by injecting a voltage ΔV supported by a power converter coupled with a capacitor and energy storage for reactive and active control. Figure 3.2 illustrates how the voltage can be modelled in series.
Where

- V_s is the source voltage (primary of DVR)
- V_L is the voltage at the load (secondary of DVR)
- V_{DVR} is generated voltage by VSC, ΔV is the total injected voltage by the DVR.

Assuming that ΔV can be expressed as $\Delta V = ZI$ then the voltage balance is given by equation 3.1 and V_L is further given by equation 3.3 below

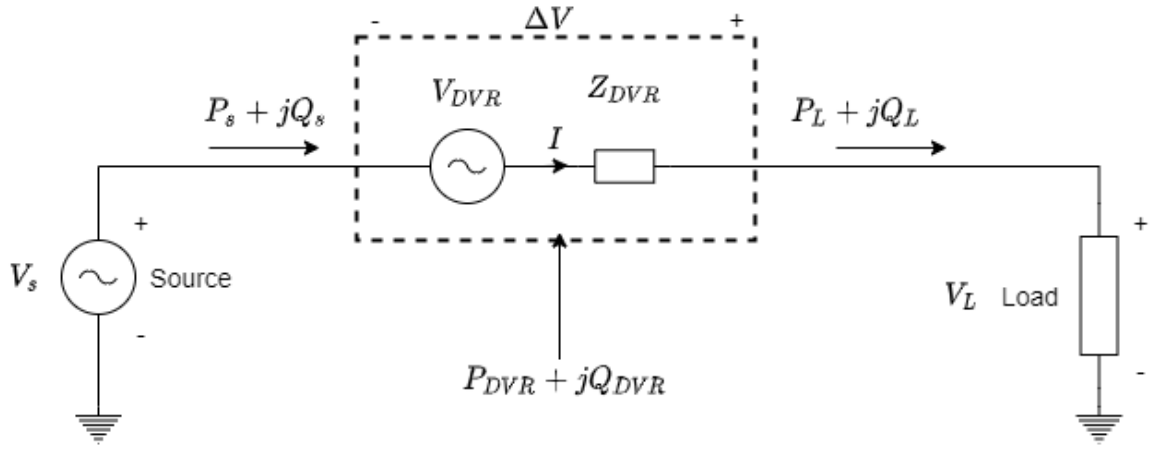

Figure 3.2: Example circuit of the DVR implementation.

$$-V_s - \Delta V + V_L = 0 \tag{3.1}$$

$$V_L = V_s + \Delta V \tag{3.2}$$

$$V_L = V_S + ZI \tag{3.3}$$

According to equation 3.3 the magnitude and phase of the voltage injected by the DVR can be varied by controlling the current in the circuit. A simplified phasor diagram for the circuit above in figure 3.2 can be seen in figure 3.3 below, which illustrates the basic fundamental principle of the device. A series connected device that only offers reactive compensation will have the same phasor diagram, but the injected voltage ΔV will then always be injected $90°$ according to the source voltage. To control the voltage to 1 pu, this effectively means that devices purely based on reactive compensation consumes more reactive power than a device which can support both reactive and active power.

According to the equations and the phasor diagram, it's important to note that as long as the injected voltage ΔV is in quadrature with the load current, the voltage can be corrected by measures of reactive power. However, the size of voltage sag being corrected by this method is limited to some method which is based on the nature of the load. At some point (size of sag), active power is needed to fully recover the voltage.

Operation Schemes

As briefly explained in the previous section with the phasor diagram, the correct control of the DVR is critical to the stability of the application. During a sag event, the response of the DVR can vary according to which voltage injection method is utilized. Since the goal of the DVR is

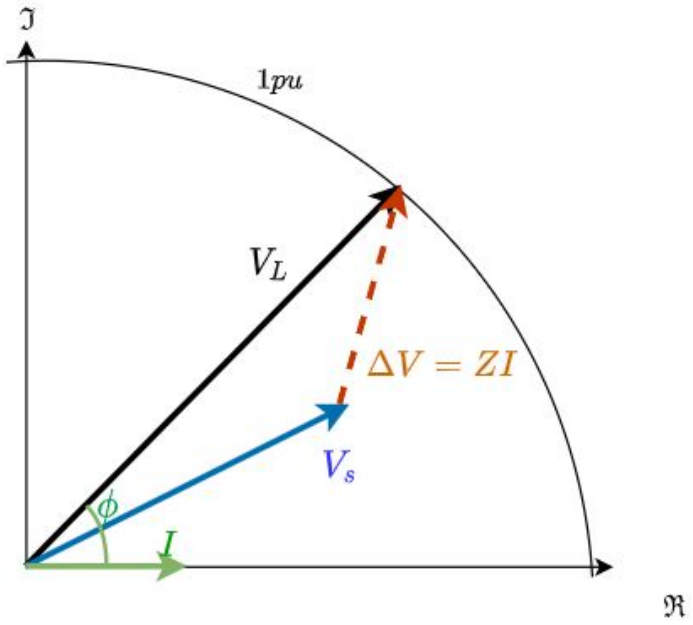

Figure 3.3: Simplified phasor diagram of a proposed SVR.

to restore the voltage on its secondary to 1 pu during a sag event, controlling the magnitude and power factor of the injected power can be done in several ways depending on different factors of the voltage sag. I.e., different load conditions, different type of voltage sags and varying power factor to mention a few. According to literature [34], there are mainly two main operation schemes controlling the injection of compensation voltage;

- **Pre-Sag Compensation:** during this control method, the DVR is continuously tracking the supply voltage during normal operating conditions. During a voltage sag event, the DVR injects the necessary active and reactive power to restore the voltage to its pre-sag conditions, meaning that both the voltage angle and magnitude will be recovered to its initial state. The amount of reactive and active power cannot be controlled and is fixed based on the measurements. The general representative phasor diagram for this situation can be found in figure 3.4b [34].

- **In-Phase Compensation:** during this control method, the DVR is functioning independently of the load current and pre-fault voltage. This means that the injected voltage will be in phase with the supply voltage, controlling the injection of active and reactive power accordingly. Phasor diagram for this situation can be found in figure 3.4a [34], and is the scheme which will be utilized in this thesis. The biggest downside of this method is the inability to correct the phase jump during a sag event, such as an induction motor start, but is significantly easier to model.

In figure 3.4, V_{grid} and V_{load} corresponds to the primary and secondary terminal voltages of the DVR. I_{load} is the load current and V'_{DVR} is the injected voltage by the DVR. δ is the phase shift

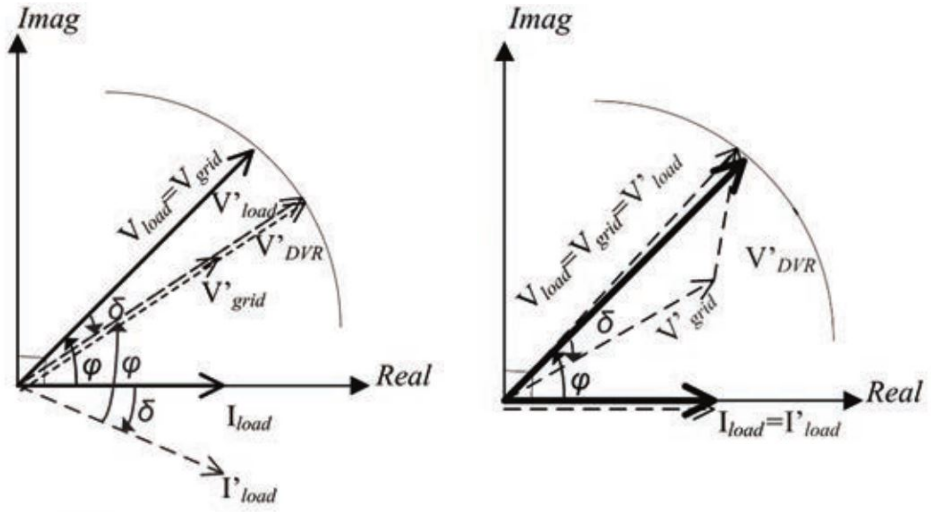

(a) In-phase compensation. **(b)** Presag-compensation.

Figure 3.4: Phasor diagrams for presag and in-phase compensation [34]

during the sag event, and ϕ is the phase displacement between the voltage and current. The prefix $'$ means the parameter after the sag event. I.e., V_{grid} and V'_{grid} corresponds to the voltage pre and post sag.

3.1.2 Fundamental Elements

Power Converter

There are several different designs of Power Converters available. In the modelled DVR a three-phase, three bridge, 6 pulse (two-level) VSC is utilized. The VSC can change the output frequency, magnitude and phase of the output signal based on the control scheme and is broadly used in FACTS applications. The basic outline of a 6 pulse VSC is found in figure 3.5. There are several different switching methods in the inverter, here one of the more suitable types are the Integrated Gate-Commutated Thyristor (IGCT) which offers low cost and snubberless operation [34]. The more important requirements of the installed power converter is high efficiency, high reliability and inherent safety [31].

Energy Storage

The coupled energy storage has one primary function, which is to deliver active power compensation to the DVR. As seen in the phasor diagram in 3.3, when the injected voltage also consists of active power - the voltage regulation control can be simplified since injected voltage based on purely reactive compensation is always injected $90°$ in phase. There are several types of potential energy storage solutions that can be coupled with the DVR such as flywheels, fuel cells and super capacitors. However, more common solutions are batteries based on lead-acid

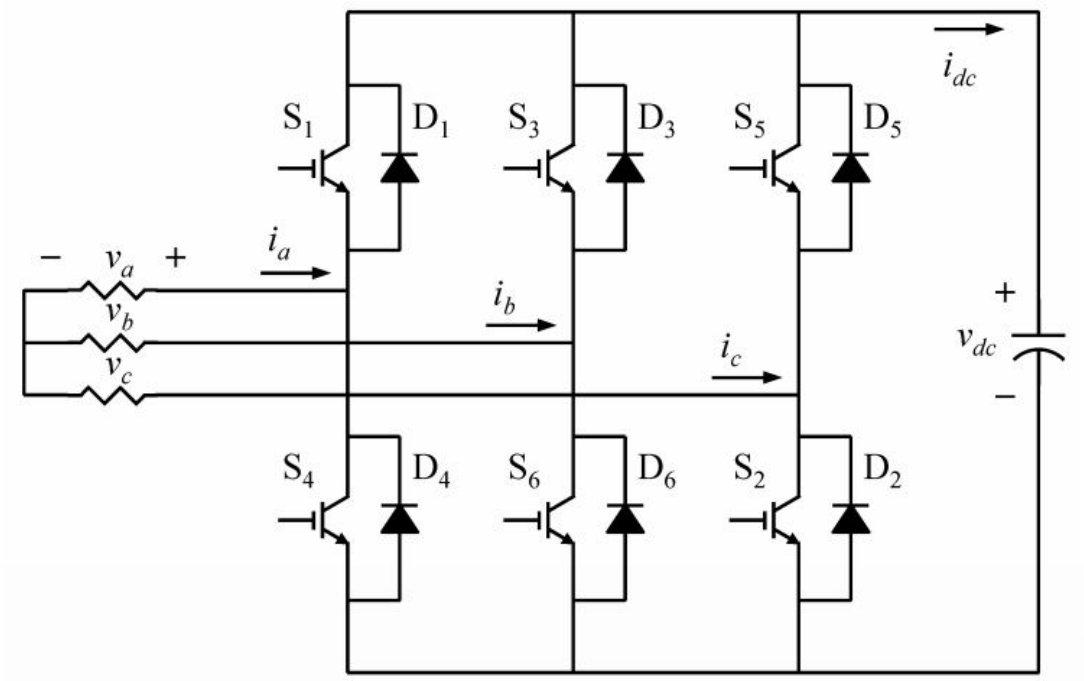

Figure 3.5: Illustrative one-line diagram of a 6 pulse VSC [29].

and lithium-ion technology [31].

There are some downsides with DVRs coupled with an active power source. One of the more important is the cost of batteries, as well as the compensation ability which will decay over time with the current technology of batteries. Besides, the matter of battery capacity should always be kept in mind as the battery has to be charged to sustain the ability to inject active power when needed. This usually happens at times of low load, but introduces a discussion about the capacity of the battery, as well as the operation scheme of the DVR and the topology of the grid itself.

Filter

The main function of the implemented filters is to decrease the amount of notable harmonics in the output signals which can cause overvoltages or cause other problems in the grid. The filter installations can be connected on both the DC side as well as the AC side - on both the HV and LV side of the injection transformers, both options having some advantages and disadvantages. In general, the installation of filters is a very customized process in regards to the actual grid, according to [31], but by installing the filter on the ”line” side of the injection transformer, the filtering does not affect the control system of the DVR. Besides, the leakage reactance of the transformer can be used as a filter inductor and is located further away from the source of the harmonics.

Injection Transformer

The injection transformer is mainly installed to minimize the voltage rating of the converter and the energy storage. However, the transformer also functions as galvanic isolation of the device which is an advantage, should faults occur in the system. At lower voltage levels, the injection transformer is not a necessity, and by removing this element - the costs can be reduced in addition to the increased system impedance of the device.

Bypass and Disconnection Equipment

The bypass and disconnection equipment are in essence smart switches which can isolate the DVR during faults and are connected in series or parallel respectively. I.e., when the DVR is in a state of no operation - the bypass switch can be closed but can be opened on short notice if sudden sags or swells should occur. In addition, the switch can be closed during faults on the line, increasing the short circuit current of the system since the series impedance of the injection transformer will be removed [31].

3.1.3 Control Scheme

In figure 3.6 a one-line diagram of the modelled DVR is illustrated. The voltage is measured at the secondary side of the transformer and relayed to the 3P Sequence Analyzer. The sequence analyzer is outputting the phase sequence components of the voltage signal such as the magnitude and phase. The magnitude of the measured signals is subtracted from the V_{ref} value set to 230V before the PI controller which then outputs the corrected signal to the implemented phase modulator (as represented in figure 9.14 in the Appendix), which offsets the signal according to each phase with $120°$. The signal is then output to the 6 pulse PWM generator. The control strategy is based on the in-phase compensation technique as explained in the previous section. A screenshot of the model can be seen in figures 9.12 and 9.13 in the Appendix, and is inspired by [19]. A short introduction of the different main elements of the control loop is done below.

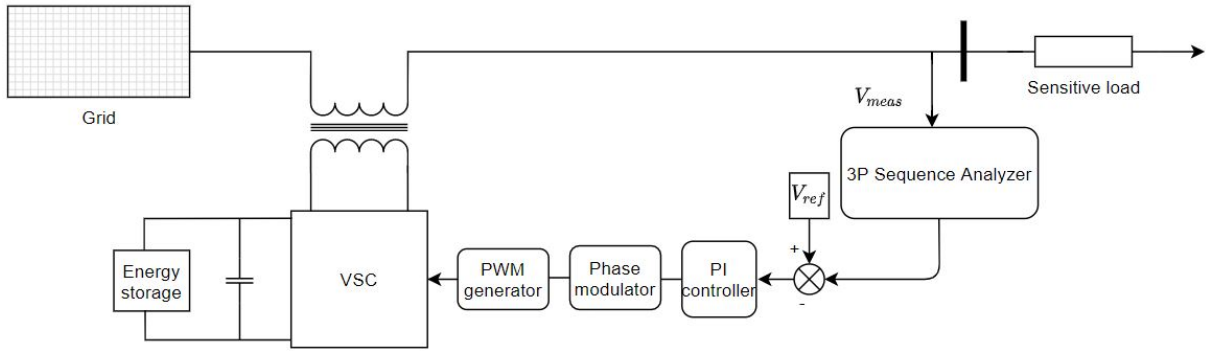

Figure 3.6: Simple one line diagram of control scheme for modelled LVR.

3P Sequence Analyzer

The Sequence Analyzer uses the voltage measurements as mentioned above to calculate the phase sequence components. The sequence voltages are internally calculated as in equations 3.4-3.6. here a equals the complex operator such that $a = 1\angle 120°$. The Sequence Analyzer then outputs the magnitude and phase of the measured signals.

$$V_1 = \frac{1}{3}(V_a + aV_b + a^2V_c) \tag{3.4}$$

$$V_2 = \frac{1}{3}(V_a + a^2V_b + aV_c) \tag{3.5}$$

$$V_3 = \frac{1}{3}(V_a + V_b + V_c) \tag{3.6}$$

PI Controller

A PI controller is utilized. Since the system is of the first order, the PI controller gives acceptable stability and can be tuned by utilizing the Ziegler Nichols method as well as experimental tuning. The transfer function of the PI controller is of the same form as in equation 4.9 with parameters as in table 3.2 below. The controller outputs the signal to a phase modulator which splits the controlled signal according to phase A, B and C with a $120°$ phase shift.

$\mathbf{K_p}$	$\mathbf{K_i}$
0.005	3000

Table 3.2: Controller parameters for the PI controller of the implemented DVR.

PWM Generator

The PWM Generator generates pulses based on the input signal which is used to control a power converter, in this case, the VSC at the core of the DVR. According to the MathWorks specifications [26], the pulses are generated by comparing a triangular carrier waveform to an external reference modulating signal. The signal from the PI controller is the reference. An example of how the PWM generator generates signals based on the carrier and modulated signal can be seen by figure 3.7.

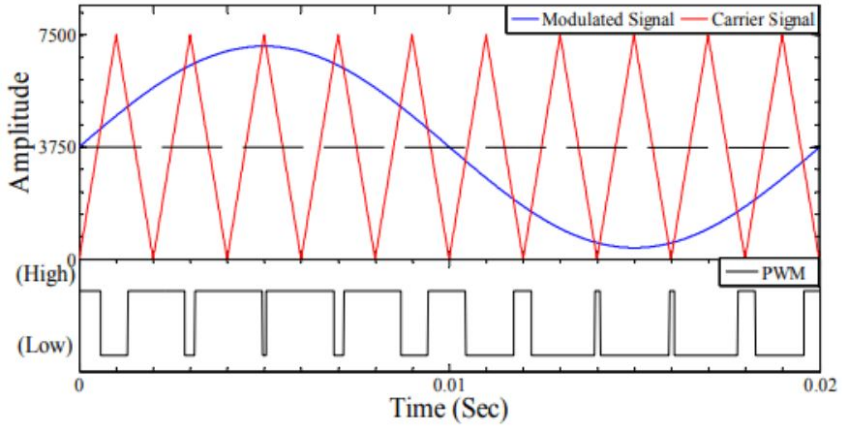

Figure 3.7: Illustration of how the PWM signal is generated based on the carrier and modulation signal [14]

3.2 Assumptions of Model

In the modelled DVR, a few assumptions has been made to simplify the model. The goal has not been to create a fully modularized model, but rather showcasing the working principle of the technology. The implemented model can be found in figures 9.12 - 9.13 in the Appendix.

- **The Energy Storage:** The energy storage on the DC side of the VSC is modelled as an ideal DC voltage source rated at 500V. All charging and discharging factors as well as degrading of the source is neglected. The capacitance of the coupled capacitor is rated at $C = 5.4 \cdot 10^{-6}$ F.
- **Filter:** Minimal amounts of filtering are installed in the model, simplifiying the calibration according to the load.
- **Bypass equipment:** No bypass equipment is modelled.

Chapter 4

The Magtech Voltage Booster

Since the MVB is a subject in this thesis, a thorough deep dive into the working principle of the technology will here be presented. The following chapter is identical to the section in the specialization project [11]. Besides, the groundwork for the Simulink model utilized in the completed simulations will be established. The Simulink model and theory is inspired by the work from a previous thesis [15].

4.1 Motivation

In short, the MVB is a series-connected transformer coupled with an autotransformer, all in series with the distribution grid as shown in 4.3, effectively functioning as an LVR as explained in the previous chapter. The company Magtech has patented a unique technology of a controllable magnetic coil (MCI) to seamlessly regulate the output voltage on the primary side of the transformer.

Other companies provide similar LVRs, like ABB and a-eberle (mentioned earlier). However, both of these applications are based on step-changing technology through switches. According to a study done by [13], a LVR should fulfil two requirements in the highest degree as possible. High robustness is important since installations like LVRs are often implemented in weak parts of the grid that are located in rural areas. Installations with moving parts are subject to fatigue and requires maintenance. Besides, the installation must affect the power quality as little as possible. It is curious that technologies that incorporate stepped control of the inductance (which is quite widespread), can cause flickers, voltage jumps/dips and other transients [13]. In the same study, a novel LVR utilizing the same MCI technology as the Magtech is established.

4.2 Working Principle and Technology

The MVB is available in two different models optimized for either IT or TN network configuration in the low voltage distribution grid. Models that are optimized for IT network configuration will function purely as voltage support, while the TN model also can contribute to increased SCC. In figure 4.1, the general block diagram of the MVB is illustrated [24]. The device is connected in series with the load on a strategic location where the voltage should be regulated. The output of the MVB is connected closest to the load. The controller unit has a set reference point close to the system voltage (in this case slightly above, 235V), and compares the output voltage of the transformer giving an output to a controller unit that rectifies the current needed from the output. The DC current controls the hysteresis of the MCI (variable induction coil), effectively changing the inductance of the autotransformer. With the magnetization of the autotransformer regulated by the MCI, the output voltage will seamlessly change in accordance with the set DC current. [15].

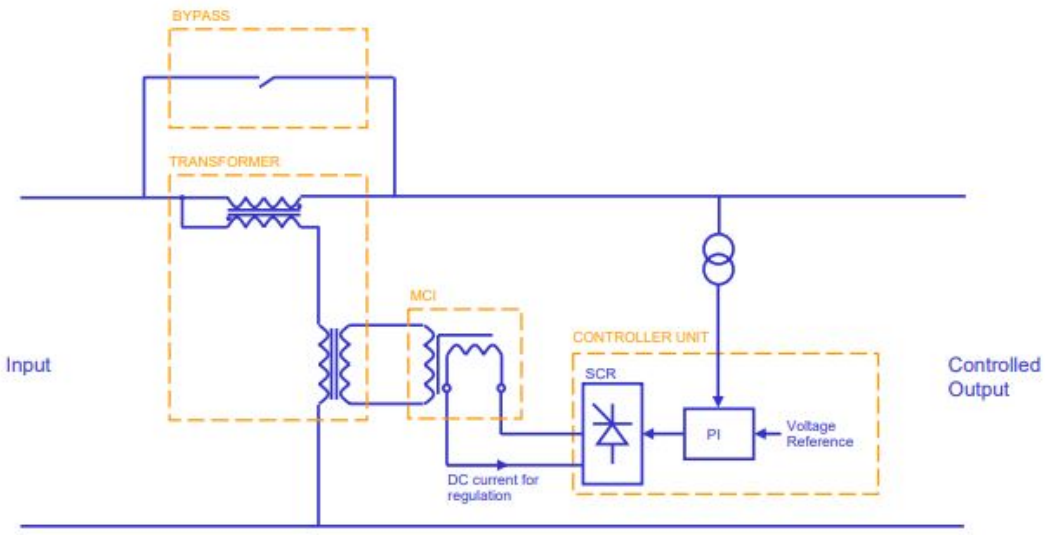

Figure 4.1: Per-phase depiction the MVB with controller, the MCI, bypass and transformer units [24].

The lower node of the autotransformer is galvanically coupled with the MCI through a power transformer (neglected further), where the value of the variable inductance of the MCI is controlled with a DC current that is rectified from the secondary side of the transformer [15] [28].

4.2.1 MCI - Magnetic Controllable Inductor

The MCI is the core technology of the MVB, making the seamless change of output voltage possible. As can be seen from figure 4.1 above, a controllable DC current i_{dc} is used to change the inductance of the main winding of the transformer through the MCI. This is possible because of the special layout of the MCI.

The MCI compromises a main and a control winding wound around an iron core, where the control winding is designed such that the magnetic field generated is orthogonal to the field generated by the main winding. A virtual air gap is created as a result of this interaction, which in turn enables the control of the inductance of the inductor through the control of the current in the control winding [28]. The relationship between the inductance of the inductor and the rectified control current is found as in equation 4.1 where $\Re_c$ and $\Re_g$ is the reluctance of the core and the virtual air gap [15].

$$L = \frac{n^2}{(\Re_c + \Re_g)} \tag{4.1}$$

It is already established that the virtual air gap is established as a result of the interaction of the two magnetic fields from the main and control windings. Adjusting the i_{dc} that circulates in the control winding will therefore directly impede the reluctance of the system, and from equation 4.1 the inductance is changed [15].

Figures 4.2a and 4.2b illustrates a core with control and main windings from Magtech [24] and a simple illustrative one line diagram where the autotransformer and MCI is sketched in.

(a) Illustration of a real MCI.

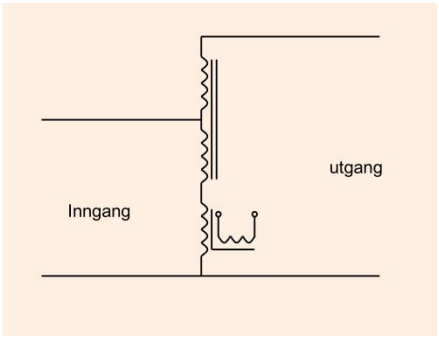

(b) Simple one-line diagram of the MVB.

Figure 4.2: Simple illustration of a one line diagram of the autotransformer and the MCI [24].

4.3 Modelling in Simulink

A simplified Simulink model is established for the MVB based on [15]. The implementation, assumptions and general model will briefly be presented in the following section.

4.3.1 Per-Phase Model

A simplified per-phase one-line diagram is shown in figure 4.3. Several simplifications and assumptions has been done relating the model to its original design, and can be listed as follows [15]

- The autotransformer is assumed ideal, with no power loss or saturation behaviour over the transformer.
- The MCI inductance has no specified restrictions on its dynamic behaviour and is purely controlled by the PI regulator of the booster.
- All effects by the power electronics in terms of dynamic behaviour and disturbances are neglected.
- The galvanic coupling of the MCI and autotransformer is neglected.

The model in figure 4.3 is the basic model implemented in Simulink, with v_{in} and v_{out} being the input and output voltage of the booster, while the i_{in} and i_{out} is the in and output currents. v_1 and v_2 represents the primary and secondary voltages of the autotransformer. i_m and v_m represents the voltage across the variable inductor and its respective current. In a future model, the losses and magnetic coupling should be included in some way - but is not pursued in this thesis.

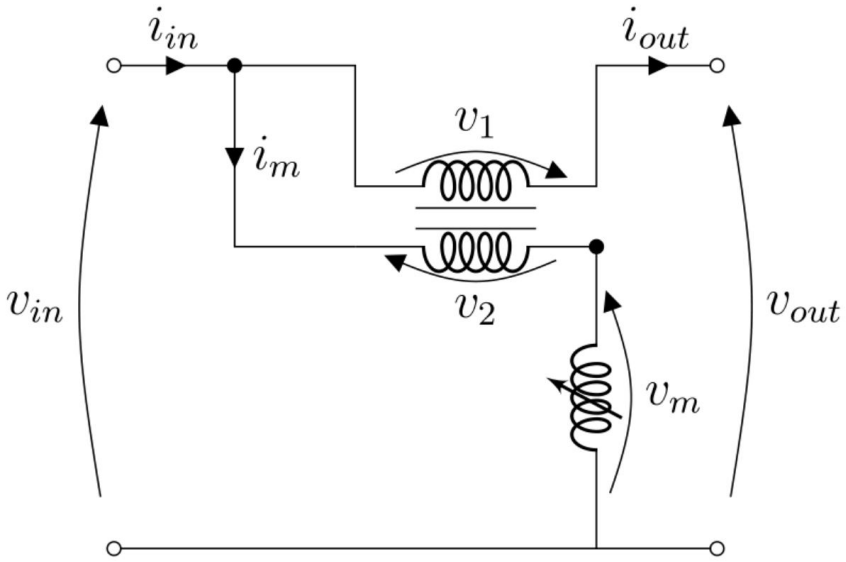

Figure 4.3: Simplified per-phase circuit of the MVB [15].

The equations controlling the dynamic behaviour (equations 4.2-4.8) of the model is derived from figure 4.3 and found by using Kirchhoff's laws and node balance from the reference point of the system [15]. The parameter z corresponds to the connected load of the MVB.

$$v_m = L_m \frac{di_m}{dt} \tag{4.2}$$

$$v_2 = nv_1 \tag{4.3}$$

$$v_{out} = v_{in} + v_1 \tag{4.4}$$

$$v_{in} = v_m + v_2 \tag{4.5}$$

$$v_{out} = zi_{out} \tag{4.6}$$

$$i_{in} = i_{out} + i_m \tag{4.7}$$

$$i_m = \frac{1}{n} i_{out} \tag{4.8}$$

4.3.2 Control System and PI Regulator Parameters

A PI regulator was chosen as the control law of the system since the system is of first order. The block diagram of the voltage control loop of the system is given in figure 4.4 [15]. The v_{out} of the booster is measured and compared to the voltage reference of the booster. The PI controller calculates the δL_m which is added to the initial inductance L_m. The value of inductance is passed on to the voltage booster, and recalculating new voltage and current values, and outputting a new value of v_{out}. The PI controller will continue to regulate the output voltage as long as there is a deviation between the reference and output.

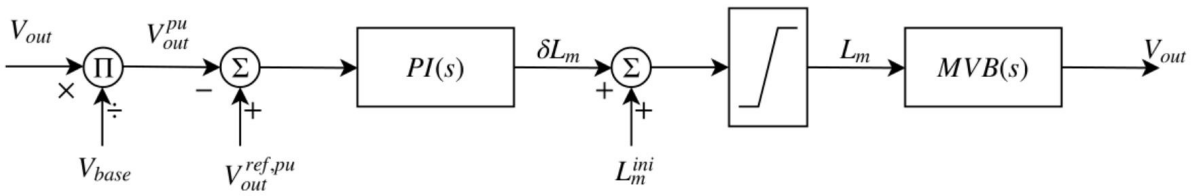

Figure 4.4: Block diagram of the voltage control loop [15].

The PI controller is on the form as in 4.9 and the K_p & K_i terms can be modified to adjust the dynamic response time.

$$h_r = K_p + \frac{K_i}{s} = K_p \frac{1 + \frac{K_p}{K_i} s}{\frac{K_p}{K_i} s} = K_p \frac{1 + T_i s}{T_i s} \tag{4.9}$$

According to the datasheet (Appendix D) of the model, the controller should have a dynamic response time of 200ms. Tuning accordingly to the appointed loads in the tests the values in

table 4.1 are chosen. An apparent weakness in this model is that different load settings require different regulator parameters. A screenshot of the Simulink representation of the MVB and its control system can be found in figure 9.9 in the Appendix.

$\mathbf{K_p}$	$\mathbf{K_i}$
-0.005	-1

Table 4.1: Controller parameters for the PI controller of the implemented MVB.

4.3.3 Steady State Model

According to [15], the model can be transformed into phasor notation. Using phasor notation, the steady-state transfer function of the MVB between V_{out} and V_{in} can be found as in equation 4.10. It should be noted that decreasing the inductance increases the output voltage V_{out} with the load and input voltage set to constant. Further, the smaller L_m is, the relative voltage drop at the output will increase.

$$\frac{\overline{V}_{out}}{\overline{V}_{in}} = Z\frac{(1+n)}{nZ + \frac{jX_m}{n}} = Z\frac{(1+n)}{nZ + \frac{j2\pi f L_m}{n}} \tag{4.10}$$

This transfer function can be plotted for different values of L_m and can be seen in figure 4.5 below with base values utilized as in table 4.2.

$\mathbf{S_{base}}[\mathbf{VA}]$	$\mathbf{V_{base}}[\mathbf{V}]$	$\mathbf{I_{base}}[\mathbf{A}]$	$\mathbf{Z_{base}}[\Omega]$
2000	230	2.89	79.35

Table 4.2: Base values used in plotting of transfer function of MVB

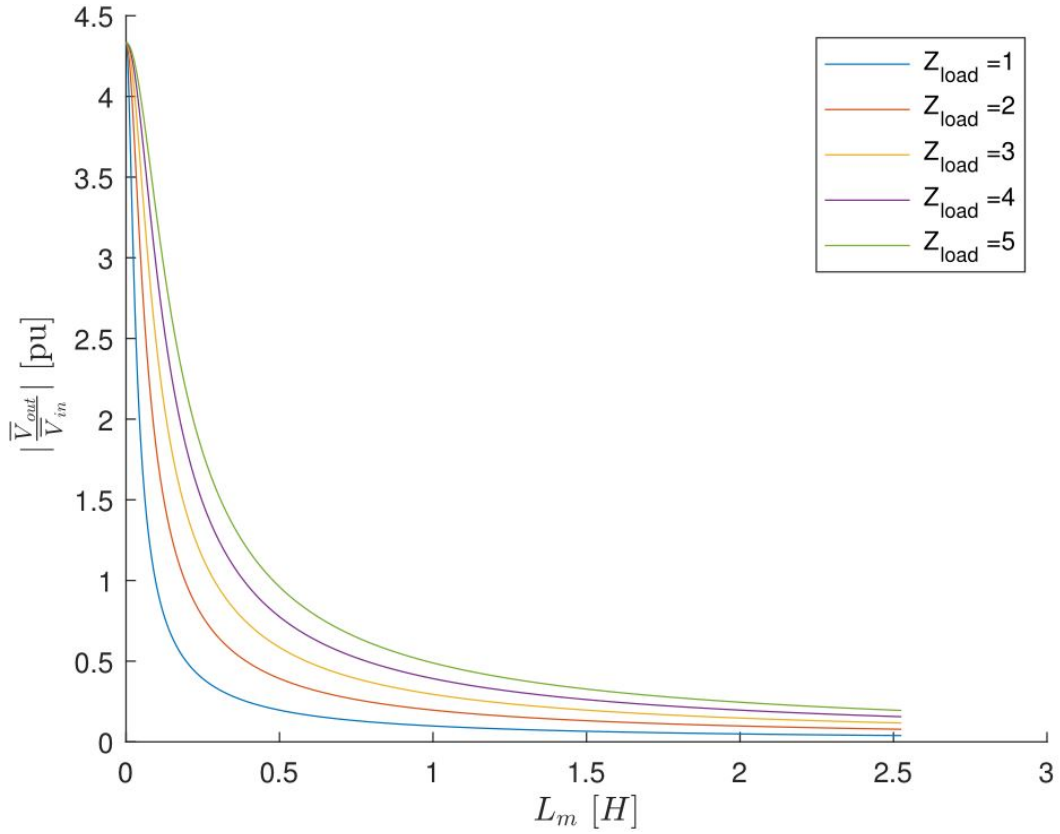

Figure 4.5: Transfer function of the MVB [15].

4.4 Results From Specialization Project

In the specialization project conducted in the autumn of 2019 [11], an actual MVB was tested in the laboratories of SINTEF, and the Simscape model which is utilized here was also implemented with a goal of localizing weaknesses in comparison with the actual device. Some key points that should be noted from start before utilizing this model can be found below and will function as error sources in analysing the later simulation results.

- Both the implemented model and the real MVB both succeeded in increasing the voltage according to the set dynamic response.
- The simulated model as well as the real MVB both consumed *significant* amounts of reactive power during operation, with a close to constant power factor if the voltage sag is subject to conditions on the secondary of the MVB. Resistive load changes were the source of the voltage changes. However, if the voltage sag was subject to factors upstream, the power factor during boosting would drastically be reduced.
- Both the implemented model and the real model experience different magnitude of the voltage drops and spikes on the output compared to the input during load changes. The significant drops in the model were explained by the nature of the transfer function, where the added reactance of the booster significantly affects the $\frac{R}{X}$ ratio of the system. This shows as the voltage drops on the secondary side were much larger on the secondary side compared to the primary. The model, however, experiences much greater drops and is a known problem. If this is to occur during the following simulations in this thesis, it should be duly noted, but not given much attention.
- The real MVB successfully boosts the voltage with a maximum deviation of 0.2 pu between the input and output, with a pick-up voltage at 0.72 where the output is then boosted to 0.92 pu.

From the specialization project, it was concluded that the MVB would function at its very best with the least chance of complications in a grid with $\frac{R}{X} > 1$, with small or no amounts of DG production as well as a total system impedance of 0.23 Ω including the MVB to maintain proper protection selectivity during faults [11]

Chapter 5

The Induction Machine

The induction machine, also known as the asynchronous machine, is an important class of electrical machines both in industry and households. According to Kothari and Nagrath [18], more than 85% of industrial motors in use as of today are of this type. The machine shares some similarities to the traditional synchronous machine, both utilizing the phenomena of rotating magnetic fields to induce voltage and generate torque.

In this thesis, a standard induction motor is implemented in the Simscape environment to be used for grid simulations in a low voltage distribution network. Induction motors are severely taxing for the low voltage grid, especially during startup with the motor pulling currents several times the size of the load current. The basic working principle of the machine, as well as the mathematical foundation of the Simscape model, will be briefly explained. Further, a method of modelling the mechanical torque by measuring the rotational speed ω_{rpm} will be presented.

Overview of the Simscape Electrical and SPS implementations of the machine can be found in figures 9.11 and 9.15 in the Appendix, respectively.

5.1 Working Principle

The Three-Phase Induction Motor is similar in construction to that of a synchronous machine, with the stator consisting of a three-phase winding engulfing the rotor. The rotor core is of laminated construction with rotor bars conveniently distributed along its horizontal axis. Further, the rotor can be of two types - wound and squirrel cage. In this model, a squirrel cage rotor is used. Contrary to the synchronous machine which operates with the rotor and stator magnetic fields locked in place, the induction machine does not produce torque at synchronous speed but has its origins in the current induction in the rotor which occurs at asynchronous speed [18].

A detailed illustration of the magneto-motive forces (MMF) and flux waves in the rotor and stator is illustrated in figure 5.1 below. The electrical torque produced is a result of the interaction between the rotor and stator fields. The further physical groundwork of the machine will not be explained further.

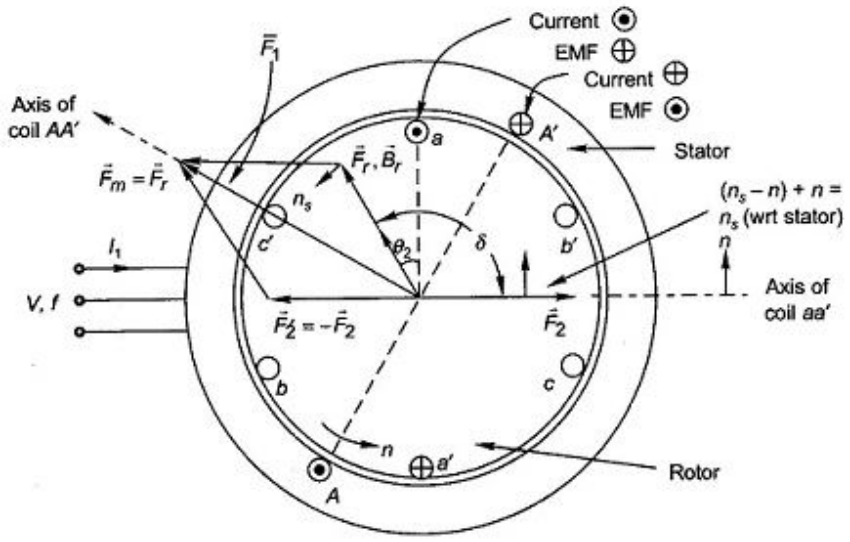

Figure 5.1: MMF and Flux waves in induction motor [18].

5.2 Basics of Simulink Model

The Simulink model of the wound rotor induction machine used is already implemented as a standardized element in the Simscape Electrical and Specialized Power Systems (SPS) toolbox library and is made up of an electrical and mechanical part. The Electrical part is represented by a fourth-order state-space model and the mechanical by a second-order system [4]. The state equations for the electrical and mechanical models will briefly be presented below. The electrical states are represented exclusively in the dq frame by utilizing the park transformation, and thus assuming constant reference frequency to avoid oscillatory transients. This makes computations and model representation significantly easier.

Electrical Model

The equivalent circuits for the d and q axes reference frames of the modelled machine are found in figure 5.2. Where the notations r and s represents rotor and stator respectively. Figures and equations are cited from the MathWorks library [4].

The stator and rotor voltages of the d and q reference frames (V_{qs}, V_{ds}, V'_{qr} and V'_{ds}) from figure 5.2 are given by equations 5.1 - 5.4 below.

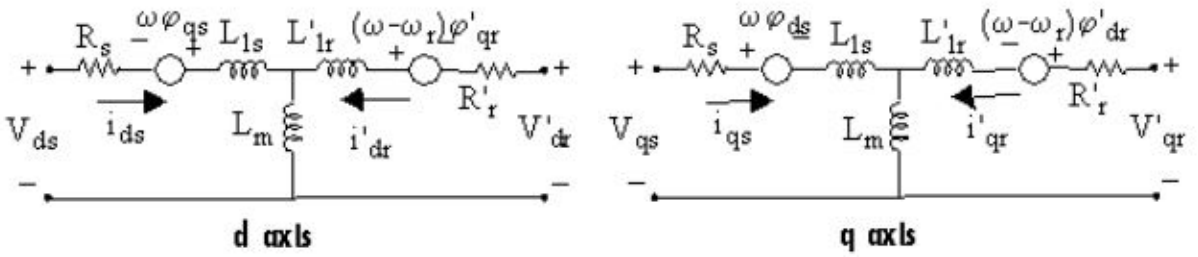

(a) Equivalent circuit d-axis frame.

(b) Equivalent circuit q-axis frame.

Figure 5.2: Equivalent circuit for d and q axes [4].

$$V_{qs} = R_s i_{qs} + \frac{d\phi_{qs}}{dt} + \omega\phi_{ds} \tag{5.1}$$

$$V_{ds} = R_s i_{ds} + \frac{d\phi_{ds}}{dt} - \omega\phi_{qs} \tag{5.2}$$

$$V'_{qr} = R'_r i'_{qr} + \frac{d\phi'_{qr}}{dt} + (\omega - \omega_r)\phi'_{dr} \tag{5.3}$$

$$V'_{dr} = R'_r i'_{dr} + \frac{d\phi'_{dr}}{dt} + (\omega - \omega_r)\phi'_{qr} \tag{5.4}$$

Further, the rotor and stator fluxes for the dq reference frame are modelled as in equations 5.5 - 5.8.

$$\phi_{qs} = L_s i_{qs} + L_m i'_{qr} \tag{5.5}$$

$$\phi_{ds} = L_s i_{ds} + L_m i'_{dr} \tag{5.6}$$

$$\phi'_{qr} = L'_r i'_{qr} + L_m i_{qs} \tag{5.7}$$

$$\phi'_{dr} = L'_r i'_{dr} + L_m i_{ds} \tag{5.8}$$

Finally, the electrical torque T_e is calculated by equation 5.9

$$T_e = 1.5p(\phi_{ds} i_{qs} - \phi_{qs} i_{ds}) \tag{5.9}$$

Mechanical Model

The mechanical model which is used for simulating the mechanical properties of the machine is represented by a two order model as given in equations 5.10 - 5.11. Equation 5.10 is also known as the swing equation and represents the change in rotational speed as the torque balance changes. T_e and T_m is the electrical and mechanical torques respectively, while H is the inertia

constant of the machine. The factor $F\omega_m$ represents the impact of viscous friction, which is usually neglected in simplified simulations [4].

$$\frac{d}{dt}\omega_m = \frac{1}{2H}(T_e - F\omega_m - T_m) \tag{5.10}$$

$$\frac{d}{dt}\theta_m = \omega_m \tag{5.11}$$

Further, the inertia J of the machine can be calculated by using equation 5.12. The inertia constant H is given in seconds and ω_{sync} is the synchronous speed of the machine given by equation 5.13 where P represents the number of poles.

$$J = \frac{2H \cdot S_{rated}}{\omega_{sync}^2} \tag{5.12}$$

$$\omega_{sync} = \frac{120 \cdot f}{P} \tag{5.13}$$

5.2.1 Modelling Mechanical Torque

The mechanical torque T_m which is applied to the machine represents a load. There are several different ways to model the applied mechanical torque, but usually, T_m is a function of the rotational speed ω. The ABC model is represented by equations 5.14 and 5.15. All factors are expressed in pu [40].

$$T_m = T_{m0}(A\omega_r^2 + B\omega_r + C) \tag{5.14}$$

$$A + B + C = 1 \tag{5.15}$$

The model constants A,B and C, as well as the inertia constant H, varies in accordance to the nature of the load. In [40], a list of constant values for common loads such as a dishwasher, heat pump/AC is readily presented. The list is presented in table 9.2 in the Appendix.

5.3 Characteristics of Model

The parameters of the three-phase squirrel cage induction machine model are presented in table 5.1. The machine is initially modelled after a small industrial load with H = 0.70 and A = 1 but is altered to decrease the starting currents by increasing the machine impedances. Zero sequence interaction and modelling of the magnetic saturation in the machine is neglected.

Parameter	Value
V_{base}	230 V
S_{rated}	4 kVA
f	50 Hz
H	0.7 s
J	0.0567 kg· m^2
P	1 pair
ω_{sync}	3000 rpm
t_{start}	2.50 s
R_{stator}	1.50 Ω
$X_{leak,stator}$	2.25 Ω
R_{rotor}	0.84 Ω
$X_{leak,rotor}$	1.03 Ω
X_{mag}	17 Ω

Table 5.1: Parameters of the three-phase squirrel cage induction machine.

Further, the torque/speed and active/reactive power characteristics as well as the power factor during startup of the machine is presented in figures 5.3, 5.4 and 5.5 below, respectively. Looking at the power consumption during startup, it should be noted that the reactive power consumption is roughly 3 pu during a direct start. This value can often be 2-3 times larger but is intentionally reduced in this thesis, enabling the implemented SVRs able to properly compile.

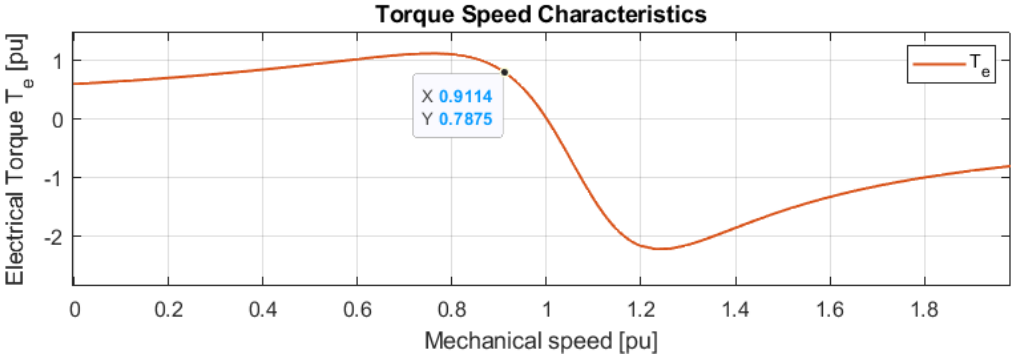

Figure 5.3: Torque Speed Characteristics of the induction machine.

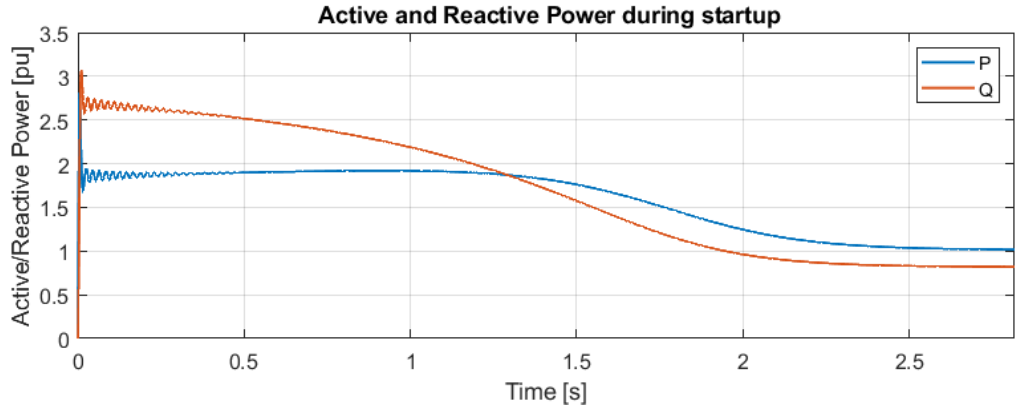

Figure 5.4: Active and reactive power characteristics of the machine during start-up.

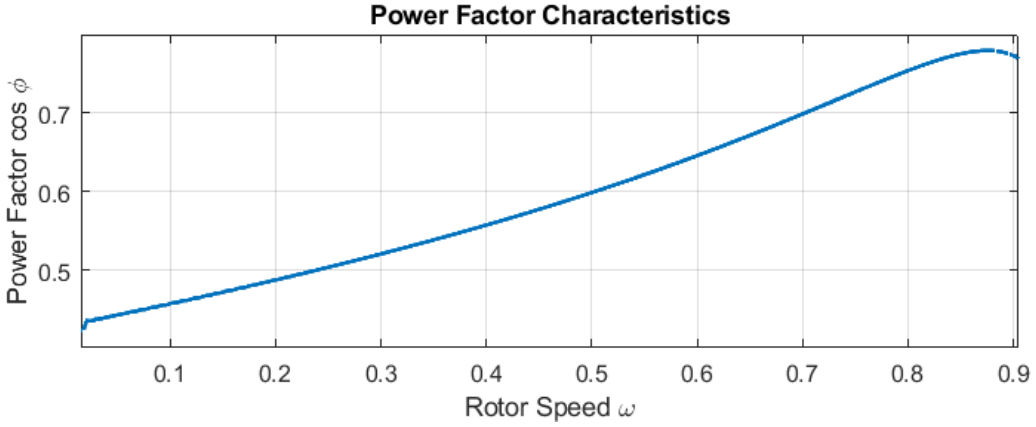

Figure 5.5: Power Factor of induction machine during start-up.

Chapter 6

Method

6.1 Modelling the case network

Data from an existing low voltage distribution grid is acquired from Elvia and modelled in two different variations in the Simscape environment in Simulink. The grid is modelled using the *Specialized Power Systems* (SPS) toolbox as well as the *Simscape Electrical* environment. The previously modelled MVB is modelled specifically for the latter environment, while the newly modelled DVR is modelled in the SPS toolbox. The two different environments give the same results in steady-state operation, and will in this section be presented as a single modelled network.

6.1.1 Grid Topology

The modelled grid is a classical 230V IT-based distribution network which can be exposed to voltage problems. In this network, an MVB is already installed at a certain node (between line 9 and 10) due to experienced voltage problems at load 1.

The topology of the network is visualized in figure 6.1 below. The length of the line segments in the figure is not representative for the actual length. The length and type of cable for each segment can be found in table 6.1. It should be noted that the voltage booster is connected 840m into the grid from the step-down transformer. In the simulations, the location of the installed modelled voltage regulator will remain the same. Figures 9.10 and 9.8 in the Appendix features screenshots of the modelled network in the SPS and Simscape environment respectively.

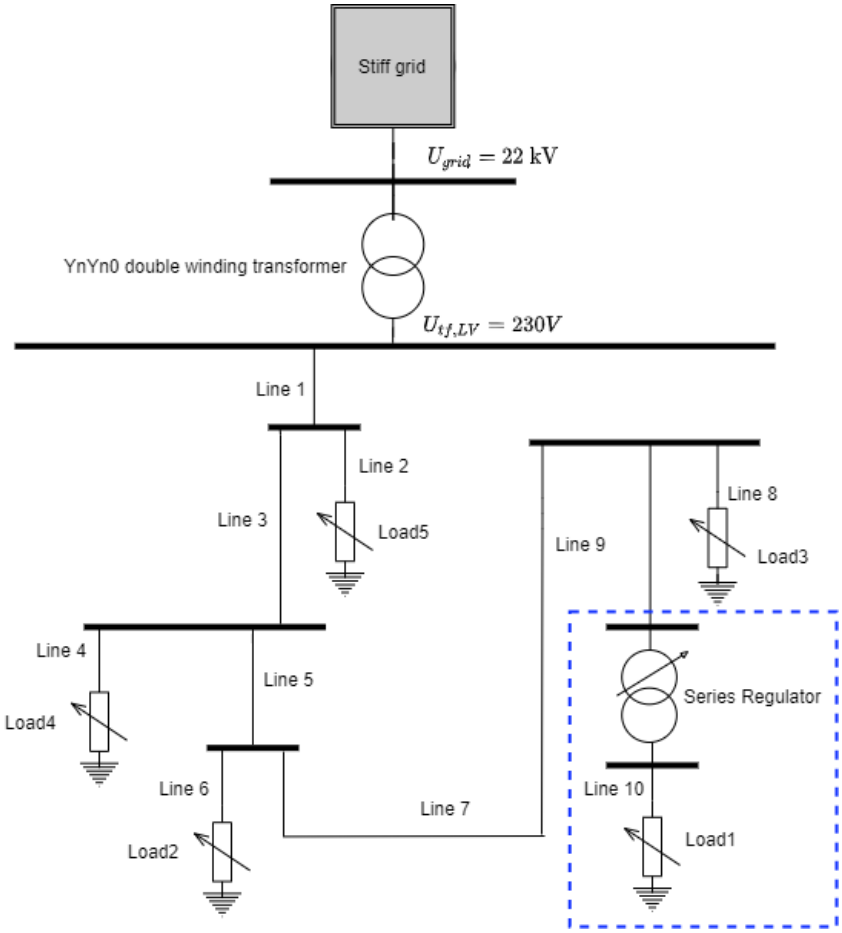

Figure 6.1: Grid topology of modelled distribution grid.

Line segment	Type	Length [m]
1	TFSP3x150 + EX95	31 + 52
2	EX25	13
3	EX95	31
4	PFSP3x50	22
5	EX25	82
6	PFSP3x25Al	27
7	EX95	54
8	EX25	96
9	Al70	638
10	Ex25	73

Table 6.1: Length and type of lines in the modelled network.

6.1.2 Load Flow Validation

Maximum load data has been acquired from Elvia along with calculated voltage readings from NETBAS, which are presented in table 6.2 along with a simple load flow analysis of the modelled grid. The load flow analysis is done in the Simulink Simscape environment.

The voltages acquired from the load flow from the modelled grid is very accurate compared to the actual readings. To further lower the voltages downstream in the grid, a minor adjustment is done by changing load 3 from 0 to 7 kW. Currently, there is no consumption at this node. The updated model then gives the voltage readings as written in the very last column of the table.

Bus	$\mathbf{P_{load}[kW]}$	$\mathbf{Q_{load}[kVAr]}$	**DSO V[pu]**	**Model V[pu]**	**Upd. Model V[pu]**
TF LV	-19 (-26)	0.160	0.999	0.999	0.994
Load 5	4	0	0.987	0.987	0.983
Load 4	7	0	0.982	0.982	0.976
Load 3	0 (7)	0	0.973	0.970	0.936
Load 2	4	0	0.969	0.968	0.951
Load 1	4	0	0.953	0.952	0.935

Table 6.2: Load Flow Analysis of case network during full load.

6.1.3 Simscape Model

Building a power system in the Simscape and SPS toolbox in Simulink is accomplished by utilizing the implemented blocks corresponding to each element such as the loads, voltage sources, distribution line models etc.. The modelling basis for the different major elements will briefly be explained below.

Numerical Solver

In Simulink, there are several implemented solver configurations that can be utilized, but in this project, the discrete trapezoidal solver is chosen with a sample time of 10^{-5} which gives satisfactory accuracy.

Voltage Source

The chosen voltage source block equals a configurable three phase voltage source which outputs the balanced phase voltages V_a, V_b and V_c as described in equations 6.1 - 6.3. No harmonic distortions are included. $V_{RMS} = \frac{22}{\sqrt{3}}$kV and $\phi = 0$.

$$V_a = \sqrt{2}V_{RMS} \cdot sin(\omega t + \phi) \tag{6.1}$$

$$V_b = \sqrt{2}V_{RMS} \cdot sin(\omega t + \phi + 120°) \tag{6.2}$$

$$V_c = \sqrt{2}V_{RMS} \cdot sin(\omega t + \phi - 120°) \tag{6.3}$$

Further, the internal impedance is modelled by the means of short circuit power level and $\frac{X}{R}$ ratio as given by table 6.3, and represents the ”stiffness” of the connected MV grid. Figure 6.2 illustrates the block representation of the three-phase voltage sources for the Simscape and SPS toolbox.

Parameter	Value
$\frac{X}{R}$	7
S_{scc}	500 kVA

Table 6.3: Internal impedance values of voltage source.

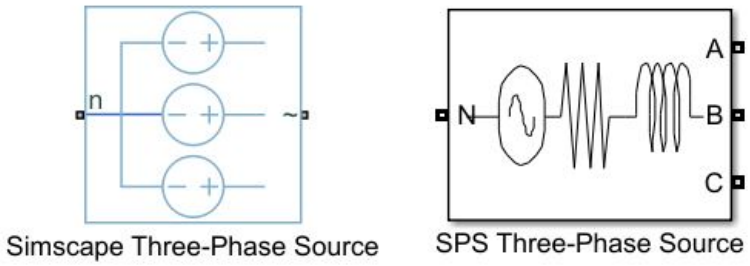

Figure 6.2: Block representation of the utilized voltage source in Simulink.

Transformer

The three-phase double winding distribution transformer is implemented by its respective block, and corresponds to the equivalent circuit in 6.3 below. The transformer parameters can be found in table 6.4 with impedance values in pu. The Z_{base} can be calculated by $Z_{base} = \frac{V_{base}^2}{S_{base}}$

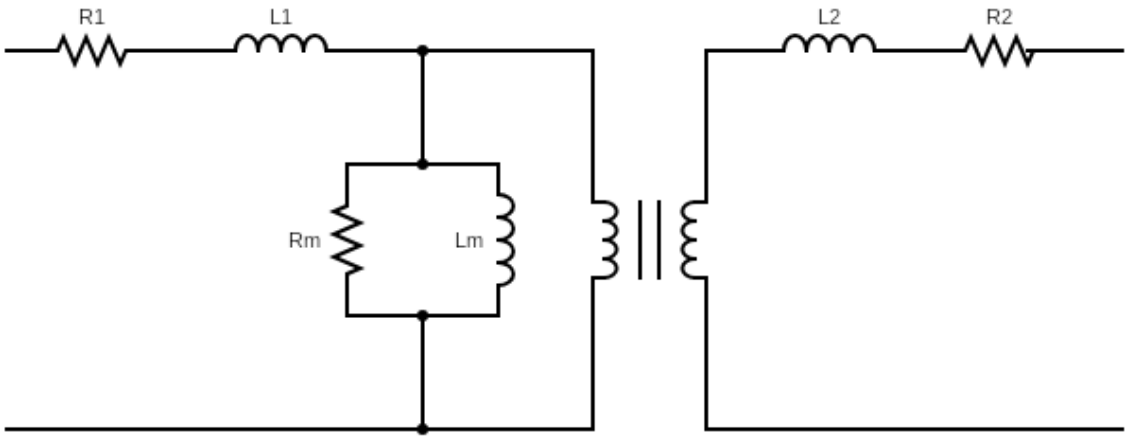

Figure 6.3: Equivalent phase diagram for the transformer model.

Parameter	Value
$V_{1,line,RMS}$	22 kV
$V_{2,line,RMS}$	230 V
S_{rated}	100 kVA
Configuration	YnYn0
R_1	0.01 pu
X_1	0.001 pu
R_2	0.01 pu
X_2	0.001 pu
R_m	500 pu
X_m	500 pu

Table 6.4: Distribution transformer parameters.

Pi-Line Model

The block used for modelling the distribution lines in the system is the integrated Three-Phase PI Section line. The PI line model connects the R and L elements in series, with the capacitive elements connected in shunts at the sending and receiving end of the segment. A circuit diagram of the model can be seen in figure 6.4 below [27].

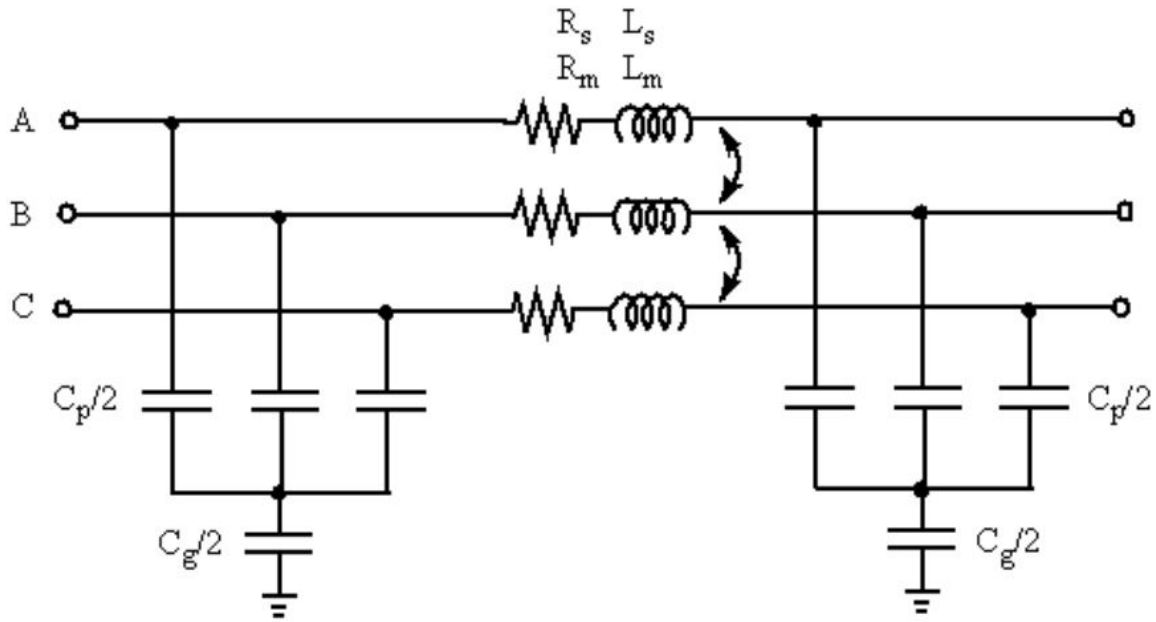

Figure 6.4: Illustration of PI-section line model.

The RLC elements in the model are calculated by equations 6.4 - 6.9 [27].

$$R_s = \frac{2R_1 + R_0}{3} \tag{6.4}$$

$$L_s = \frac{2L_1 + L_0}{3} \tag{6.5}$$

$$R_m = \frac{R_0 - R_1}{3} \tag{6.6}$$

$$L_m = \frac{L_0 - L_1}{3} \tag{6.7}$$

$$C_p = C_1 \tag{6.8}$$

$$C_g = \frac{3C_1C_0}{C_1 - C_0} \tag{6.9}$$

In these equations R_1, L_1, C_1 corresponds to the positive sequence parameters, while R_0, L_0 and C_0 corresponds to the negative sequence parameters.

The line data used to calculate the necessary parameters are collected from external sources and

standards like REN [32], and can be found in table 9.1 in the Appendix.

Load

The modelled system consists of a total of 5 households consuming a set amount of power at unity power factor, i.e., the loads are PQ dependent. The loads are connected in delta, giving a line voltage of 230V over the load resembling an IT configuration. Figure 6.5 shows the block representation of the loads utilized.

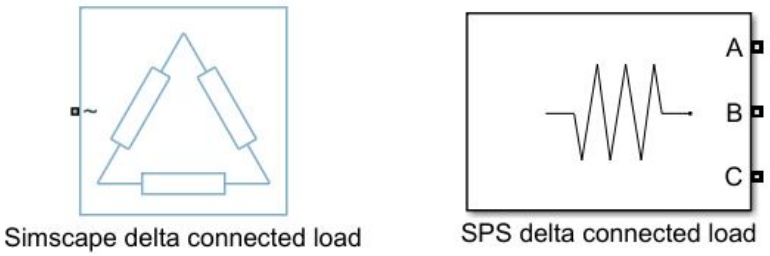

Figure 6.5: Block representation of the utilized delta connected load model in Simulink.

Per Unit system

In the following simulations, the results will be mainly presented using per unit (pu) terminology. Notable base values used for presentation are found below in table 6.5.

Parameter	Base Value
Voltage	230 V
Active Power	4000 W
Reactive Power	4000 VAr
Apparent Power	4000 VA
Rotational Speed	3000 rpm
Frequency	50 Hz

Table 6.5: Some notable base values in the pu system.

Chapter 7

Simulation Results

This chapter will be divided into three sections, with the first section presenting the induction machines impact on the voltages in the distribution grid as a whole as well as the startup process of the machine. The two next sections will investigate the behaviour of both the modelled voltage regulators with the machine implemented in parallel with the existing resistive load of 7 kW at load 1. Due to the nature of the voltage regulators, the MVB will be connected during the whole period while the DVR will be connected at 200ms after the machine is connected.

Several points of interest will be investigated such as

- Active and reactive consumption/injection of the regulator.
- Dynamic voltage response.
- Voltage impact of regulators in the network as a whole.
- Line losses upstream of regulator.

Scenario 1: Induction Motor Start with no Voltage Regulation

Induction motor start with no voltage regulation. The induction machine is connected at $t = 0.5\text{s}$ and the motor's impact on the voltage profile of the system will be investigated. Besides, the motor start characteristics as well as electrical torque with voltage controllers connected will be presented.

Scenario 2: Induction Motor Start with MVB

The induction machine is connected at $t = 0.5\text{s}$. The MVB is connected throughout the whole simulation, since there is no limit on the capacity of the booster. Additional simulations to investigate power losses across line segment 9 will be done.

Scenario 3: Induction Motor Start with DVR

The induction machine is started at $t = 0$s, DVR is connected at $t = 0.2$s. The DVR relies on an energy source to be able to supply active power to affect the voltage, meaning that the DVR will only be connected to compensate for greater voltage sags and swells. Additional simulation to investigate power losses across line segment 9 will be done.

Clarification for Simulations

Since the induction machine is modelled and simulated in two different Simulink environments (Simscape Electrical and SPS) the transient behaviour of the machine differs marginally, but will not impact the conclusions in any important way. However, the stationary conditions before and after startup are identical.

7.1 Induction Motor Start with no Regulation

The voltage profile of the whole network during the start of the machine can be seen by figure 7.1, with some key values described in table 7.1. It is quite clear that the direct start method is severely taxing for the voltages.

Bus	$\mathbf{V_{pre,start}}$	$\mathbf{V_{min,transient}}$	$\mathbf{V_{SS,start}}$	$\mathbf{V_{post,start}}$
Secondary Transformer	0.99	0.98	0.99	0.99
Load 5	0.98	0.97	0.97	0.98
Load 4	0.97	0.96	0.97	0.97
Load 3	0.94	0.90	0.91	0.92
Load 2	0.95	0.92	0.93	0.94
Load 1	0.93	0.83	0.85	0.89

Table 7.1: Voltage profile in system during start of motor with no voltage control.

Machine Start Characteristics with Regulation

The startup time, speed and torque with and without the MVB/DVR is plotted in figures 7.2 and 7.3 while some key values are presented in table 7.2. As expected, the machine starts slower with a reduced voltage at its terminals. Further, the difference in torque shape should be noted between the MVB and the DVR case from figure 7.3, with the DVR introducing significant noise to the electrical torque.

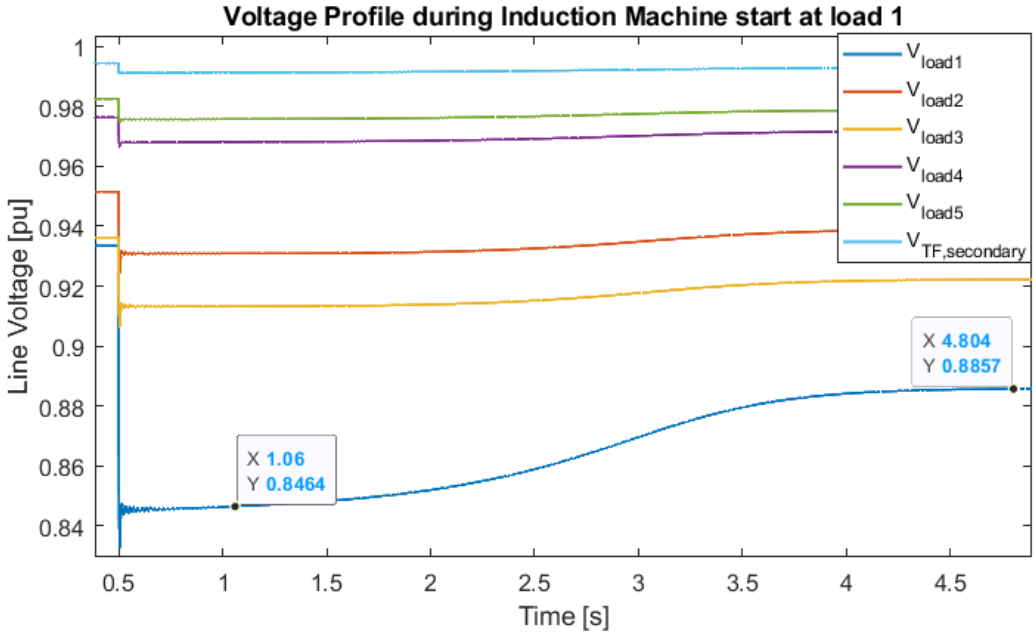

Figure 7.1: Voltage profile during the motor starting.

	MVB	**DVR**	**No regulation**
ω_{start} [pu]	0.91	0.90	0.87
t_{start} [s]	2.49	2.56	4.00

Table 7.2: Rotor speed ω and startup time with the MVB and DVR and no regulation.

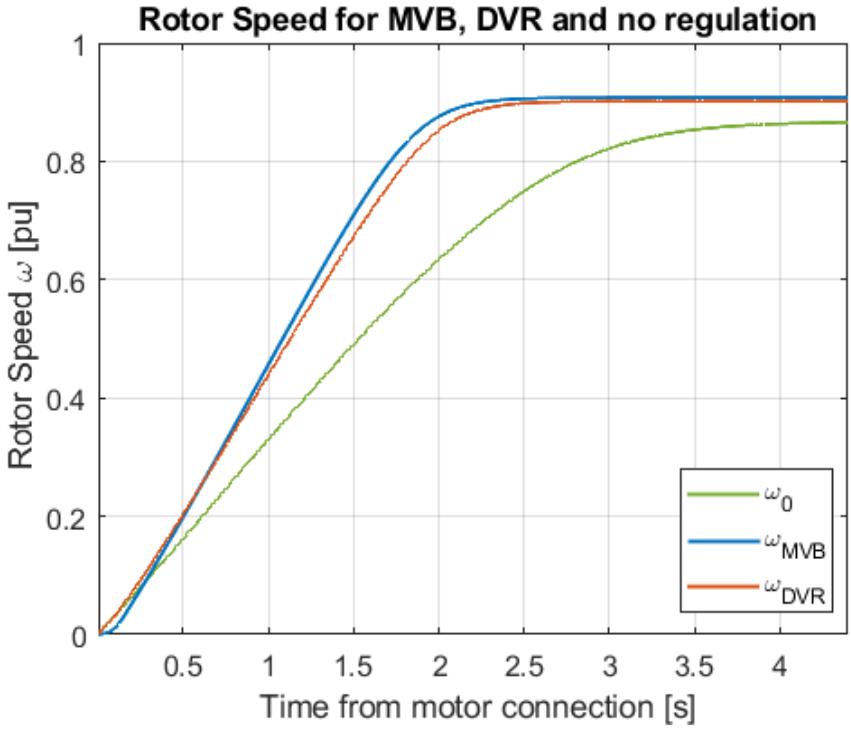

Figure 7.2: Startup speed of machine with/without MVB and DVR connected.

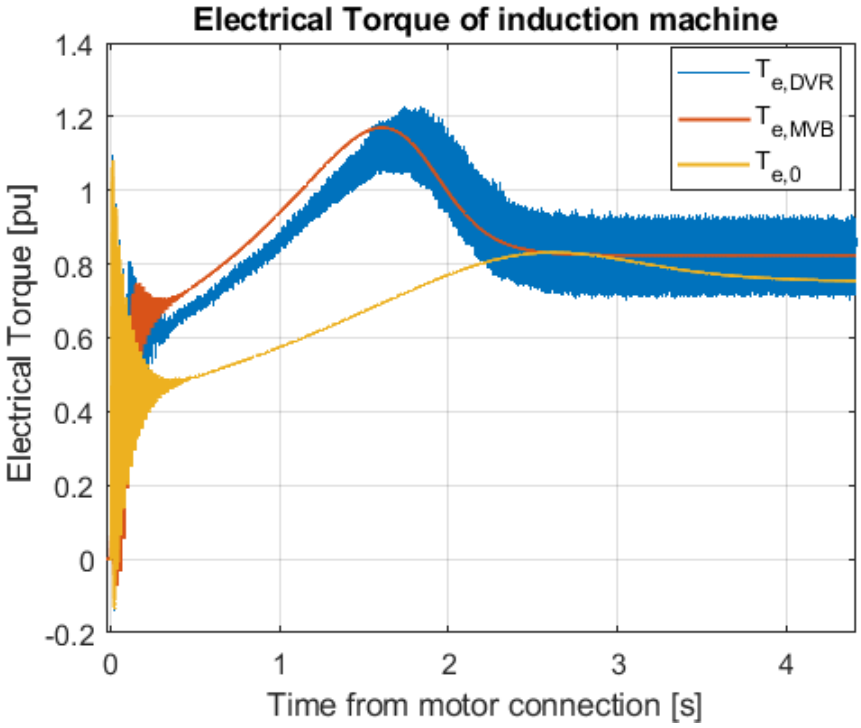

Figure 7.3: Startup electrical torque of machine with/without MVB and DVR connected.

7.2 Induction Motor Start with Implemented MVB

In this simulation, the induction motor is connected in parallel at load 1 at $t = 0.5\text{s}$ with the modelled MVB connected throughout the whole simulation.

7.2.1 Voltages and Distortions

The voltages on the primary and secondary side of the MVB is plotted in figure 7.4. At $t = 0.5\text{s}$ the motor is connected. The voltage drop on the secondary side of the MVB is extremely significant, with a measured lowest value of 0.3 pu before the controller kicks in. After 200ms the voltage is regulated back to its reference of 1.02 pu. The voltage drop on the primary of the MVB is measured at 0.74 pu.

There is no significant noise on the voltage signal in the model. The whole voltage profile of the system is plotted in figure 9.3 in the Appendix.

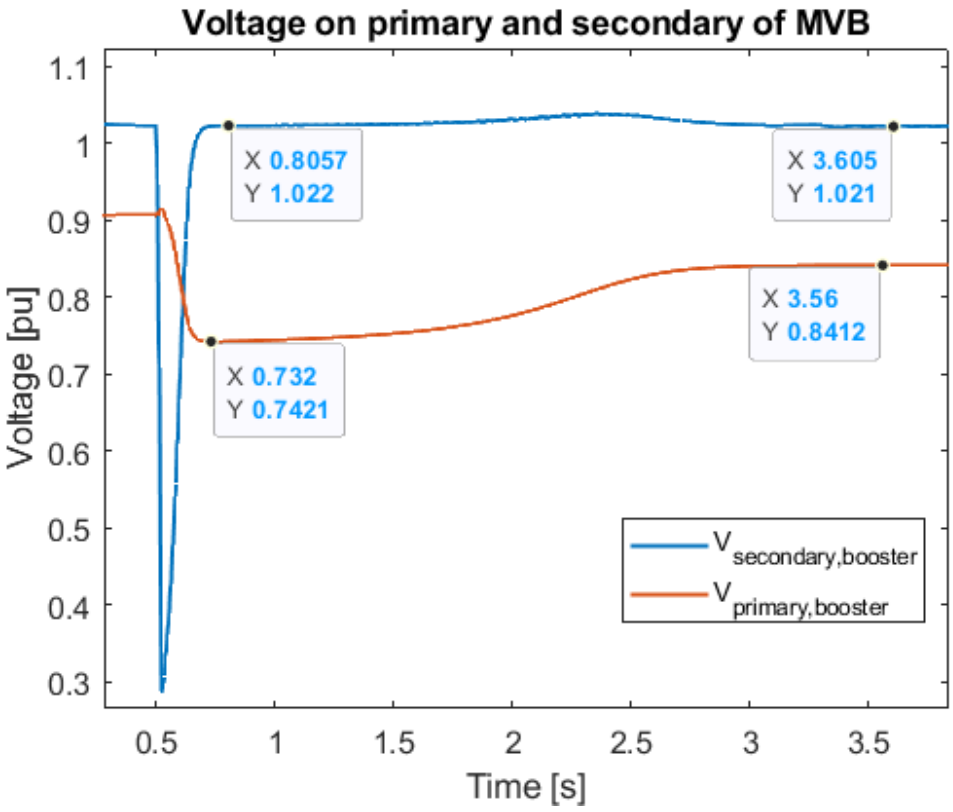

Figure 7.4: Voltages measured on primary and secondary side of MVB.

7.2.2 Power Characteristics

The reactive power consumption measured on the input of the MVB (difference of input and output, reactive power consumption of the machine is removed), as well as the power factor $\cos\phi$ measured at the input, is plotted in figures 7.5 - 7.6 below. The modelled MVB does not consume active power. The active and reactive power measured on the primary and secondary of the MVB can be observed in figures 9.6 - 9.7 in the Appendix. As expected, the measured active power is identical on in and output.

The power factor is drastically changed during the first 200ms as a result of controller transients, but looking away from this deviance the power factor is in the area of 0.51-0.56.

The power consumption of the induction machine during startup with the MVB connected can be seen in figure 9.4 in the Appendix.

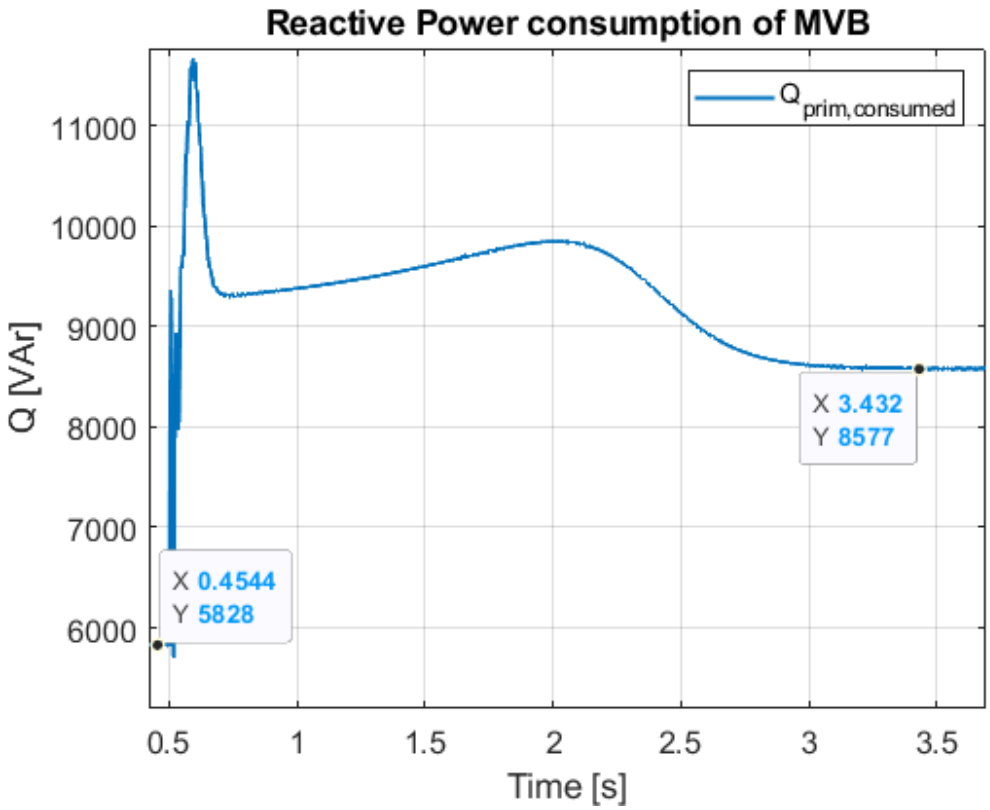

Figure 7.5: Reactive power consumed by MVB.

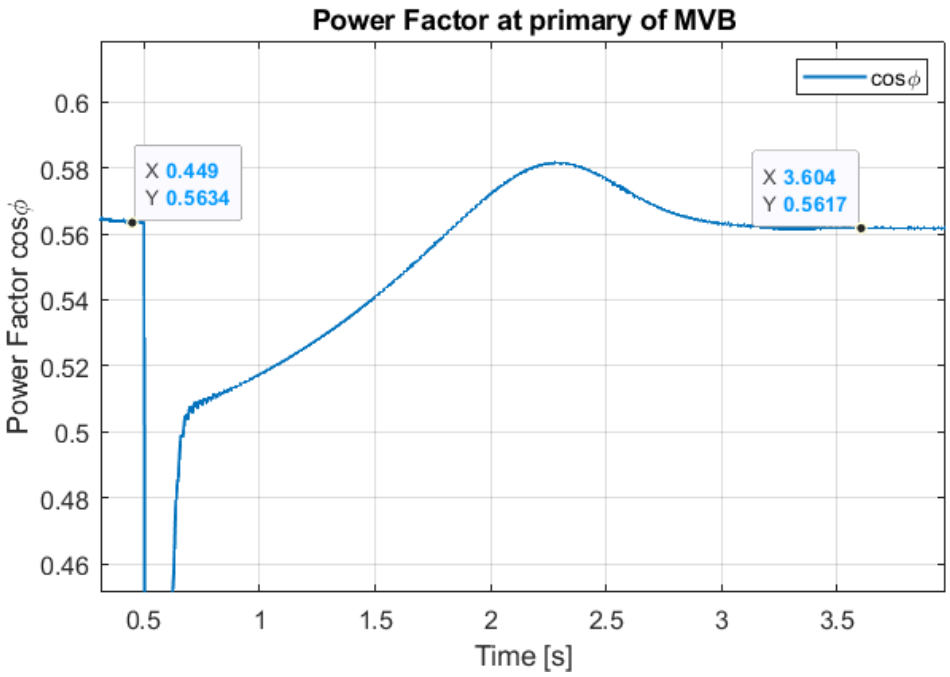

Figure 7.6: Measured Power Factor at input.

Voltage Impact of MVB at Select Nodes

To properly emphasize how the additional reactive power consumption of the MVB further affects the voltages in the system, the voltages at loads 2 and 3 as well as the primary of the MVB is plotted in figure 7.7. The switching events of this simulation are found in table 7.3 below.

Event	**t [s]**
Motor connection	0.5
MVB connection	0.7

Table 7.3: Switching events of simulation

After the MVB is connected it uses approximately 200ms to clear any transients (the transient increase can be neglected). Notable values are found in table 7.4. As shown in the figure, the measurements are done such that the only factor affecting the voltage is the presence of the MVB.

The voltage drop difference at the primary of MVB illustrates the effect of how the different $\frac{R}{X}$ ratio of distribution cables and overhead lines differ. I.e., right before the MVB a 640 m long line segment of Al70 is installed, which haves a $\frac{R}{X}$ factor of 0.8, which is why the relative voltage drop with and without the MVB is greater here than at load 2 and load 3. The active and reactive power consumption of this line can found in the next paragraph.

Location	$\mathbf{V_0}$ **[pu]**	$\mathbf{V_{MVB}}$ **[pu]**
Load 2	0.93	0.90
Load 3	0.91	0.88
Primary MVB	0.86	0.74

Table 7.4: Voltages at load 2, load 3 and primary of MVB with and without MVB connected.

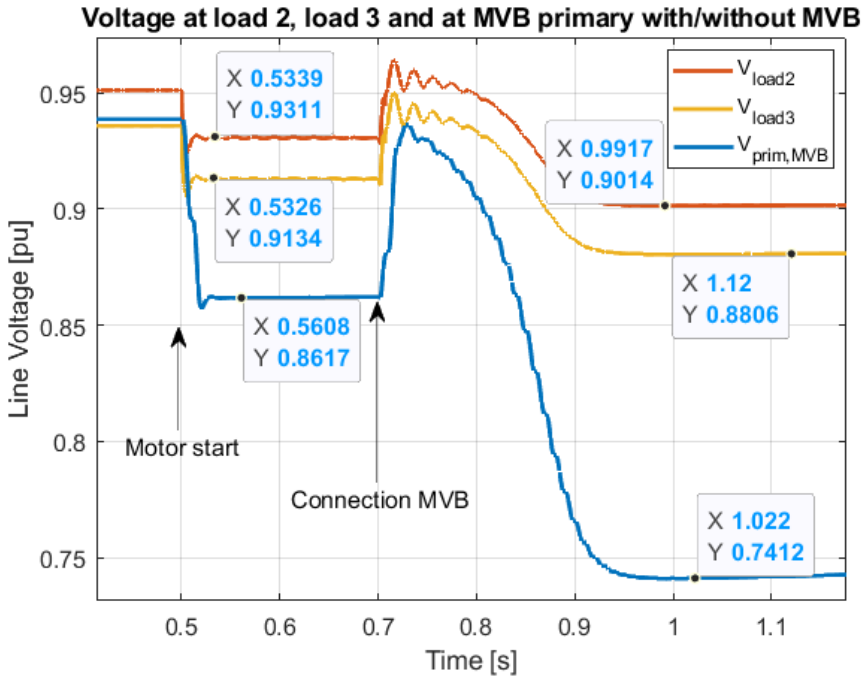

Figure 7.7: Voltages at load 1, load 2 and primary of MVB with and without MVB connected

Active and Reactive Power Consumption of Line 9

The active and reactive power consumption of line segment 9 with and without the MVB connected can be seen in figures 7.8a and 7.8b respectively. The line in question is of the Al70 type with a length of 640m. According to the line data from 9.1, the $\frac{R}{X}$ factor of this line is roughly 0.8, which seems accurate looking at the losses. There is a significant difference in the losses which can be explained by taking into consideration the increased current drawn by the MVB, and that the losses are proportional with the square of the current.

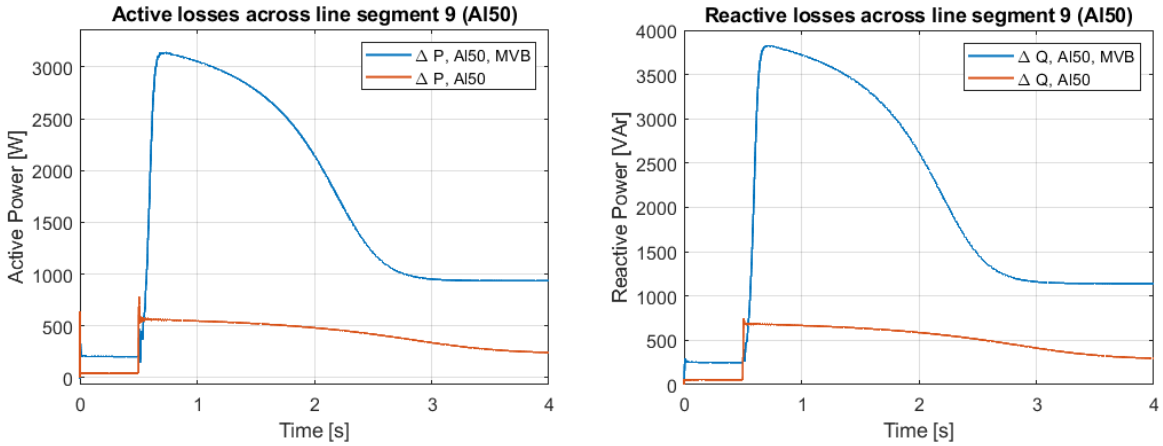

(a) Active power losses.

(b) Reactive power losses.

Figure 7.8: Losses across line segment 9

7.3 Induction Motor Start with implemented DVR

7.3.1 Voltages and Distortions

The motor is connected at $t = 0$s and the DVR is connected at $t = 0.2$s.

The voltages on the primary and secondary side of the voltage regulator are presented in figure 7.9 below. The bus voltages of the whole system are presented in figure 9.2 in Appendix B. From the same figure it can be seen that the voltages upstream of the DVR are not impacted in anything but some added noise from the VSC. The noise can be seen from figure 7.11 below, and is prone to further discussion.

The LVR is tuned such that the dynamic response is set to roughly 150ms during full load as can be confirmed by the voltage response. The transient increase which can be observed during the connection is assumed to be a switching transient in accordance with the connection of the injection transformer. The voltage is fully restored to 1 pu, but at the moment the machine has

fully started, the output voltage overshoots and stabilizes at 1.05 pu. This stable overshoot is peculiar as the sequence analyzer which governs the controller is giving another value as seen in figure 7.10. The voltage is measured at the very same point.

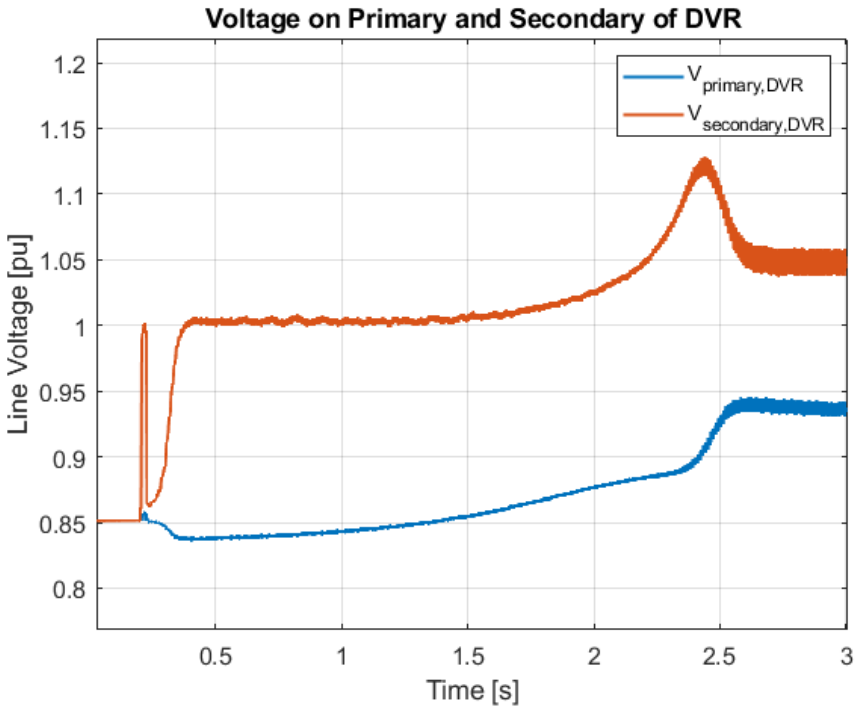

Figure 7.9: Voltages measured on primary and secondary side of DVR during induction machine start.

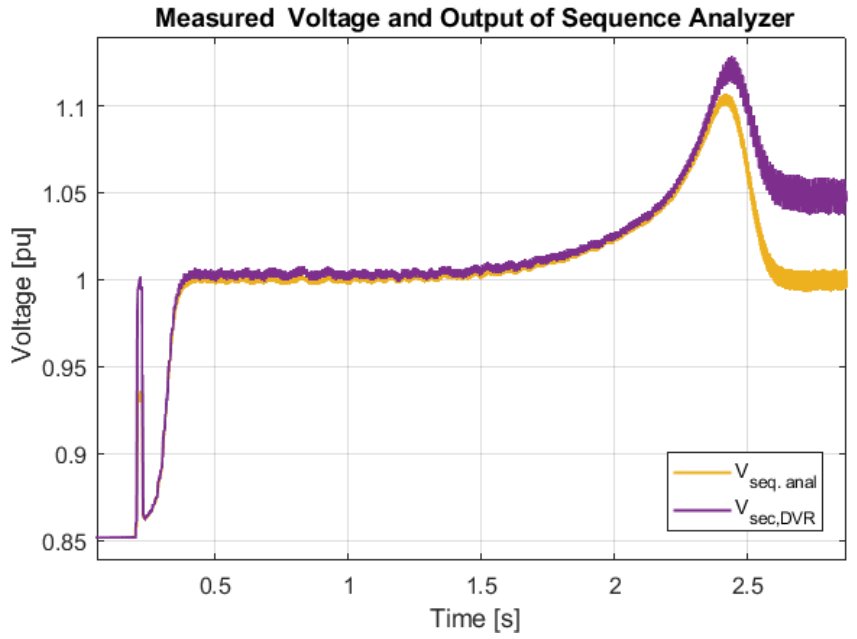

Figure 7.10: Measured voltage at secondary side of DVR and magnitude output of the phase sequence analyzer.

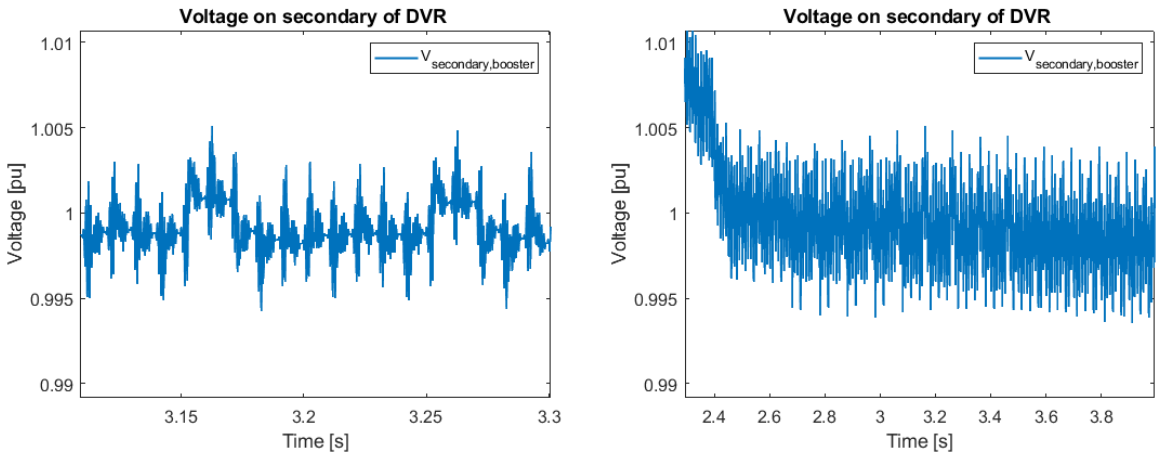

(a) Voltage at load 1 during LVR in operation.

(b) Same signal as figure on left, but zoomed in.

Figure 7.11: Voltage at load 1 during operation of the DVR, zoomed in such that the noise is visible.

7.3.2 Active and Reactive Power

The injected active and reactive power by the DVR is plotted in figure 7.12 below. At the end of the startup ΔQ is negative. This means that the delivered reactive power measured on the input is greater than the output, suggesting that the transformer is consuming some reactive power from the grid.

The power consumption of the induction machine during startup with the DVR connected can be seen in figure 9.5 in the Appendix.

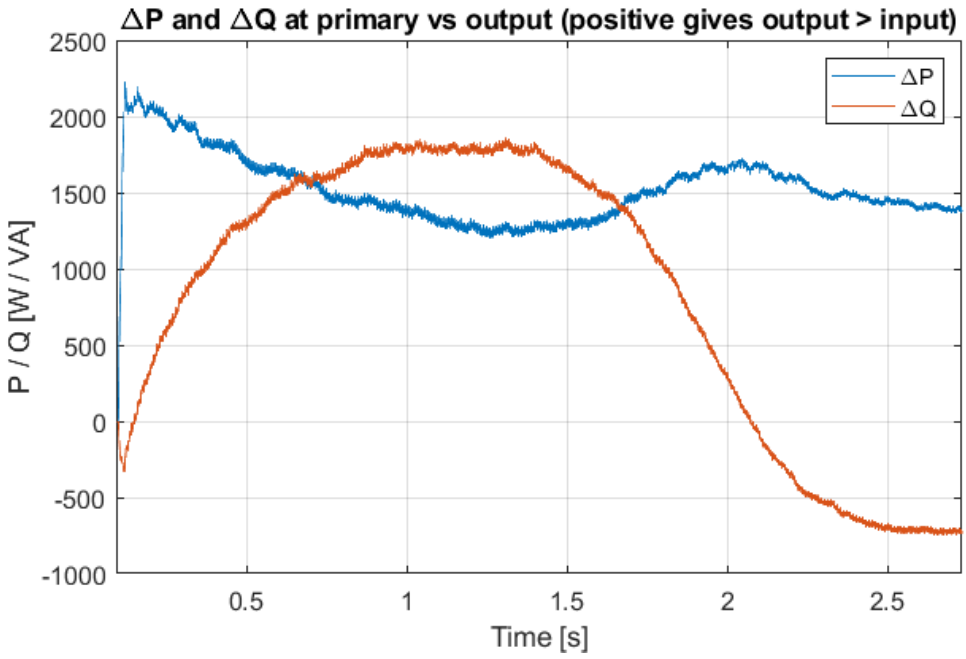

Figure 7.12: Injected power by DVR. Positive value gives output $>$ input.

Active and Reactive Power Consumption of Line 9

The active and reactive power consumption of line segment 9 with and without the DVR connected can be seen in figures 7.13a and 7.13b respectively. These figures confirm that the power losses over this line with the DVR connected are significantly reduced in comparison with the MVB scenario, since the DVR is not consuming any extra current of magnitude.

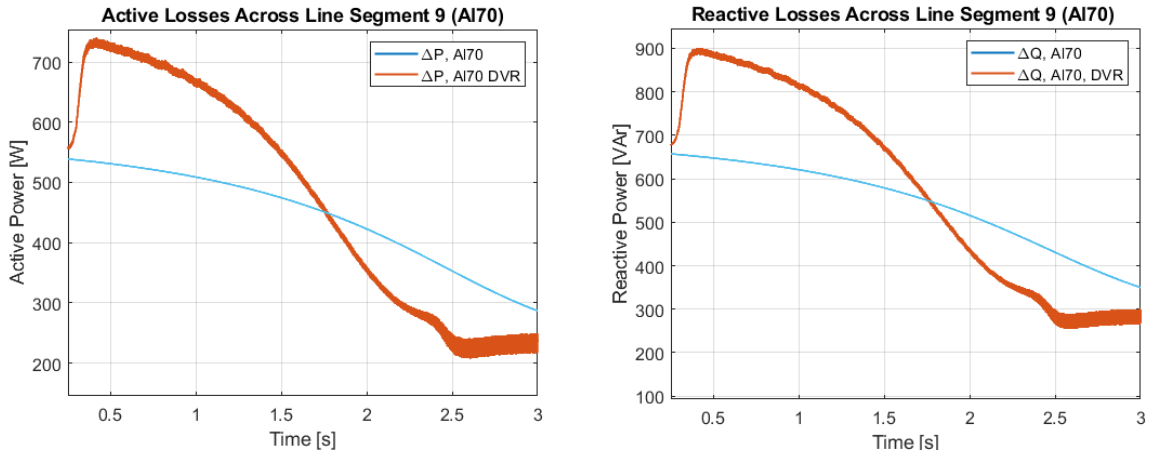

(a) Active power losses.

(b) Reactive power losses.

Figure 7.13: Losses across line segment 9 with and without the DVR connected

Chapter 8

Analysis and Discussion

In this section, the results will be discussed individually for all three scenarios, and in a broader context concerning voltage regulation in low voltage distribution networks.

8.1 Scenario 1 - No Regulation Device

As can be seen from the results, and already mentioned, the induction machine start in this simulation introduces significant voltage drops all across the system, which in turn can lead to voltage instability. The transient power consumption of the modelled induction machine is reduced by increasing the impedance of the machine in order for the modelled voltage regulators to compile. A real machine has the potential of consuming 6-7 pu of the rated power during startup, further emphasizing the significance of the induction motors behaviour in weak distribution grids.

8.2 Scenario 2 - With Implemented MVB

The MVB as well as the modelled DVR, are both controlled by a PI regulator system with a manual setpoint of parameters. This implies that the dynamic response is fully controllable, giving the measured result of 200ms to be expected.

By analysing the active and reactive power measurements on the input from figure 7.6, it should be noted that the power factor is varying during the startup, but is drastically decreased in the first transients of the induction motor startup. The power factor is roughly 0.56 before and after the machine is started, which corresponds to the results from the specialization project - where the power factor have minor variations if the load changes are subject at the secondary of the booster. The secondary voltage is recovered as expected and the induction machine starts up

quite cleanly with the MVB, further emphasizing that the model works.

In the voltage response, the known phenomena where the voltage drop on the secondary is greater than the primary is present [11]. In the simulations, the initial voltage drop during connection of the induction motor before the controller reacts is measured to roughly 0.3 pu on the secondary side, while the voltage drop on the primary is measured to 0.74 pu. The value of 0.3 pu is an anomaly with the model (which has been elaborated upon in [11]), and should not be given too much consideration. However, the measured voltage at the primary of 0.74 pu is of particular interest.

This value is significantly lower than the lowest measured voltage with the DVR implemented and showcases that the reactive power consumed by the MVB is of importance, which also can be seen by figure 7.7 and table 7.4. The reactive power consumption introduces additional voltage drops which increase with decreasing $\frac{R}{X}$ factor. The line segment prior to the MVB is a 640m long Al70 with $\frac{R}{X}$ ratio of roughly 0.8 (table 9.1 in Appendix). The active and reactive power consumption at this line segment with and without the MVB connected, as well as with and without the DVR, is visualized by figures 7.8a - 7.8b and 7.13a - 7.13b respectively. The power losses increase with the square of the current according to $S_{loss} = I^2Z$ where Z is the line impedance.

From the specialization project, it could also be recalled that the MVB failed to boost the voltage if the primary voltage was below roughly 80%, further emphasising that the total voltage drop at the terminals of the MVB has to be above this value, even in operation. Additional voltage drops are measured at loads 2 and 3 which further indicated the problematic impact of the device.

Summarized

In general, the MVB by its general design works splendidly to boost the voltage utilizing the MCI, and is best suited in grids where the degree of voltage transients and the SCC is low. This implies that the system impedance of the grid seen from the sensitive load is too large due to the sheer length and quality of the distribution lines/cables. The MVB can then boost the voltage, with small consequences in the grid as a whole as long as the $\frac{R}{X}$ factor is greater than 1. The MVB is constantly consuming reactive power during operation which leads to additional voltage drops in the system which increases with decreasing $\frac{R}{X}$. Possible solutions to solve the reactive voltage drops across the Al70 line could be by installing a series capacitor to offset the reactance, but most likely not realistic due to economic considerations.

Simply put, the MVB should be installed in a grid where the additional reactive power does not

lead to additional problems for other loads, and there is a problem with consistent undervoltages during peak loads. The general location of undervoltages are far downstream in the grid where the SCC is low, whereas the MVB is usually utilized before one or two households since voltage regulation at the distribution transformer can introduce overvoltages at loads upstream.

8.3 Scenario 3 - With Implemented DVR

Similarly to the MVB, the DVR is controlled by a PI regulator with set parameters such that the dynamic response is approximately 150ms. This can be seen by 7.9. In the models, it is important to note that the PI controller can be tuned as wished. It is already mentioned that a power electronics based regulator (FACTS device) is among the fastest applications for equalizing voltage sags and swells, and can be observed by how fast the DVR reacts to the voltage sag introduced by the induction machine. Tuning the regulator to operate even faster could have been done as well as connecting it quicker.

The voltage response on the primary and secondary side of the DVR is found in figure 7.9. The temporal overshoot which occurs at the moment of connection is neglected and assumed to be a controller/transformer transient. The voltage on the secondary side is restored to 1 pu during the startup of the machine before the DVR further injects until the secondary voltage is measured at 1.05 pu after the machine is fully started. The reasons why the DVR is overshooting the reference of 1 pu after the machine is started is a bit unclear since the phase sequence analyzer is measuring the voltage at 1 pu and not 1.05 pu according to figure 7.10. The cause probably lies in the measurement method of the sequence analyzer.

The degree of noise is much more substantial with the DVR implemented compared to the MVB, which is natural due to the implementation of the VSC. Noise and harmonics occurring as a result of the implementation of power electronics based devices are well-known phenomena. According to FoL [21], there are several restrictions regarding the generation of harmonics and noise, which can lead to voltage instability and general problems with electrical devices connected to the grid. I.e., there is measured significant noise on the electrical torque of the induction machine with the DVR connected, which can cause unneccesary wear and tear on the machine in the long run. The noise can be reduced by adjusting regulator parameters, changing the VSC parameters as well as implementing filters (though expensive) as explained in chapter 3.

Looking at the active and reactive power injection by the DVR from 7.12, it can be observed that the magnitude of injected active and reactive power is not constant. However, the injected

values are enough to sustain the voltage over the load close to 1 pu. The explanation of the varying active and reactive power injection lies in how the DVR is modelled. By utilizing the in-phase compensation method as explained in chapter 3 the DVR injects voltage in phase with the existing voltage to restore the magnitude, but not the phase itself as shown in figure 3.4a. As the power consumption of the induction machine varies according to its startup characteristics, the DVR is simply injecting power according to the voltage angle at load 1, giving a voltage input at a variable angle. It should be noted that the DVR is consistently injecting the missing voltage supported by around 1.5-2.0 kVA of power, and is enough to successfully boost the voltage from 0.85 pu to the reference of 1 pu.

Measures to deload the line can also be achieved with the DVR through more advanced control, such that the DVR supplies even greater amounts of necessary power - further decreasing the power consumed from the grid. Besides, choosing different capacitance rating of the capacitor as well as the voltage across the energy storage affects the performance of the device.

A FACTS based series voltage regulator such as the DVR is more robust and effective than LVRs of the switching or MCI type during situations of transient activity leading to great voltage sags. This is due to the installed energy storage device on the DC side that supply the active power (which is assumed charged during times of low power demand). Further, since the DVR (ideally) is not consuming any reactive power during its operation, induced voltage drops at other locations upstream of the device are avoided, contrary to the MVB. However the injection transformer will consume some amounts of reactive power due to its internal impedance as shown in figure 7.12.

The reactive power needed for compensation is produced by the device, and the active power needed to fully recover the voltage during large contingencies is available as long as there is capacity in the energy storage. This is of major importance comparing the device to the MVB, as the MVB consumes reactive power from the grid to support the injected voltage. The fact that the DVR can support limited quantities of active power however emphasizes the fact that the DVR should not be used for continuous compensation of active power losses of the line or the load.

The DVR is by the completed simulations working as it should by utilizing the series-connected transformer and injecting the missing voltage backed by the required active and reactive power supported by the capacitor and the energy storage on the DC side of the VSC. However, the control of the VSC could have been even more profound. I.e., by decoupling the currents into the $dq0$ plane by the park transformation, it would be more seamless to control both the active and reactive power injection separately.

Summarized

Installing fast-acting regulation devices such as the modelled DVR is a great choice to mitigate large temporary voltage transients caused by i.e., an induction motor start, and can according to literature even be used to counteract harmonic distortions created by other installations at consumers. Additionally, the DVR can be used to support important loads from temporary short circuits upstream for a limited amount of time as long as there is capacity in the energy source supplying the active power. This is a major advantage comparing the DVR to the MVB since the latter is heavily dependent on reactive power consumed from the grid to control the injected voltage. The DVR is only dependent on the VSC and the capacity of the energy storage, meaning that the induced voltage impacts upstream in the grid can be drastically reduced in addition to relieving stressed line segments in the grid.

Installing a regulation device of this nature may not however be the best solution for a grid with low short circuit capacity due to high system impedance, contrary to the MVB or other LVR types. This is mainly because active compensation requires available stored energy in the energy storage, like a charged battery. In a distribution grid with mostly $\frac{R}{X} > 1$ and low SCC, the voltage is subject to crossing the undervoltage barrier of 10% at full load due to active power losses over greater periods of time which the energy storage is depleted. In this case, the MVB is the better choice due to its consistent voltage performance during steady-state operation and its economic advantage. The DVR is though more robust and can be used for unlimited reactive power compensation (limited by the power rating of the device), but it should again be noted that devices based on FACTS technology are significantly more expensive than more simple installations like LVRs based on tap changing or the MVB, and the increased voltage drop and stress on lines are often acceptable compared to the extra cost of investment.

The voltage regulators modelled in this thesis are meant for localized regulation downstream in older low voltage grids. Proper coordination between different voltage regulation measures such as the impact of OLTC distribution transformers in union with more local devices such as shunt connected FACTS devices and series-connected LVRs is an exciting topic as every single grid is unique in different ways. In the future with the implementation of even more DG units, devices based on FACTS technology in union with energy storage has a unique property of storing excess energy during situations with low consumption and high production, instead of installing reactive sinks that simply consume energy instead of utilizing it effectively.

Another important consideration is the impact of the short circuit currents which can occur

during faults, where series installed voltage regulators of the LVR type have a negative effect on this current - making it even smaller, introducing selectivity problems in the calibration of relays and fuses. Both the MVB and the DVR have bypass switches that ideally bypasses the short circuit current after a set amount of time, but properly calibrating these measures are no easy task - and with the main goal of these devices to be as cost-effective as possible, it is crucial that the degree of modularity is high. This topic is not profoundly treated in this thesis, but measures to apprehend this problem is of vital importance regarding the safety of supply during load. Further researching this field of study with emphasis on bringing a greater understanding of the implications of installing voltage regulation devices concerning relay and fuse selectivity is an interesting and deeply relevant topic for future studies.

Chapter 9

Conclusion

One of the goals of this thesis was to compare the performance of the two implemented SVRs on a scientific basis in the modelled distribution grid. A modelled 4 kVA induction motor is connected in parallel at load 1 to simulate a taxing dynamic voltage distortion to properly challenge the voltage regulators. According to the simulations, both the DVR and the modelled MVB manages to successfully regulate the voltage back to its reference, but there are significant differences in how the applications impact the grid as a whole during operation.

Due to its nature, the MVB is consuming significant amounts of reactive power from the grid during operation which effectively introduces new voltage drops in the system. This trend increases with the decreasing $\frac{R}{X}$ factor of the network impedance. During the machine startup, the voltages at the primary of the booster, load 2 and 3 are experiencing notable voltage drops which is a direct result of the consumed reactive power. The difference is largest at the primary of the booster, where the difference is 0.74 pu with the MVB connected and 0.86 pu without, which is explained by the Al70 line spanning before the MVB with a $\frac{R}{X} = 0.8$, highlighting the reactive losses.

The DVR on the other hand injects voltage through the means of the internal VSC and can supply active compensation due to its design with an energy storage connected on the DC side of the converter. The DVR does not introduce additional voltage drops like the MVB since the reactive and active power needed to control the injected voltage is supplied from the device itself. This makes the DVR potent for protecting sensitive loads during taxing dynamics, even sustaining voltage over the load if a short circuit upstream in the grid occurs. The limiting factor is the power rating of the device as well as the capacity of the energy storage. For the DVR to contribute with active power to restore the voltage, however, it's crucial that there is available energy in the energy storage. I.e., the energy storage has to be charged by the grid, and should be charged during periods of low load.

As a result, the DVR is not well suited in a grid where the SCC is low with a resistive $\frac{R}{X}$ factor where undervoltages can occur consistently due to active power losses through the lines at full load. In this case, the MVB is the better choice due to its consistent voltage performance during steady-state operation and the lower cost. The DVR is though more robust, but it should be noted that devices based on FACTS technology are significantly more expensive than installations like LVRs based on tap changing or the MVB. The increased voltage drop and stress on lines are often acceptable compared to the extra cost of investment, especially since installing these devices are supposed to be a cheaper alternative to reinvesting in the infrastructure of the grid itself.

Through the theory which is presented and the simulations that are done, it can be concluded that SVRs like the MVB and DVR works splendidly to boost the voltage downstream in a grid where the degree of voltage transients and short circuit capacity is low, giving undervoltages that consist over time. This holds as long as the reactive power consumed by the regulator does not initialize further voltage drops of significance due to the low $\frac{R}{X}$ factor of the network impedance. The DVR will not function properly in situations which consistently requires active power compensation since the capacity of active power often is limited. The DVR is, however, operating fast with great precision. No voltage drops are introduced upstream due to reactive consumption and are a great alternative to effectively mitigate any sudden voltage sags, harmonics and general transient behaviour. Introducing the DVR in grids with problems like the ones previously mentioned can be of great help, especially coupled with energy storage systems such as batteries.

9.1 Further Work

The two modelled series voltage regulators are both viable devices, but there exist a number of other technologies such as other shunt connected FACTS devices like the STATCOM and the SVC. In [15] a similar study was done with the STATCOM, yielding quite good results. Modelling an SVC in a similar environment as done in this thesis would be interesting.

Conducting further modelling studies with the DVR, removing assumptions and properly implementing a more robust control system would make the model even more precise, yielding better results in the simulations. The same can be said about the MVB, as the implemented model clearly has weaknesses compared to the real-life tested device according to [11].

Repeating the last paragraph from the discussion:
Another important consideration is the impact of the short circuit currents which can occur during faults, where series installed voltage regulators of the LVR type have a negative effect on this current - making it even smaller, introducing selectivity problems in the calibration of relays and fuses. Both the MVB and the DVR have bypass switches that ideally bypasses the short circuit current after a set amount of time, but properly calibrating these measures are no easy task - and with the main goal of these devices to be as cost-effective as possible, it is crucial that the degree of modularity is high. This topic is not profoundly treated in this thesis, but measures to apprehend this problem is of vital importance regarding the safety of supply during load. Further researching this field of study with emphasis on bringing a greater understanding of the implications of installing voltage regulation devices concerning relay and fuse selectivity is an interesting and deeply relevant topic for future studies.

Bibliography

[1] a eberle. Datasheet - lvrsys^{TM}. www.a-eberle.de. (Accessed on 10/12/2019).

[2] B. J. Baliga. *The IGBT device: physics, design and applications of the insulated gate bipolar transistor*. William Andrew, 2015.

[3] G. Celli, F. Pilo, G. Pisano, V. Allegranza, R. Cicoria, and A. Iaria. Meshed vs. radial mv distribution network in presence of large amount of dg. In *IEEE PES Power Systems Conference and Exposition, 2004.*, pages 709–714. IEEE, 2004.

[4] M. H. Center. Model the dynamics of three-phase asynchronous machine, also known as induction machine - simulink. https://www.mathworks.com/help/physmod/sps/powersys/ref/asynchronousmachine.html. (Accessed on 16/05/2020).

[5] Circuitglobe. What is series compensation? advantages & location of series capacitors - circuit globe. https://circuitglobe.com/series-compensation.html#:~:text=Series%20Compensation,the%20impedance%20of%20the%20system. (Accessed on 10/06/2020).

[6] E24. Bygger kraftlinjer for 140 mrd. https://e24.no/energi/i/rL646w/bygger-kraftlinjer-for-140-mrd. (Accessed on 16/12/2019).

[7] EnergiNorge. Ansvar for nettdrift må desentraliseres. https://www.energinorge.no/fagomrader/stromnett/nyheter/2018/ansvar-for-nettdrift-ma-desentraliseres/. (Accessed on 16/12/2019).

[8] EnergiNorge. Drift og utvikling av kraftnettet – utforming av dso-rollen. https://www.energinorge.no/contentassets/2858551aafa94bb798d89a8edf15a42b/drift-og-utvilkling-av-kraftnettet---rapport-05-12-2018.pdf. (Accessed on 16/12/2019).

[9] Enova. Solenergi — enova. https://www.enova.no/privat/alle-energitiltak/solenergi/. (Accessed on 02/12/2019).

[10] eSmartSystems. Effektiv nettdrift i en digital verden. https://response.esmartsystems.com/effektiv-nettdrift-i-en-digital-verden. (Accessed on 18/12/2019).

[11] A. Festøy. Voltage regulation in low voltage distribution grids - a study of different technologies and implementation of the magtech voltage booster, December 2019.

[12] G. Herold. Why is resistance of a transmission line negligible and the resistance of a distribution system is considered to be predominant? https://bit.ly/2AbmDOg. (Accessed on 06/06/2020).

[13] M. Holt, J. Maasmann, and C. Rehtanz. Line voltage regulator based on magnetic-controlled inductors for low-voltage grids. *CIRED-Open Access Proceedings Journal*, 2017(1):278–281, 2017.

[14] M. Issa, H. Ibrahim, A. Ilinca, R. Lepage, and M. Ghandour. Integrated a variable frequency drive for a diesel generating set using the genset-synchro concept. *International Journal of Engineering and Technical Research*, 8:232–239, 08 2019.

[15] A. S. Karoui. Short circuit capacity improvement tecniques for low voltage distribution grid, June 2018.

[16] H. Kirkeby and H. Seljeseth. Utfordrende elektriske apparater. *Sintef Energi AS,[Internett]. Available: http://www. sintef. no/contentassets/8f3be4a5285b4a7a85a2987a9d397615/rapporter/9.3 _kirk eby_henrik—utfordrende-elektriske-apparater. pdf*, 2014.

[17] M. L. Kolstad, S. Garnås, and B. N. Torsæter. *Dagens teknologi for spenningsregulering*. SINTEF, 8 2018.

[18] D. P. Kothari and I. Nagrath. *Electric machines*. McGraw-Hill Education, 2018.

[19] S. R. Kumar and S. S. Nagaraju. Simulation of d-statcom and dvr in power systems. *ARPN Journal of Engineering and Applied Sciences*, 2(3):7–13, 2007.

[20] M. L. Kolstad. Alternative tiltak for å øke tilknytningskapasitet i distribusjonsnett. 2016.

[21] Lovdata. Forskrift om leveringskvalitet. https://lovdata.no/dokument/SF/forskrift/2004-11-30-1557. (Accessed on 27/11/2019).

[22] Lovdata. Forskrift om sikkerhet ved arbeid i og drift av elektriske anlegg - lovdata. https://lovdata.no/dokument/SF/forskrift/2006-04-28-458. (Accessed on 16/12/2019).

[23] J. Machowski, J. Bialek, J. R. Bumby, and J. Bumby. *Power system dynamics and stability*. John Wiley & Sons, 1997.

[24] MagTech. Microsoft word - model overview mvb medium voltage 29.03.11 eng_rev0.doc. https://www.slo.lv/upload/catalog/vidspriegums/magtech_voltage_booster_medium_290311_eng.pdf. (Accessed on 07/11/2019).

[25] N. Mahmud and A. Zahedi. Review of control strategies for voltage regulation of the smart distribution network with high penetration of renewable distributed generation. *Renewable and Sustainable Energy Reviews*, 64:582–595, 2016.

[26] MathWorks. Generate pulses for pwm-controlled 2-level converter - simulink. https://www.mathworks.com/help/physmod/sps/powersys/ref/pwmgenerator2level.html. (Accessed on 24/06/2020).

[27] MathWorks. Implement three-phase transmission line section with lumped parameters - simulink. https://www.mathworks.com/help/physmod/sps/powersys/ref/threephasepisectionline.html#:~:text=Description,lumped%20in%20a%20PI%20section.&text=This%20method%20of%20specifying%20line,the%20three%20phases%20are%20balanced. (Accessed on 06/06/2020).

[28] N. A. Moerman. Conversion and control of electrical energy by electromagnetic induction, July 17 1979. US Patent 4,161,772.

[29] Z. Pavel and J. Ramirez. Modeling of multi-pulse vsc based sssc and statcom. https://www.scirp.org/pdf/JEMAA20100300005_20130005.pdf. (Accessed on 13/05/2020).

[30] S.-E. Razavi, E. Rahimi, M. S. Javadi, A. E. Nezhad, M. Lotfi, M. Shafie-khah, and J. P. Catalão. Impact of distributed generation on protection and voltage regulation of distribution systems: A review. *Renewable and Sustainable Energy Reviews*, 105:157–167, 2019.

[31] V. Remya, P. Parthiban, V. Ansal, and B. C. Babu. Dynamic voltage restorer (dvr)–a review. *Journal of Green Engineering*, 8(4):519–572, 2018.

[32] REN. Distribusjonsnett - tekniske verdier; nr 8041. (Accessed on 06/06/2020).

[33] REN. Ren-nytt, nr. 2 - 2017. https://www.ren.no/doc/api/rest/download/rennytt/201702, 2017. (Accessed on 19/12/2019).

[34] A. K. Sadigh and K. M. Smedley. Review of voltage compensation methods in dynamic voltage restorer (dvr). In *2012 IEEE Power and Energy Society General Meeting*, pages 1–8, 2012.

[35] P. Sarathy and P. Raghav. Analysis and optimization of medium voltage line voltage regulators. Master's thesis, NTNU, 2018.

[36] Siemens. Fitformer reg - the adaptable distribution transformer. https://assets.new.siemens.com/siemens/assets/api/uuid:d0ffd90a-9079-46e8-b3a3-09b67c2933bc/version:1563441916/fitformer-ipdf-en.pdf. (Accessed on 16/12/2019).

[37] SNL. nettsystem – store norske leksikon. https://snl.no/nettsystem. (Accessed on 07/12/2019).

[38] S. A. Taher, H. T. Fard, and E. B. Kashani. New switching approach for dvr using one cycle control method. *Ain Shams Engineering Journal*, 9(4):2227–2254, 2018.

[39] M. A. Tayyab, M. Vaziri, A. Yazdani, and M. Zarghami. Distributed generation effects on voltage profile of distribution grid with svc and smart inverter. In *2015 IEEE Power Energy Society General Meeting*, pages 1–5, July 2015.

[40] T. van Cutsem. Dynamics of the induction machine. https://studylib.net/doc/18650338/dynamics-of-the-induction-machine, November 2015. (Accessed on 13/05/2020).

[41] Wikipedia contributors. Flexible ac transmission system — Wikipedia, the free encyclopedia. https://en.wikipedia.org/w/index.php?title=Flexible_AC_transmission_system&oldid=929250576, 2019. (Accessed on 16/12/2019).

[42] Wikipedia contributors. Distributed generation — Wikipedia, the free encyclopedia. https://en.wikipedia.org/w/index.php?title=Distributed_generation&oldid=960882408, 2020. (Accessed on 12/02/2019).

Appendix

9.2 A: Line Data and other Tables

Line Type	$\mathbf{R}[\frac{\Omega}{\mathrm{km}}]$	$\mathbf{X}[\frac{\Omega}{\mathrm{km}}]$	$\mathbf{C_{line}}[\frac{nF}{\mathrm{km}}]$	$\mathbf{C_{line,ground}}[\frac{nF}{\mathrm{km}}]$
TFSP 3x150Al	0.206	0.072	0.60	1.19
PFSP 3x50Al	0.641	0.079	0.53	1.08
PFSP 3x25Al	1.200	0.082	0.42	0.82
EX95	0.320	0.076	0.52	1.09
EX25	1.200	0.082	0.28	0.55
Al70	0.256	0.312	4.48	11.91

Table 9.1: Line parameters for utilized cables/overhead lines in the test grid [32].

	Type	R/X-rate	Konfigurasjon
Lavspenning	TFXP 4x50 Al	8,11	1 kV, fireleder uten skjerm i jord
	TFXP 4x95 Al	4,21	1 kV, fireleder uten skjerm i jord
	TFXP 4x240 Al	1,74	1 kV, fireleder uten skjerm i jord
	EX 3x50 Al	8,11	1 kV, hengeledning
	EX 3x95 Al	4,16	1 kV, hengeledning
	EXW 3x150 Al	2,86	1 kV, hengeledning
Høyspenning	FeAl 35 (56-AL1/ 9-ST1A)	1,34	24 kV luftledning, 1,5 m faseavstand
	FeAl 50 (80-AL1/ 13-ST1A)	0,97	24 kV luftledning, 1,5 m faseavstand
	FeAl 95 (151-AL1/ 25-ST1A)	0,54	24 kV luftledning, 1,5 m faseavstand
	BLX 3x50	1,92	24 kV, hengeledning
	BLX 3x95	1,09	24 kV, hengeledning
	BLX 3x150	0,66	24 kV, hengeledning
	TXSE/TSLE 3x1x50 Al / 16	3,05	24 kV, flat forlegning
	TXSE/TSLE 3x1x95 Al / 25	1,60	24 kV, flat forlegning
	TXSE/TSLE 3x1X240 Al / 35	0,69	24 kV, flat forlegning

Figure 9.1: $\frac{R}{X}$ ratio of some typical overhead lines and cables in both the low and high voltage distribution grid [17].

Component	**A**	**B**	**C**	H(s)
Heat pump / AC	0.2	0	0.8	0.28
Refrigerator/freezer	0.2	0	0.8	0.28
Dishwasher	1	0	0	0.28
Clothes washer	1	0	0	1.50
Clothes washer	1	0	0	1.30
Pumps, fans, other motors	1	0	0	0.70
Small industrial motor	1	0	0	0.70
Large industrial motor	1	0	0	1.50
Power plant auxiliaries	1	0	0	1.50
Agricultural water pump	1	0	0	0.40

Table 9.2: Different constants for ABC torque model for induction machine [40].

9.3 B: Measurements and additional graphs from simulation

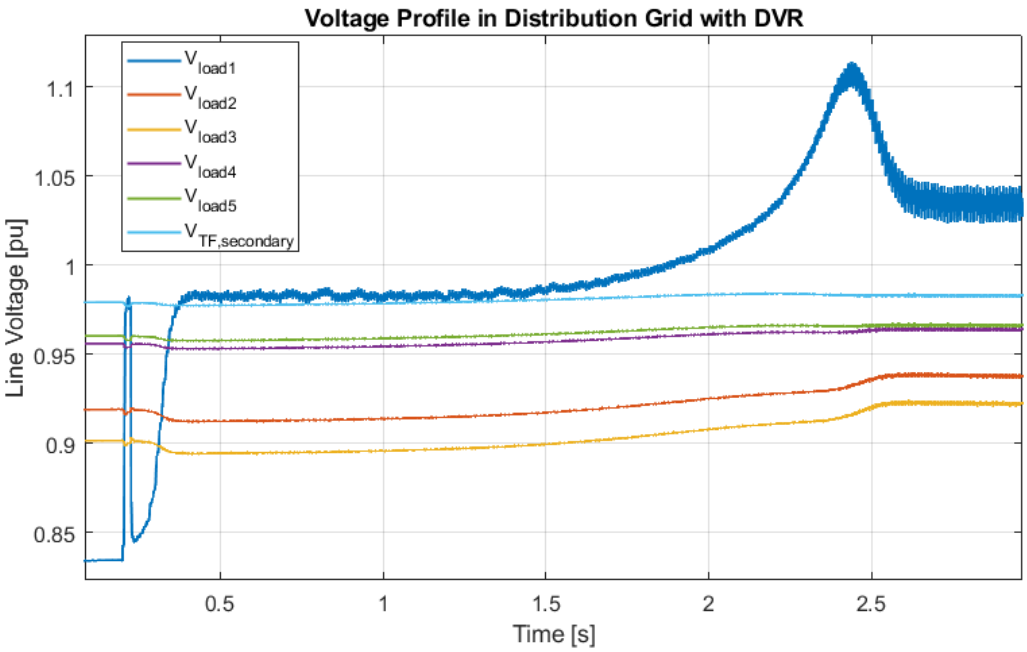

Figure 9.2: Voltage profile of the whole distribution grid during DVR connected and induction machine startup.

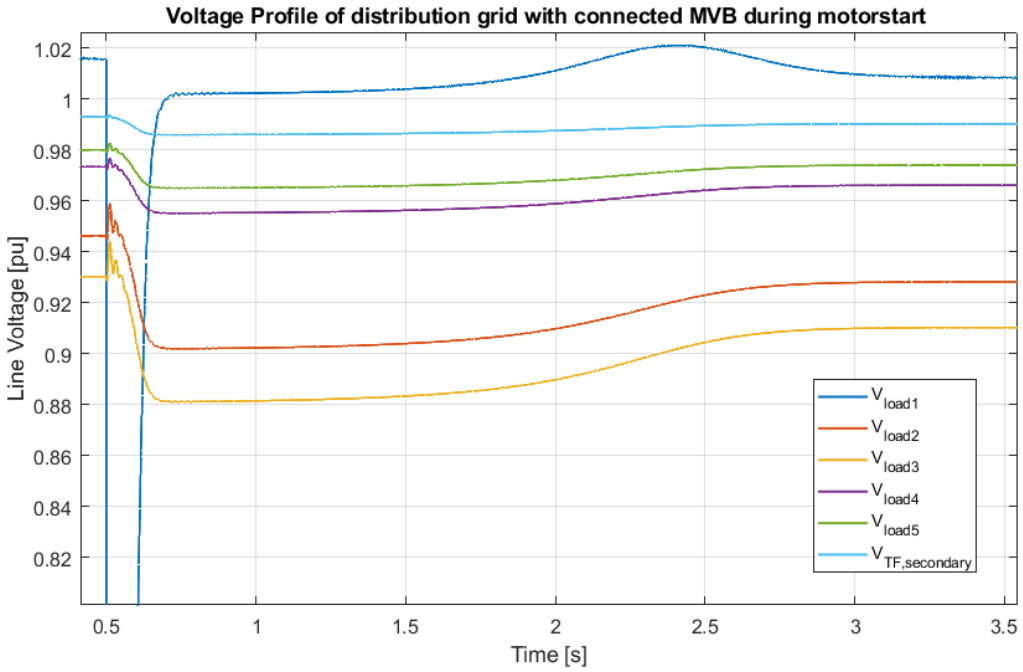

Figure 9.3: Voltage profile of the whole distribution grid during MVB connected and machine startup.

9.3.1 Induction Machine Start Power Measurements

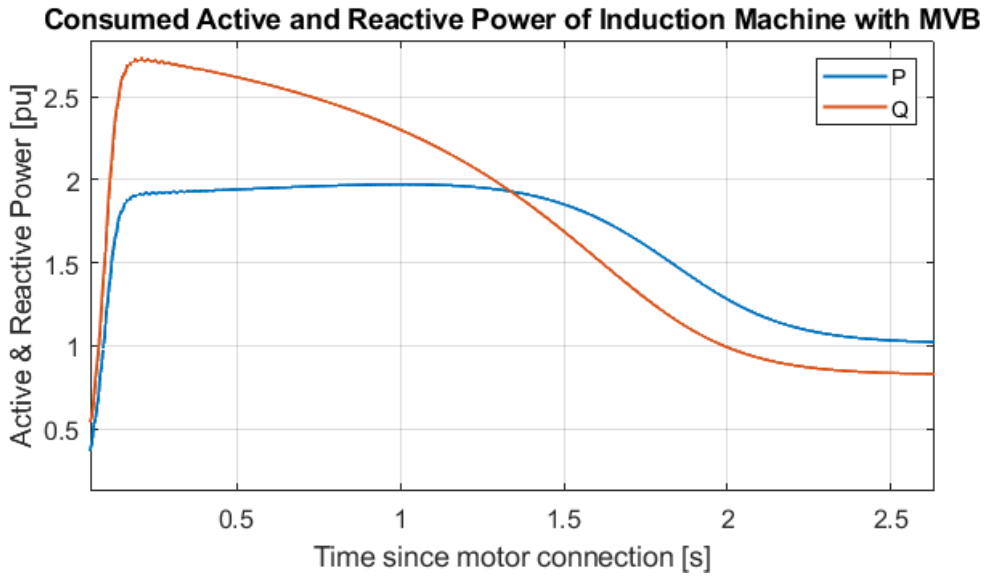

Figure 9.4: Active and Reactive Power consumption of induction machine during startup with MVB connected. $S_{base} = 4000$ VA.

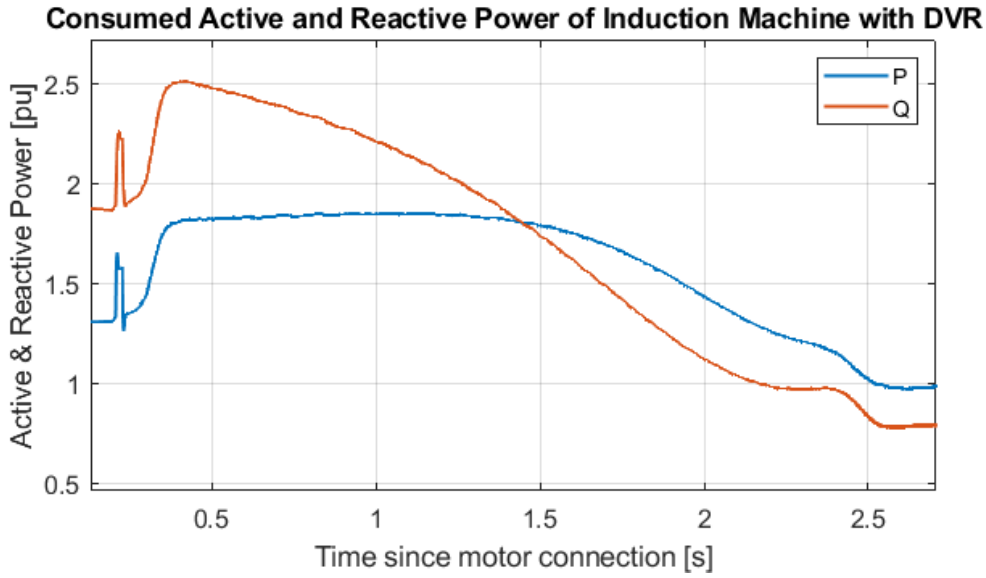

Figure 9.5: Active and Reactive Power consumption of induction machine during startup with DVR connected. $S_{base} = 4000$ VA.

9.3.2 Active and Reactive Power at input and output of MVB

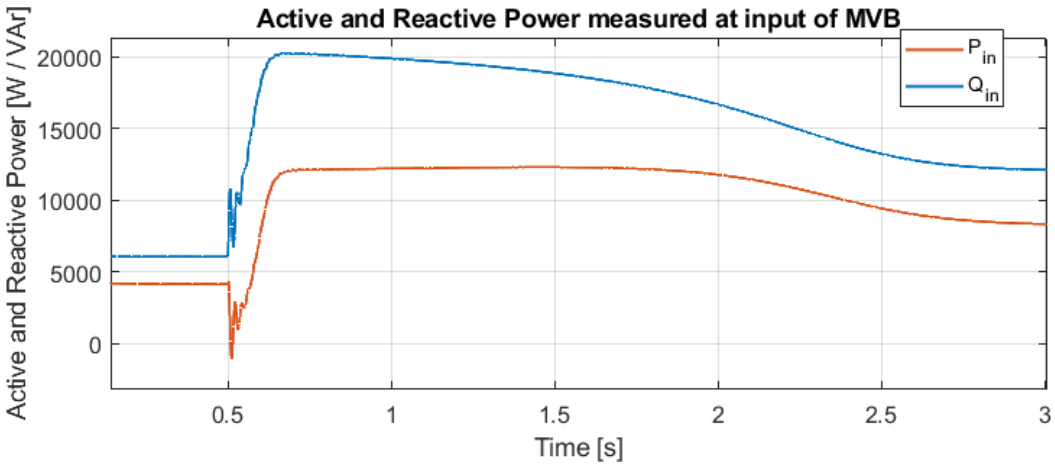

Figure 9.6: Active and Reactive Power measured at input of MVB during induction machine startup.

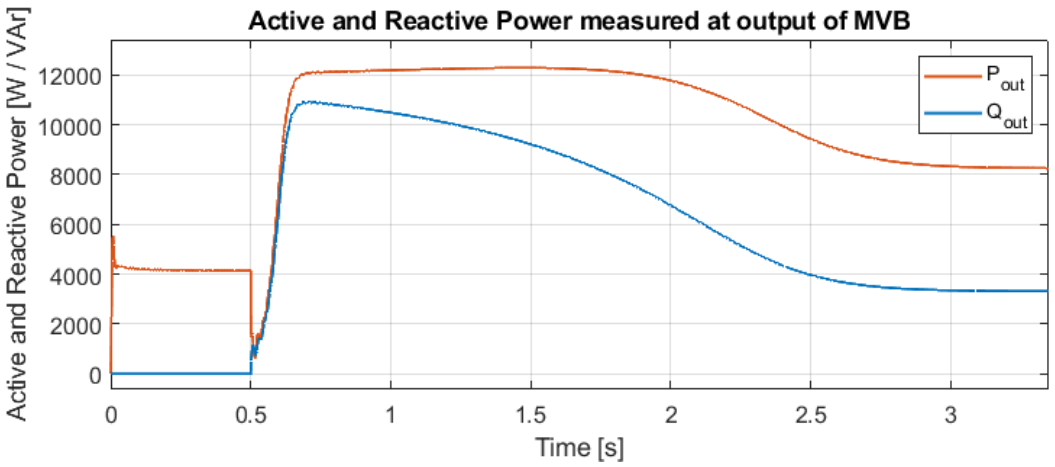

Figure 9.7: Active and Reactive Power measured at output of MVB during induction machine startup.

9.4 C: Simulink Models

9.4.1 Simscape

Modelled Grid

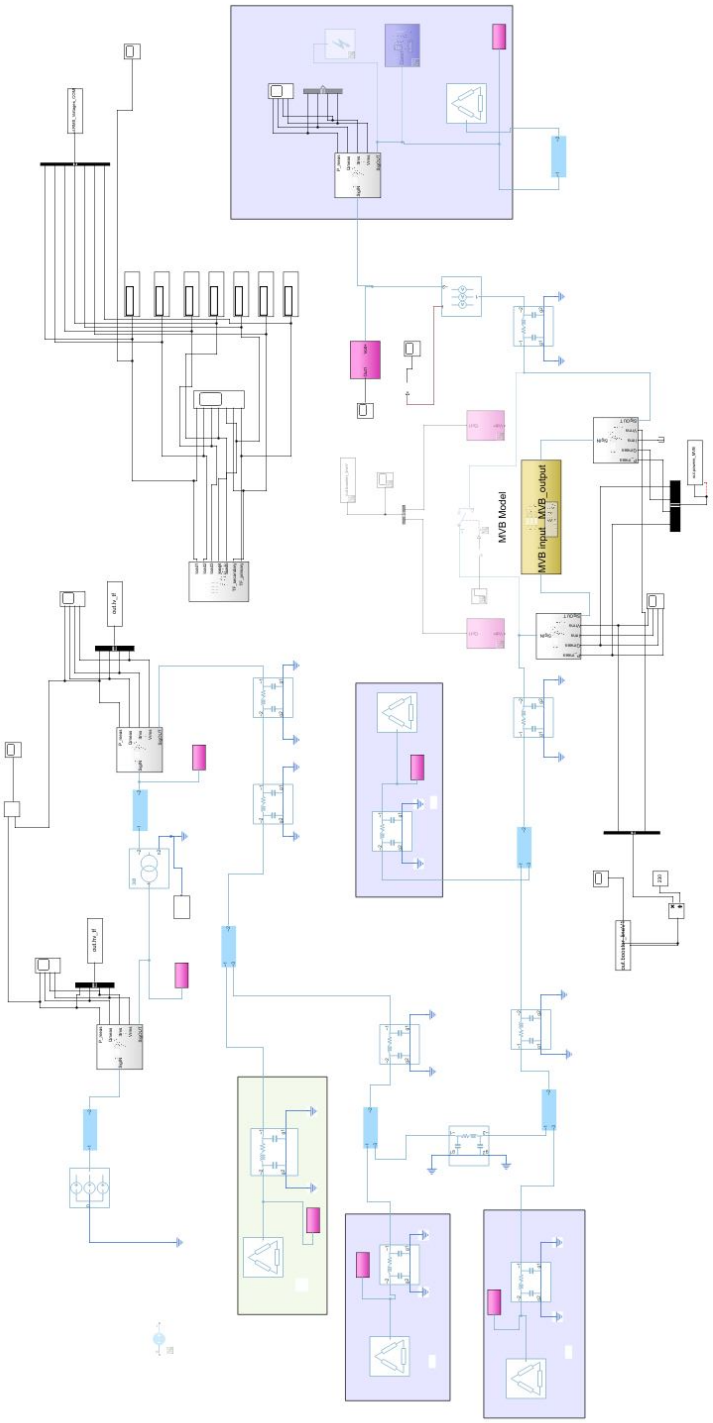

Figure 9.8: Modelled low voltage distribution network in the Simscape environment.

Magtech Voltage Booster

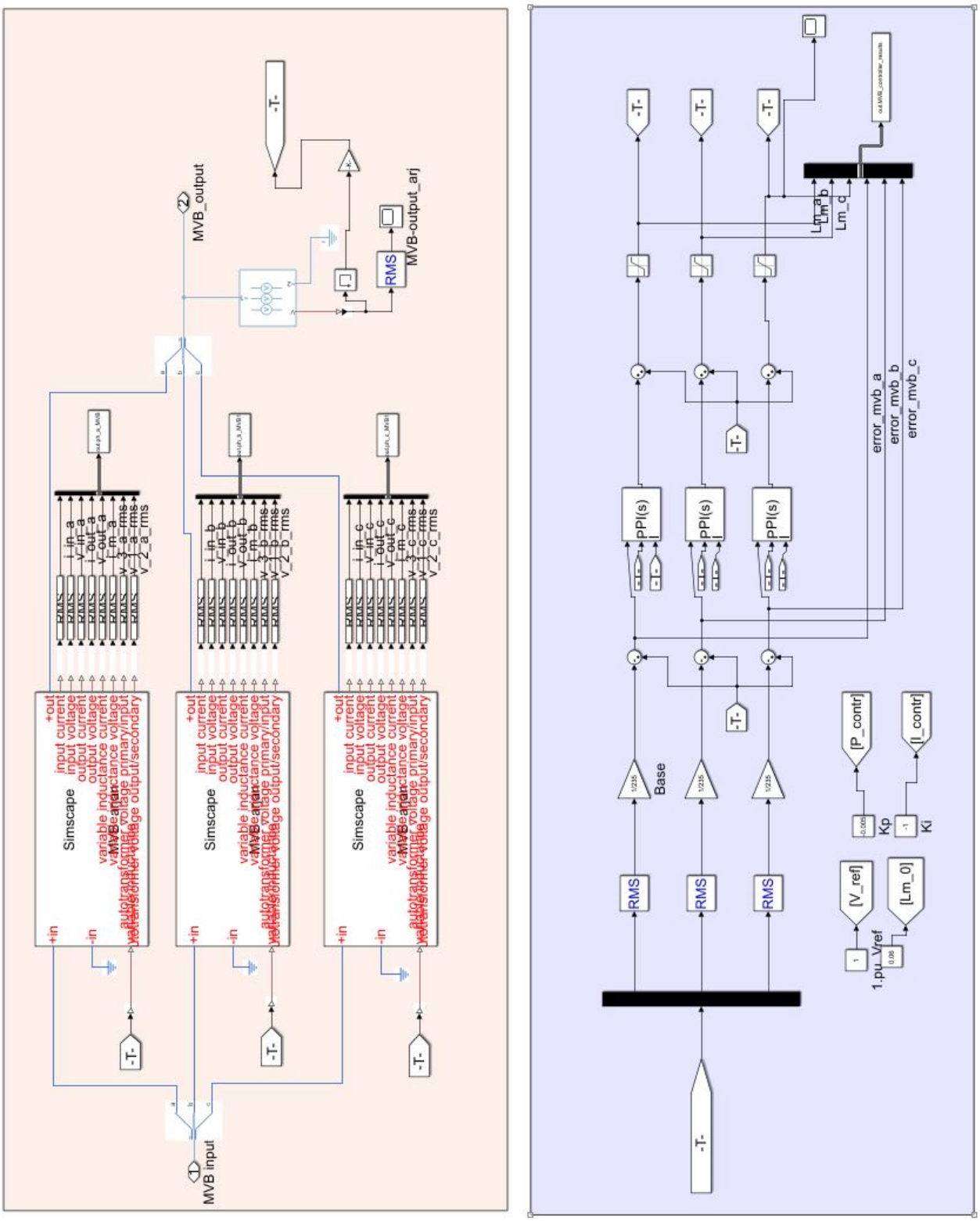

Figure 9.9: Modelled MVB and control system.

9.4.2 Specialized Power Systems

Modelled Grid

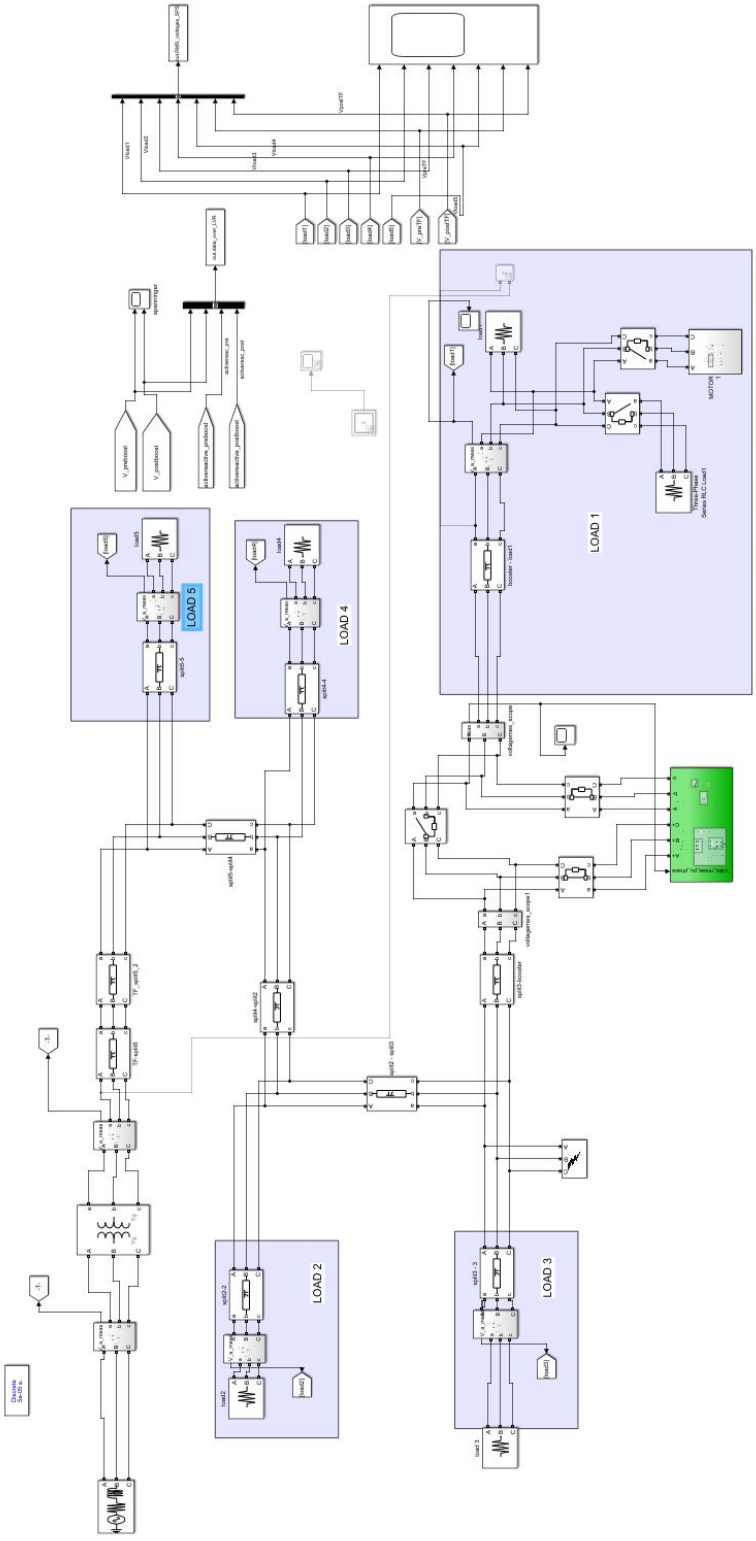

Figure 9.10: Modelled low voltage distribution network in the SPS environment.

Induction Machine Model

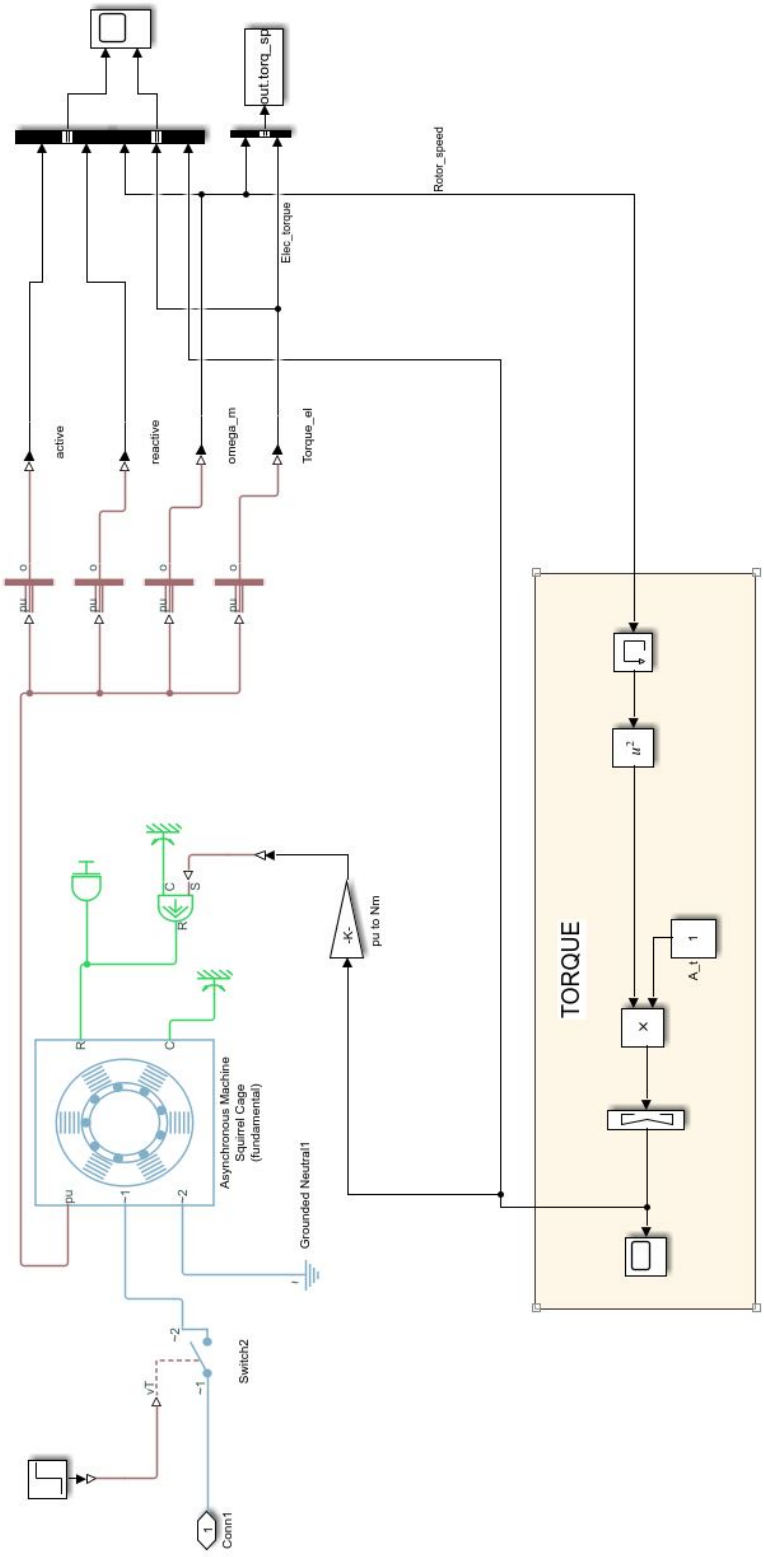

Figure 9.11: Induction Machine Model in the Simscape environment.

Dynamic Voltage Restorer - Overview

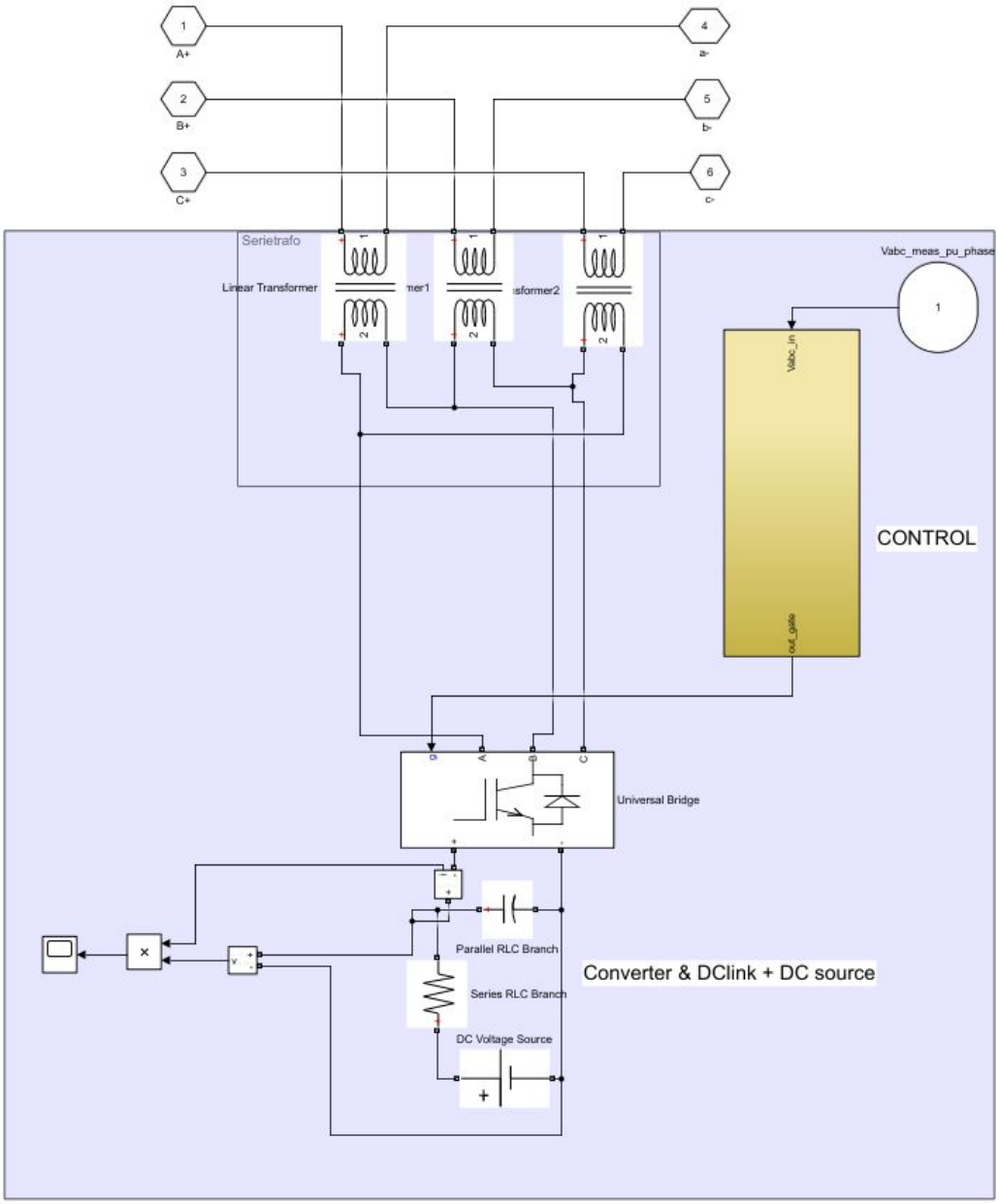

Figure 9.12: Overview of DVR model.

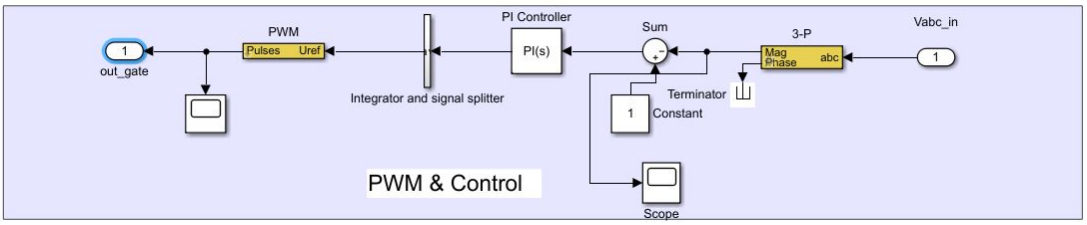

Figure 9.13: Control and PWM generator of DVR model.

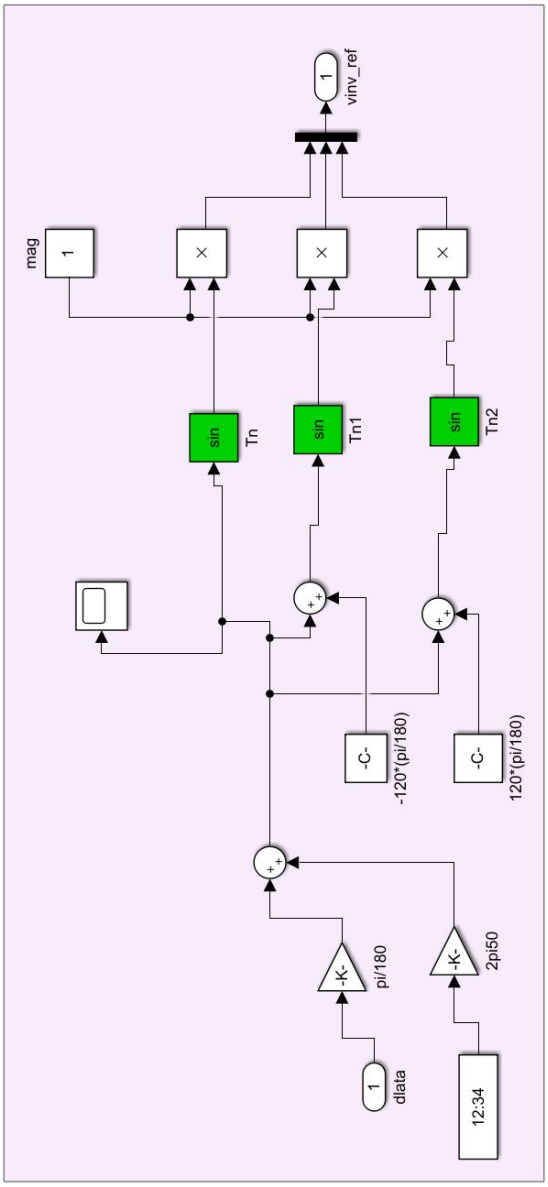

Figure 9.14: Phase modulator of DVR [19].

Induction Machine Model

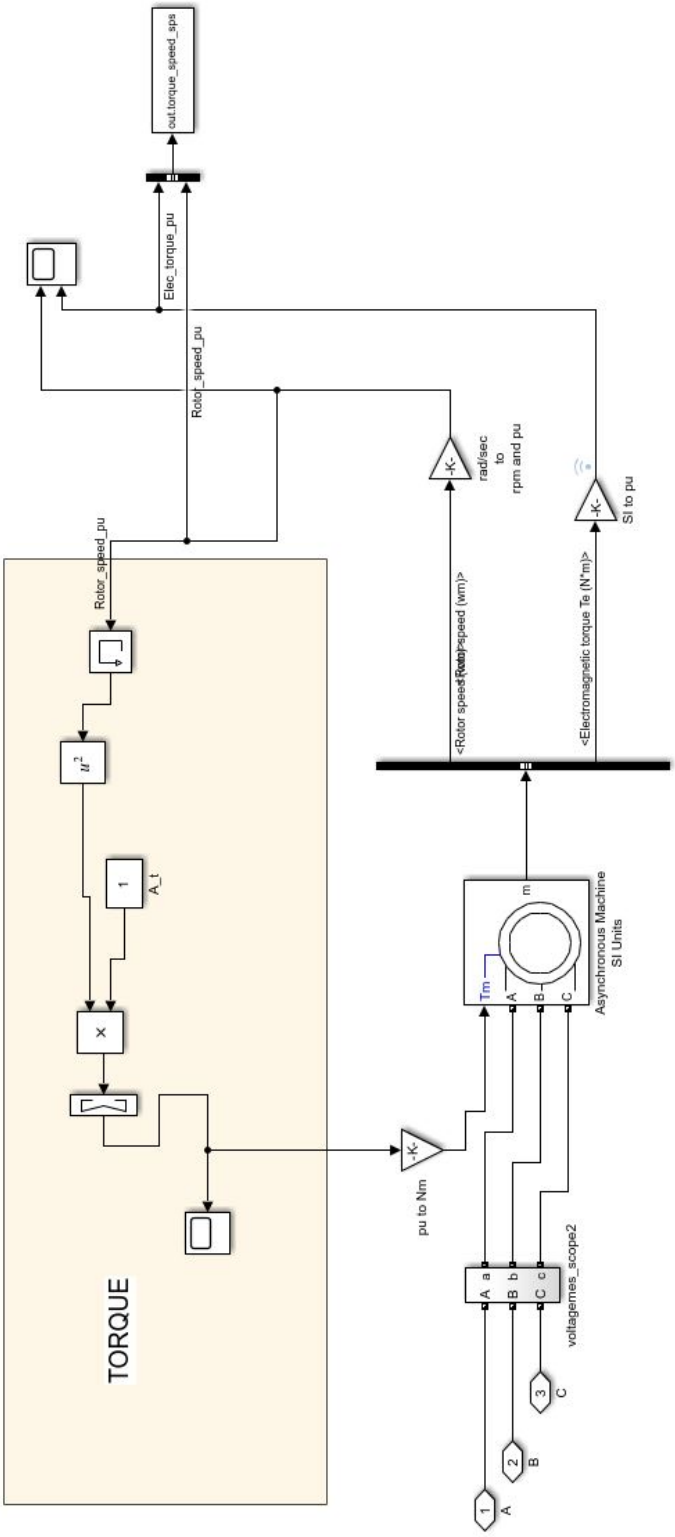

Figure 9.15: Induction Machione Model in the SPS environment.

9.4.3 Initialisation Matlab Script

Contents


```
%%Initialise testnetwork
f = 50;
S_base = 100*10^3; %VA
V_base = 230; %V,rms
Zbase_machine = V_base^2/S_base;
omega_b = 2*pi*f;
e = 10^(-9);
a = 1;


%%TF

Rprimary = 0.01;
Lprim = 0.001/(100*pi);
Rsecond = 0.01;
Lsecond = 0.01/(100*pi);
Rsat = 500;
Xsat = Rsat;
```

Induction motor pu values (Used in testing)

```
poles = 2;
connection_time_motor=0.5;
Srated = 4000;
Sbase = Srated;
V_base_machine = V_base;
I_base = Sbase/(V_base*sqrt(3));
omega_sync = 120*f/poles;
H = 0.7; %[s]
omega_rads = omega_sync*pi/30; %[rad/s]
J = Srated*2*H/(omega_rads)^2; % kgm*^2

Lbase = Zbase/(2*pi*f);
Tbase = Sbase/(100*pi);
inertia = J;
torque_constant = 2;

%%NOT PU
Rs = 0.25*6;
Rr = 0.14*6;
X_stator = 0.9*2.5;
Xrotor = 0.41*2.5;
Lrotor = Xrotor/(2*pi*f);
Lstator = X_stator/(2*pi*f);
Xm = 17;
Lm = Xm/(2*pi*f);
```

PU

```
Rs_pu = Rs/Zbase;
Rr_pu = Rr/Zbase;
X_stator_pu = X_stator/Zbase;
Xrotor_pu = Xrotor/Zbase;
Lrotor_pu = Lrotor/Lbase;
Lstator_pu = Lstator/Lbase;
Xm_pu = Xm/Zbase;
Lm_pu = Lm/Lbase;



c0 = @(Cg,Cp) Cg*Cp/(Cg+3*Cp);
```

Linedata (R[ohm/km], X[ohm/km], Clineline[F/km], Clineground[F/km], Czeroseq)

```
TFSP_3x_150Al = [0.206*a 0.072*a 0.6*e 1.19*e];
EX95 = [0.32*a 0.076*a 0.52*e 1.09*e];
PFSP3x50Al = [0.641*a 0.079*a 0.53*e 1.08*e];
EX25 = [1.2*a 0.082*a 0.28*e 0.55*e];
PFSP3x25Al = [1.2*a 0.082*a 0.42*e 0.82*e];
Al50 = [0.256*a 0.312*a 4.48*e 11.91*e];

TFSP_3x_150Al_c0 = [0.206*a 0.072*a 0.6*e 1.19*e  1.19*e];
EX95_c0 = [0.32*a 0.076*a 0.52*e 1.09*e 1.09*e];
PFSP3x50Al_c0 = [0.641*a 0.079*a 0.53*e 1.08*e 1.08*e];
EX25_c0 = [1.2*a 0.082*a 0.28*e 0.55*e 0.55*e];
PFSP3x25Al_c0 = [1.2*a 0.082*a 0.42*e 0.82*e 0.82*e];
Al50_c0 = [0.256*a 0.312*a 4.48*e 11.91*e 11.91*e];
```

Published with MATLAB® R2019b

Tekniske data

Modell	MVB40-230	MVB125-230	MVB70-400	MVB160-400	MVB250-400
Distribusjonssystem	IT	IT	TN / TT	TN / TT	TN / TT
Frekvens [Hz]	50	50	50	50	50
Spenning [volt] (3 – fase)	230	230	230 / 400	230 / 400	230 / 400
Nominell last [kVA]	10	32	30	70	112
Last, 6 timer, @20°C, inngangsspenning 195 V [kVA]	16	50	50	110	170
Nominell strøm [A]	25	80	40	100	160
Strøm, 6 timer, @20°C, Inngangsspenning 195 V [A]	40	125	70	160	250
Setpunkt utgangsspenning [V]	235	235	235	235	235
Spenningsløft [%] (symmetrisk last)	0…+17	0…+20	0…+15	0…+15	0…+10
Spenningsløft, -reduksjon [%] (ubalansert last)	0…+17	0…+20	0…+28, 0…-7	0…+28, 0…-7	0…+18, 0…-7
Dynamisk respons [ms] [1]	150	200	150	200	200
Tomgangsstap [W] [2]	180	220	180	220	220
Virkningsgrad [%] [3]	95-97	95-97	97-99	97-99	97-99
Power factor [cos φ] [3]	0,96-0,97	0,96-0,97	0,98-0,99	0,98-0,99	0,98-0,99
Harmonisk forvrengning [%] [3]	1-4	1-4	1-5	1-5	1-4
Mekaniske dimensjoner					
Bredde x Høyde x Dybde [mm]	754 x 928 x 539	1003 x 1190 x 648	754 x 928 x 539	1003 x 1190 x 648	1003 x 1190 x 648
Vekt [kg]	390	750	390	750	750
Kabel tilkobling [Copper mm²]	≤ 16	≤ 50	≤ 16	≤ 50	≤ 70
Olje [liter]	75	158	75	158	158
Kapsling	Galvanisert	Galvanisert	Galvanisert	Galvanisert	Galvanisert
Features					
Bypass @ U_out ±15% eller høy temp - Ingen spenningsbortfall - Automatisk restart	√	√	√	√	√
Klarer 100% ubalansert last og opprettholder alle fasespenninger	50%	50%	√	√	√
Enpolt korslutningsstrøm øker med typisk 60% eller mer i svake nett	Uforandret	Uforandret	√	√	√
Ingen bevegelige deler i kraftkrets	√	√	√	√	√
Vedlikeholdsfri	√	√	√	√	√
Levetid kraftkrets som vanlige distribusjonstransformatorer	√	√	√	√	√
Rask installasjon < en dag	√	√	√	√	√

Opsjon: SSP = Short-Circuit Safety Protection, 3-polt effektbryter installert på utgang, FR3 = miljøvennlig organisk olje.
[1] – fra null spenningsløft til maks boost [2] – null spenningsløft [3] - nominell last, varierende spenningsløft

http://www.magtech.no/

Patent nr.: NO 317045 US 6,788,180 B2

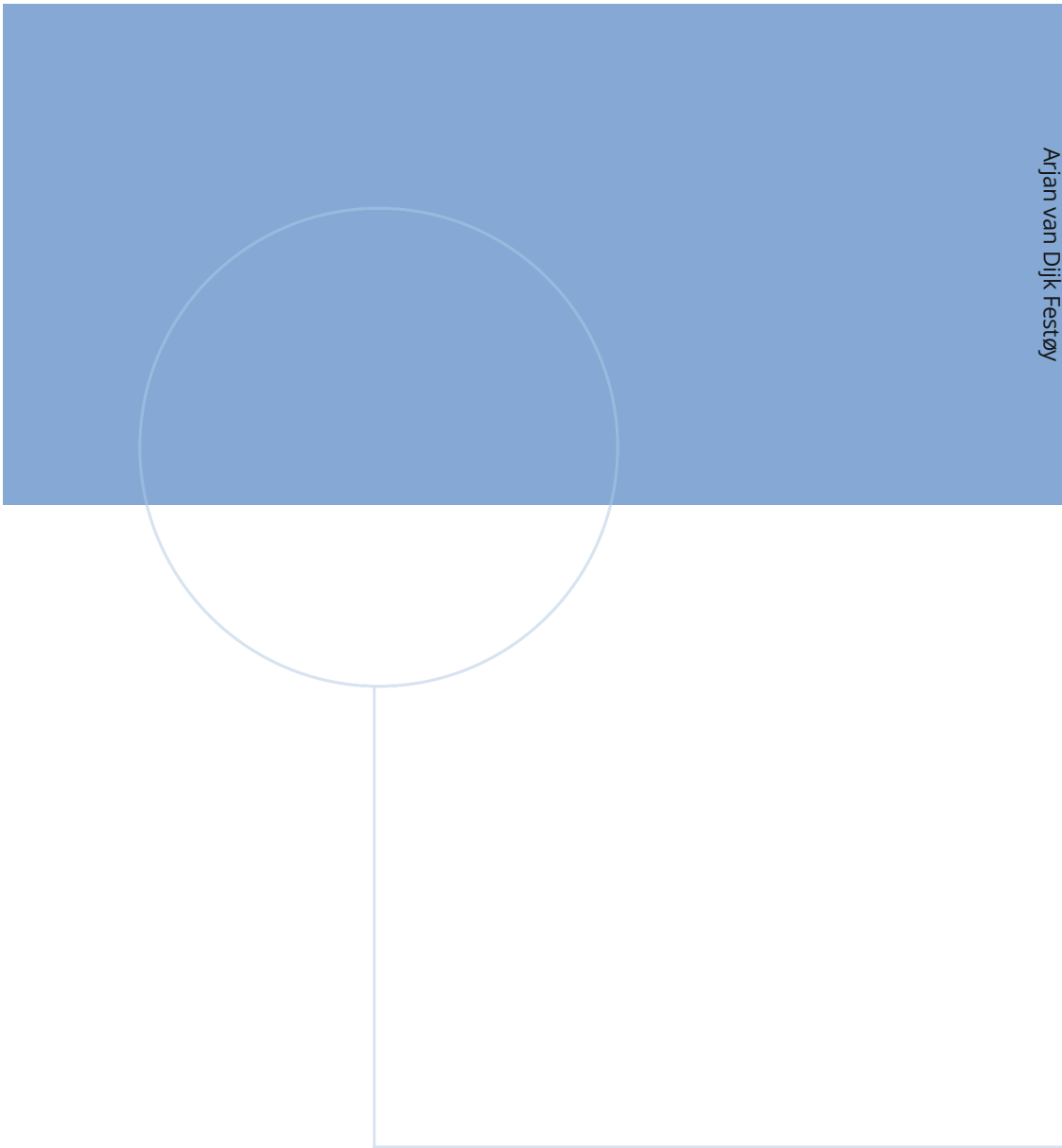

Arjan van Dijk Festøy

NTNU
Norwegian University of
Science and Technology